Modelling nearshore currents driven by waves and set-up gradients

Pieter van der Linde
Master thesis, January 2011

Woods Hole Oceanographic Institution 1930
TU Delft Delft University of Technology
USGS science for a changing world
Deltares Enabling Delta Life

Deltares

“Modelling nearshore currents driven by waves and set-up gradients”

NCEX

By

Pieter van der Linde
1092057

Delft, January 2011

This research has been done for the partial fulfilment of requirements for the Master of Science degree in Civil Engineering at the **Delft University of Technology**, Delft (NL).

Graduation committee:

Prof. dr. ir. M.J.F. Stive	Delft University of Technology
Ir. D.J.R. Walstra	Delft University of Technology / Deltares
Ir. J.J. Schouten	Deltares
Dr. ir. G.J. de Boer	Delft University of Technology / Deltares
Dr. J.H. List	United States Geological Survey
Dr. B. Raubenheimer	Woods Hole Oceanographic Institute

Abstract

Client	USGS – United States Geological Survey WHOI – Woods Hole Oceanographic Institute
Title	Modelling nearshore currents driven by waves and set-up gradients

Abstract

During the fall of 2003, an extensive measurement campaign called the “Nearshore Canyon Experiment” (NCEX) was set up along the coast of La Jolla, California. The project site covered an area in which two submarine canyons are located, respectively La Jolla and Scripps Submarine Canyon. Over 20 institutions collaborated on recording the hydrodynamics and morphological changes. The collective objective of these institutions was to gain more insight into nearshore processes.
The canyons are responsible for substantial changes in wave energy distribution over an alongshore distance of a few hundred meters. The irregular wavefield that arises in the direct vicinity of the canyons results in a complex nearshore circulation and morphological changes in the surfzone.
The following research objectives were proposed for this study: 1) “What is the relative contribution to the alongshore current of (i) alongshore water level gradients due to the alongshore variation of wave set-up and (ii) obliquely incident waves?” And 2) “Can the numerical model Delft3D reproduce the order of magnitude and direction of the nearhore currents?”
This master thesis describes the hydrodynamic circulation in the nearshore of the measurement campaign and the results of the numerical model Delft3D for two specific cases, respectively a day with wind sea and a day with swell waves. The incident waves drive currents and create wave set-up. Owing to the influence of the submarine canyons, alongshore gradients develop in the wavefield. It is concluded that the influence of the submarine canyons becomes more prominent in case of swell waves and therefore a larger alongshore set-up gradient arises. In both the observations and the model predictions an alongshore current develops strong enough to counteract the wave-driven flow.

Author	Pieter van der Linde	
Date	2011/01/31	
Review	D.J.R. Walstra	
	J.G. Boon	
	P. van der Linde	
Project number	1203349	
Keywords	Delft3D, NCEX, refraction, set-up gradient, wave-driven current.	
Status	Final	

Acknowledgements

It is a pleasure to thank all the people who have contributed to the realization of this thesis. It would not have been possible without the support and encouragement of my graduation committee, Prof. dr. ir. Marcel Stive (Delft University of Technology), Ir. Dirk-Jan Walstra (Delft University of Technology/Deltares), Ir. Jan-Joost Schouten (Deltares) and Dr. ir. Gerben de Boer (Delft University of Technology/Deltares).

I also owe my gratitude to Dr. Britt Raubenheimer (WHOI) and Dr. Jeff List (USGS) for all their support and the facilities they offered during my stay in Woods Hole. Their dedication and genuine sympathy made working with them a real privilege.

Furthermore, I would like to thank Dr. Steve Elgar, Dr. Bob Guza, Dr. Britt Raubenheimer and their field crew for collecting a phenomenal dataset during the “Nearshore Canyon Experiment”, which I used for this research. In addition, I would like to thank the Office of Naval Resources’ Coastal Geosciences program and the National Science Foundation for providing funding for the measurements.

A special thanks goes out to my fellow students and friends, to whom I have many good memories. Daan, Emiel, Frauke, Gerard, Marius, Bhaskar and Sam, thanks for listening, playing soccer, playing softball, fishing, watching Dutch soccer games or joining me on a trip.

Finally, I would like to show my deepest gratitude to my parents, sisters and brother, who have always supported me and I love very much.

Pieter van der Linde

Delft, January 2011

Summary

In this research, the performance of Delft3D is examined in simulating nearshore currents driven by waves and set-up gradients. Data from the Nearshore Canyon Experiment forms the basis for this study.

Introduction
During the fall of 2003, an extensive measurement campaign called the “Nearshore Canyon Experiment” (NCEX) was set up along the coast of La Jolla, California. The project site covered an area in which two submarine canyons are located, the La Jolla and Scripps Submarine Canyon. The canyons stretch from about 200m from the shore to about 3km offshore. Over 20 institutions collaborated on recording the hydrodynamics and morphological changes. The collective objective of these institutions was to gain more insight into nearshore processes.

The project site of NCEX is well known to surfers, as this spot is one of the most powerful surf breaks in southern California. The surf break is caused by the steep bathymetry of the Scripps and La Jolla Canyon. The canyons are responsible for substantial changes in wave energy distribution over an alongshore distance of a few hundred meters. The irregular wavefield that arises in the direct vicinity of the canyons results in a complex nearshore circulation and morphological changes in the surfzone.

Theory
Previous studies using data from NCEX demonstrated that waves experience both refraction and reflection near the submarine canyons. Resulting in a focussing effect of wave energy north of Scripps Canyon (indicated “H” in Figure I). The surface gravity waves are convergent, wave energy coming directly from the ocean combines with wave energy refracted over the canyon. Due to the focussing effect of the wave energy, locally higher waves were observed in the surfzone.

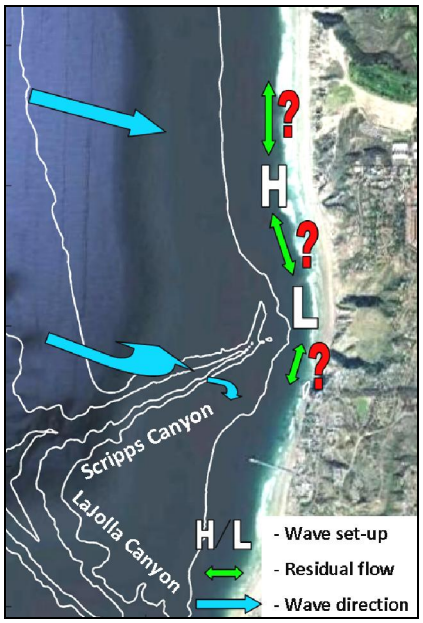

Figure I Physical processes

Near the focus zone, the incident waves approach the coast at an angle relative to the shoreline. Due to this oblique angle of incidence, an alongshore wave-driven flow is generated. As the wave direction is convergent to “H” (Figure I), also a convergent alongshore wave-driven flow develops.

Direct wave forcing from obliquely-incident waves is in general the main driving force of alongshore currents. However, observations of the measurement campaign showed alongshore flows in opposite direction compared to the direction of the wave forcing (“green arrows” in Figure I). The driving mechanism for this opposite alongshore current is caused by an alongshore wave set-up gradient. Wave set-up is a local increase of the mean water level generated by wave action. The cross-shore pressure gradient of the mean sloping water surface balances the gradient of the incoming momentum. The wave set-up varies with the wave height in the alongshore direction, so also an alongshore gradient develops, which is responsible for a pressure gradient forcing an alongshore flow.

Objective

The above described physical processes suggest that the alongshore flow can be opposite to the direction of the wave forcing when a substantial water level gradient develops. In this study is these theories are tested using the process-based numerical model Delft3D, which simulates underlying physical processes.
Hence, the following objectives are formulated:

"What is the relative contribution to the alongshore current of (i) alongshore water level gradients due to the alongshore variation of wave set-up and (ii) obliquely incident waves?"

"Can Delft3D reproduce the order of magnitude and direction of the nearshore currents?"

Results

To investigate the relevant physical processes and the performance of Delft3D, two case studies are described in this study. The first case study treats the observations of October 10th, 2003, and the second study of October 28th, 2003. On October 10, a convergent alongshore flow was observed. On this day, relatively high waves with a short period and a northwestern peak direction propagated shoreward, which is indicated as wind sea. Conversely, on October 28, a diverging alongshore flow was observed, which was a day with relatively low, southwestern swell waves.

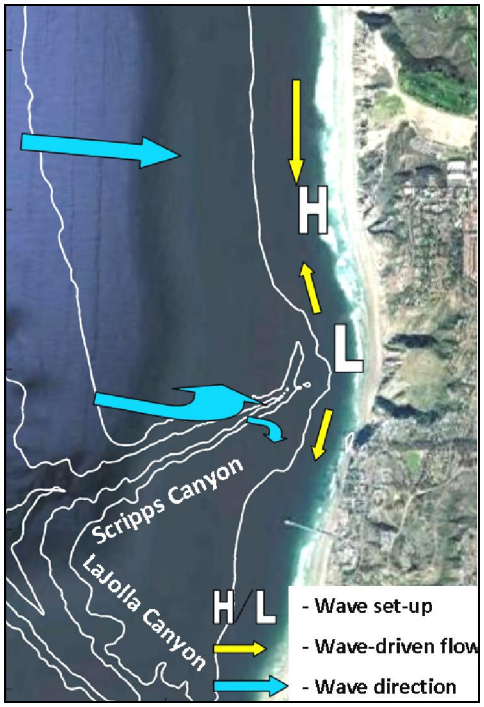

Figure II Wave-driven flow on October 10, 2003 Convergent to focus zone "H"

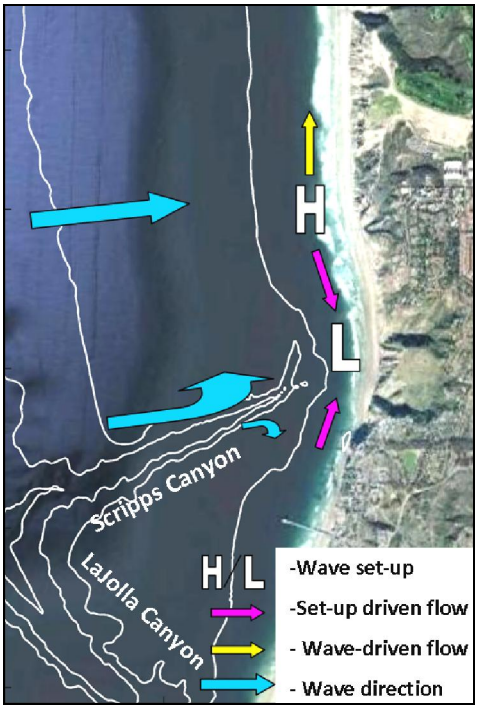

Figure III Set-up driven flow on October 28, 2003 Divergent from focus zone "H"

First, the model is calibrated by comparing observed and predicted waves further offshore. Observations were used from wave buoys deployed at 35m water depth and at the rim of Scripps Submarine Canyon. Secondly, the model predictions of waves and currents within the surfzone are compared with the observations. Data of the pressure sensors at 2.5m water depth are used for this comparison.

Both the predicted and observed significant wave heights increase alongshore towards the focus zone (see Figure IV, which illustrates the effect of diffraction predicted by Delft3D). The alongshore gradient of the observed significant wave height is also predicted according to observations. Furthermore, the wave field appears to have larger gradients in significant wave height on October 28 than on October 10.

On October 10 the alongshore wave setup gradient is smaller than on October 28. Although the predicted wave set-up shows some deviations compared to the observed wave set-up, the model does reproduce alongshore trends. In both cases, the wave set-up decreases in northward and southward direction from the focus zone.

The model predictions for alongshore currents for October 10 show a convergent flow and for October 28 a divergent flow. These predictions are according the observations. The cross-shore currents show more deviations. These deviations are attributed to the comparison of a depth averaged flow velocity with an observation at 30cm from the bottom, while prior studies demonstrated that cross-shore flow velocities strongly vary over the water column. The predicted rip current on October 10 is therefore hard to verify, however its existence is likely since the alongshore flow is converging.

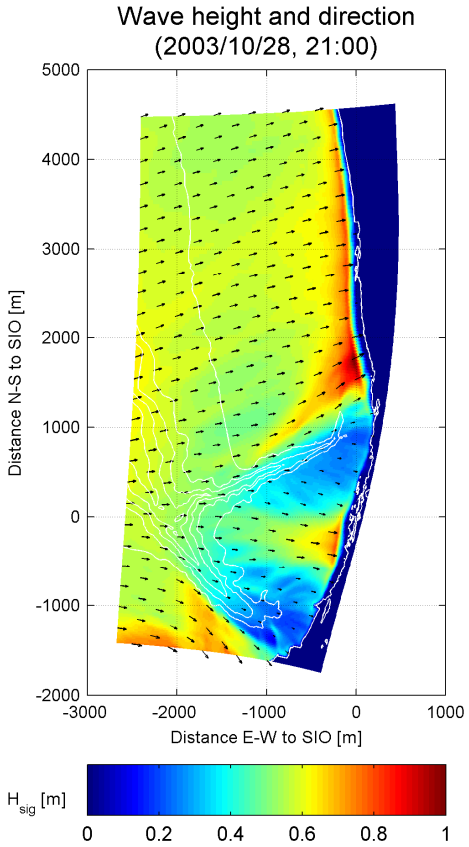

Figure IV H_{sig} and mean wave direction small wave grid

Conclusions

The main conclusions of this study are listed in the following:

- Alongshore wave set-up gradients become more evident in the simulation of October 28. This is addressed to the fact that offshore waves have longer periods and experience more influence from the canyon.
- Model predictions agree that when a larger set-up gradient develops, the alongshore flow is able to contradict the direction of wave forcing.
- Delft3D reproduces both the convergent and the divergent alongshore flows with a reasonable agreement to the observations.
- Delft3D reproduces a rip current in case converging wave-driven flows are dominating, further cross-shore observations show significant deviations.

Contents

List of Tables

List of Figures

1 Introduction

This study has been executed to contribute to the understanding of the hydrodynamic processes in the coastal environment. This chapter briefly describes the importance of our coastal system, and the "Nearshore Canyon Experiment" (2003). Furthermore, the problem description, the study objectives, and finally a reader's guide is given.

1.1 General

Water covers about 70 percent of the world's surface, and plays a crucial role in our ecosystem. The oceans regulate our earth's weather and climate, provide habitat for an enormous number of plants and animals, provide human food, and control the evolution of our ever-changing coastlines [d'Angremond and Pluim-Van der Velden, 2001]. More than half the world's population, which is more than 2.7 billion people, live within a 100 km distance from the coast, and is directly dependent on the coastal environment for living and working. Therefore, understanding the behaviour of the coastal system is essential for sustainable usage.

The total length of the world's coasts is about 504,000km [Stive, 2006]. The transition between land and water is an unstable area where waves, currents, and water levels interact with the underlying sediments. At many places, the coast is densely populated, with infrastructure that often restricts the freedom of shorelines to erode when processes remove sediment. Understanding how different processes develop and affect the coast in one location will help to understand and forecast coastal behaviour at other places in the world. In this way, better decisions can be made when considering coastal zone management.

Many processes in the ocean are still poorly understood. The physical processes responsible for the morphological changes along the coast are mainly caused by surface gravity waves and nearshore currents, which can create gradients in sediment transport leading to erosion and accretion. To gain more insight in coastal processes an extensive field campaign, known as the "Nearshore Canyon Experiment" (NCEX), was carried out during fall 2003 near La Jolla at the Southwest coast of California; U.S.A. [Thomson et al., 2007]. During this experiment, many measurements were conducted, including water levels, waves, currents and morphology. By analyzing these data, the interaction between the hydrodynamics and the bathymetric variations can be investigated.

The most outstanding characteristic of the NCEX project site is the presence of the Scripps and the La Jolla submarine canyons, responsible for several physical processes. According to Thomson et al. [2007] these canyons modify the propagation of incident surface gravity waves, resulting in strong alongshore variations in waves and currents.

1.2 Problem definition

To forecast the coastal evolution, a basic requirement is an understanding of the forces driving nearshore currents. For alongshore currents, the main forces are the radiation stress gradients resulting from obliquely incident waves approaching the coast, and the alongshore pressure gradient resulting from alongshore variations in wave set-up. Observations during NCEX pointed out that these forcing terms can be of the same order of magnitude [Apotsos et al., 2008].

Strong alongshore variations in wave conditions result from steep gradients in the bathymetry associated with canyons. At some locations the waves converge at a so-called “focus zones” while in other places where waves diverge, “shadow zones” are created. Alongshore-varying wave heights and angles result in a non-uniform forcing of alongshore currents. Furthermore, variations in wave height between focus and shadow zones result in an alongshore variable wave-induced set-up, resulting in an alongshore sea-surface gradient that can also drive alongshore currents [Apotsos et al., 2008]. The sea surface gradient generates an alongshore pressure gradient can be the dominant forcing mechanism. For example, at Delray Beach the alongshore irregularities on the shoreface influenced the wave climate in such a way that variations in shoreline set-up caused alongshore gradients in currents that created erosional hot spots at the shore [Hartog et al., 2008; Benedet and List, 2008].

The forcing of alongshore currents by obliquely incident waves is a known phenomenon. The development of alongshore currents related to alongshore set-up variations is not yet fully understood. In order to better understand the processes, the numerical hydrodynamic and morphological model Delft3D is used. After testing and validation against the NCEX data set, the model can be used to determine the contribution of the individual forcing mechanisms in driving nearshore flows at NCEX.

1.3 Objective

The aim of this research is to gain more insight into the driving forces behind the alongshore currents in vicinity of the submarine canyons. Two main questions are formulated.

Question one:
“What is the relative contribution to the alongshore current of (i) alongshore water level gradients due to the alongshore variation of wave set-up and (ii) obliquely incident waves?”

Question two:
“Can Delft3D reproduce the order of magnitude and direction of the nearshore currents?”

These two main questions are the central issue of this study. Answering these questions will be done by addressing several sub-questions. The sub-questions are split into two groups, containing questions about the physical processes and the model performance.

Relevant physical processes:
- How does the wave energy propagate across the submarine canyon?
- Does the canyon have more effect on longer waves?
- What is the incident wave angle relative to the shore?
- Does wind have an important role on the nearshore currents?

Model:
- Are the wave heights predicted correctly within the surfzone?
- Do waves have the correct angle of incidence relative to the shore?
- Can the numerical model reproduce wave set-up, and its alongshore variations?

1.4 Methodology and report outline

The methodology in this report can be divided into the following steps:

Chapter 2: Outlines of the “Nearshore Canyon Experiment” (NCEX) and the data used for this research.
Chapter 3: Describes the general the set up of the numerical model Delft3D used for this research.
Chapter 4: Describes three calibration steps of the wave simulation, using data from offshore deployed wave buoys.
Chapter 5: Compares model results with the field observations within the surfzone. Deviations are considered and explained if possible.
Chapter 6: Draws conclusions and recommendations.

The approach for this research is based on these steps.

The second chapter contains a detailed description of the NCEX measurement campaign. The project site is described geographically together with the executed measurements. Two specific cases are considered in detail in this study; a day on which wind waves were prevailing and one day on which the swell waves were. Together with a brief overview it is explained why these particular cases are selected. This provides insight in the hydraulics. The last paragraph contains a description of related literature, which is helpful to understand what is happening and to verify model results.

Chapter 3 presents a general introduction of the numerical model Delft3D, followed by a description of the computational grids, boundary conditions and settings, as it has been used for this investigation.

Chapter 4 describes three calibration steps of the wave computation in the numerical model Delft3D. Deviations in time-series and wave spectra are used to determine, which settings have to be adjusted.

Chapter 5 presents the model results together with the observed data. First, calculated wave heights and currents are compared with observed data to demonstrate if the model is reasonably capable of reproducing the physical processes. Deviations from the observations are discussed and clarified as much as possible.

Conclusions and recommendations for further research are addressed to chapter 6.

2 Measurement campaign (NCEX)

The Nearshore Canyon Experiment (NCEX) was a multi-institution field study that occurred from September 16 until December 15 of 2003, with each institution having its own observation period, to collect nearshore hydrodynamic and morphological data. The objective of this experiment is to gain better insight of the effect of the bathymetry with a steep slope on surface gravity waves and on the nearshore wave-driven currents. Several instruments recorded the waves and currents at the project site.

In the first section, a general description of the project site is given. The second section describes the deployed instruments and their locations during the experiment. In section three the selection of two specific cases is explained. Finally, in section four several previous studies of other authors are summarized considering the physical processes observed at the NCEX project site.

2.1 Project site description

NCEX was executed north of the curving Pacific coastline of La Jolla in Southern California, with instruments deployed from La Jolla Shores to Torrey Pine Beach [Thomson et al., 2007, 2008; Apotsos et al., 2008]. See Figure 2.1 for the topography. Offshore of the experiment site, two deep (more than 100 m) submarine canyons, viz.: La Jolla Canyon and Scripps Canyon extend from a few hundred meters from the shore (about 10m water depth) to about 3km offshore (about 550m water depth).

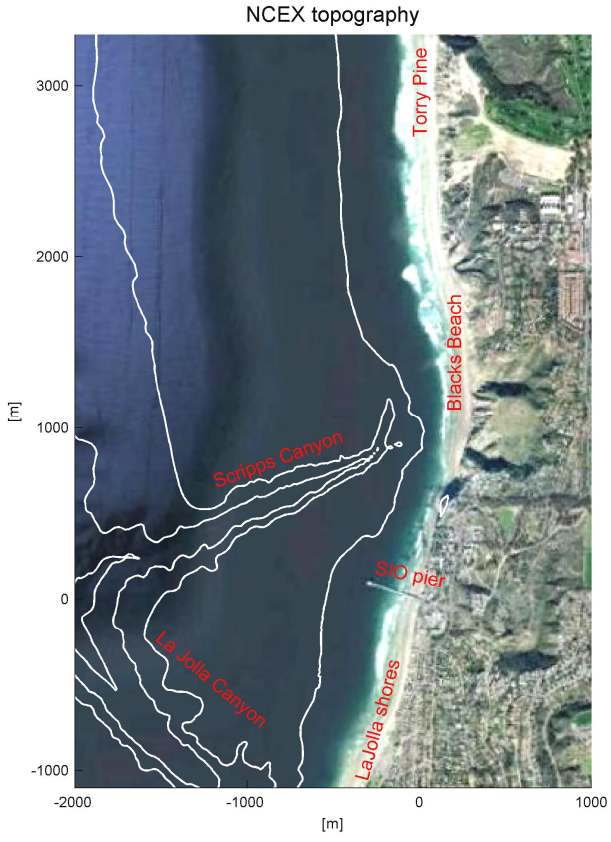

Figure 2.1 Topography of NCEX project site

The presence of the submarine canyons result in complex wave propagation patterns. The waves refract and reflect on the canyon slopes, schematically indicated in Figure 2.2. North of Scripps Canyon, wave energy comes directly from the ocean and combines with wave energy refracted over the canyon. A so-called “focus zone” develops, which is known to surfers as one of the most powerful surf breaks in southern California. Onshore of the canyon where the wavefield is diverging a so-called “Shadow Zone” develops. Thomson et al. (2005, 2007), have described in more detail the effect of the canyon with respect to reflection and refraction. This will be discussed in more detail in Chapter 2.4.1 to form a theoretical base.

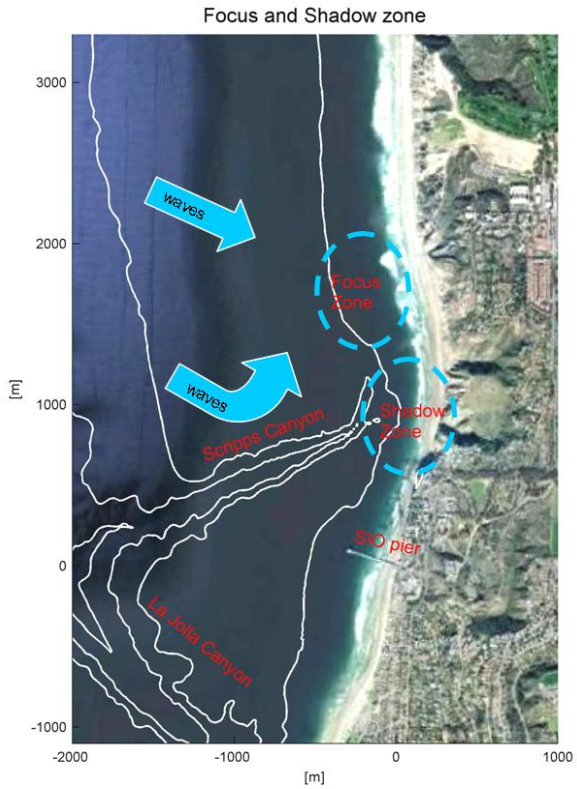

Figure 2.2 Direction of wave propagation due to Scripps Canyon

A photograph in Figure 2.3 shows the convergent wave field north of Scripps Canyon. Long crested swell waves (blue highlighted) coming directly from the ocean approach the coast perpendicular, while at the same time refracted waves from the canyon (orange highlighted) set in from the south relative to the shore normal.

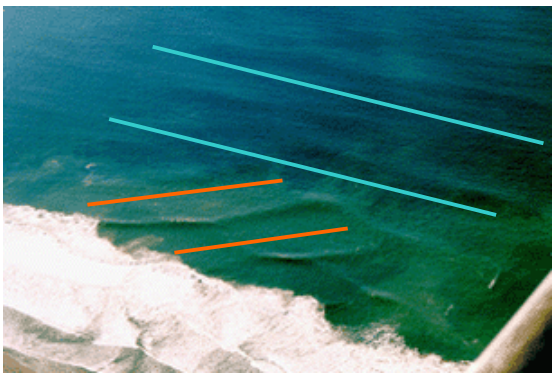

Figure 2.3 Complex wavefield at Black's Beach, Photo by S. Elgar [http://science.whoi.edu/users/elgar/NCEX/ncex-nearshore.html]

Figure 2.4 Offshore directed jet at Black's Beach, Photo by S. Elgar [http://science.whoi.edu/users/elgar/NCEX/ncex-nearshore.html]

This irregular wavefield is causing a complex nearshore circulation along Black's Beach. In Figure 2.4 a spot in front of Black's Beach is shown where alongshore flows often converge creating a rip current extending into the ocean and even crossing the 10m depth contour.

2.2 Instruments and data collection

In this paragraph the instruments, which were deployed during the experiment, are described. Each instrument is described as follows:

- location where it was deployed
- kind of data it recorded and its sampling interval
- observation period

2.2.1 Pressure gauge

The National Oceanic and Atmospheric Administration (NOAA) has deployed a tide gauge at the west end of the Scripps Institution of Oceanography pier (SIO pier) in about 7m water depth, indicated in Figure 2.1.

The tide gauged provides the water level relative to mean sea level every 6 minutes. This mean sea level is based on the epoch of 1983-2001. NOAA had already established this tidal gauge since 1924 and put the present installation in to work on September 20, 1988.

A tide gauge is located inside a submerged pipe (water can enter through the bottom), which reduces the wave fluctuations. Gauges ignore variations caused by waves with periods shorter than minutes. An electronic sensor records the height of the water level relative to datum water level.

2.2.2 Wave Buoys

The Coastal Data Information Program (CDIP, http//cdip.ucsd.edu/) monitors waves along the United States Pacific coast. Five Datawell Directional Waverider Buoys recorded wave energy, wave direction, and sea water temperature near Scripps Canyon in 20 to 120m water depths and two buoys were deployed farther North in about 35m water depth, see Figure 2.5.

A similar directional buoy was situated about 11km offshore of Torrey Pines Beach in about 550m water depth.
Each buoy estimates the wave energy and directions from measurements collected with internal accelerometers, and pitch and roll sensors [Datawell, 2009]. Wave spectra are computed for sampling periods that are about 30 minutes in duration. All buoys were active throughout the measurement campaign.

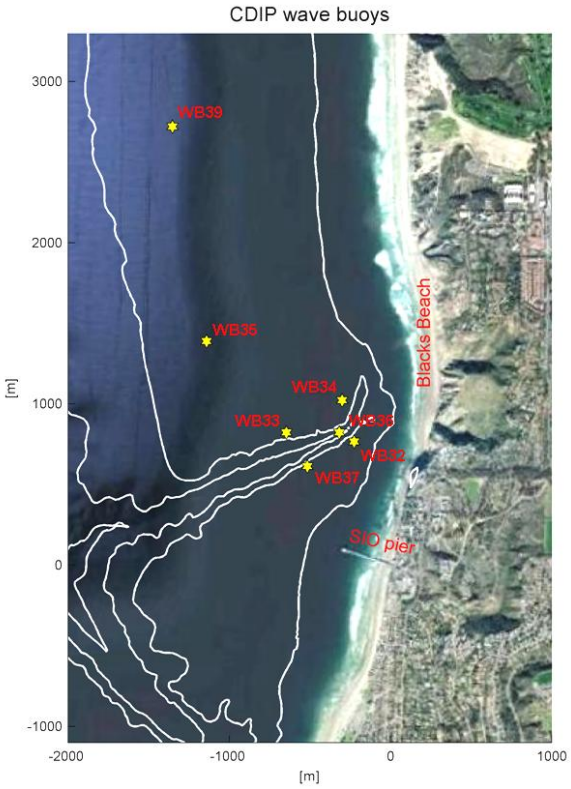

Figure 2.5 Location Wave Buoys

Figure 2.6 Datawell Directional Waverider Buoy [http://cdip.ucsd.edu/]

2.2.3 Nearshore pressure and velocity sensors

Along Black's Beach, an array of pressure and velocity sensors was set up from October 1st till November 20th. This array consisted of 9 transects perpendicular to the coast over an alongshore distance of approximately 2km. These transects lay roughly 1000, 1149, 1300, 1450, 1911, 2069, 2321, 2450, and 2700m north of the SIO pier indicated in Figure 2.7 [Apotsos et al, 2008].

At the -1.0m and -2.5m isobaths of every transect a Paroscientific pressure gauge was buried and a SonTek ADV current meter was co-located about 30 to 60cm above the bed. At the crossing of the -5.0m depth contour with the eight cross-shore transects a self-recording co-located pressure gauge and SonTek Triton current meter were deployed.

The instruments at the 1m depth contour fall dry during low tide. Therefore, the time-series of the observations at this depth contour show gaps.

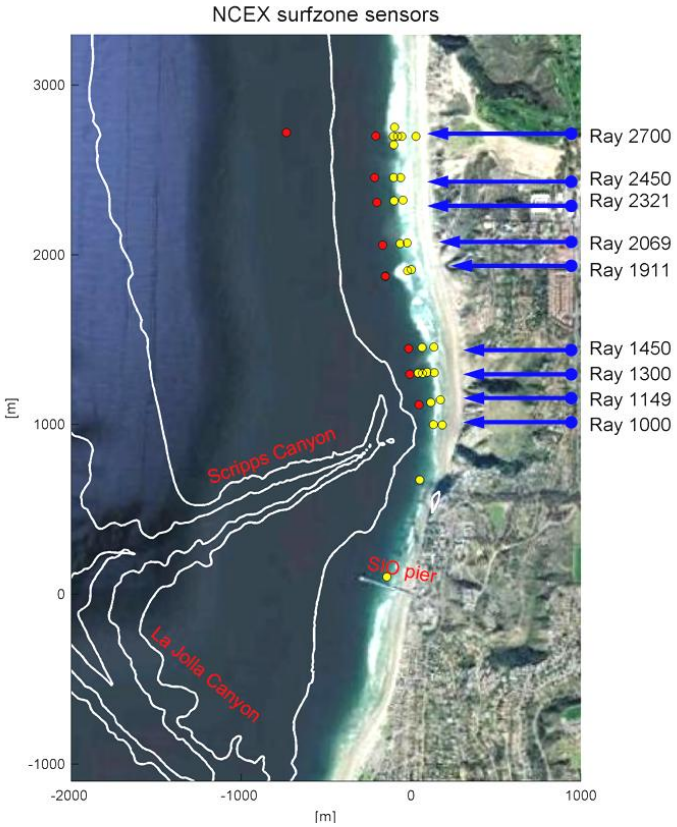

Figure 2.7 Location of current sensors and co-located pressure sensors

The pressure sensors were sampled at 2 or 16Hz for 51.2 minutes starting every hour. These hourly long data samples were divided into 8.5-minute long records to decrease the influence of non-stationarity due to depth changes caused by tidal elevation.

The rotation of every transect was determined relative to magnetic north to deploy the current meters perpendicular to the coast. This was done to record the currents in alongshore and cross-shore directions of the curving coastline. Hereby, the currents directed onshore and northward were considered positive.

2.2.4 Depth soundings

The National Ocean Survey (NOS) mapped the bathymetry of the NCEX project site using depth soundings in 1932 and in 1972. In 2001, the bathymetry over the submarine canyons was updated using swath sonar technology (WHOI), which consisted of a seabeam mounted on a ship.

During the experiment, the shallow nearshore bathymetry in front of Black's Beach was surveyed to about 6m water depth approximately once a week. This was done using the Coastal Bathymetry Survey System (CBASS), which consists of a jet ski with a Differential Global Positioning System (DGPS) [Lippmann and Smith, 2008].

2.2.5 Wind gauge

NOAA collected wind records with a wind gauge at the west end of the SIO pier, indicated in Figure 2.1. The gauge is mounted 19.4m above MSL. Measurements were made using an

RM Young digital anemometer [http://cdip.ucsd.edu/]. The data samples are hourly and describe mean direction and velocity throughout the hour.

2.2.6 Summary

In Table 2.1 a summary is given of the instruments described in this section.

Instruments	Position	Data type
Pressure gauge	West end SIO pier	Tidal elevation
Wave Buoys	- One about 11km offshore of Torrey Pines beach (550m depth) - Two North of Scripps Canyon (35m water depth) - Five around Scripps Canyon (20-120m water depth)	Directional wave spectra
Pressure gauges and co-located current meters	In surfzone at 1, 2.5, and 5m water depth at 1000, 1149, 1300, 1450, 1911, 2069, 2331, 2450 and 2700m North of SIO pier.	- Significant wave height - Water level - Flow velocity
Depth soundings	- Submarine canyons - Surfzone	Bathymetry
Wind gauge	West end SIO pier	Wind speed

Table 2.1 Summary of deployed instruments.

2.3 Observed data and case studies

Two specific days during the measuring campaign are found to be useful in this research, viz. October 10 and October 28 of 2003. On October 10, wind waves were observed with northwest peak direction causing a converging alongshore current in front of Black's Beach. Conversely, on the 28th of October swell waves were observed with a southwestern peak direction forcing a diverging alongshore current.

As all the data of the deployed instruments described in the previous paragraphs would be too abundant to show, this section mainly concentrates on the physical circumstances of the two days of the case studies. This section is subdivided into the observed physical features of tide, waves, currents, bathymetry and wind.

2.3.1 Tide

The tidal elevation during October and November 2003 is represented by Figure 2.8. The tide has a diurnal character with a strong semi-diurnal distortion. During the one and a half month of field project, three spring tides occurred, of which the second one had the largest amplitude of about 1.20m and the other two had amplitudes of 0.9m maximum. During neap tide, the amplitude reaches to 0.5m.

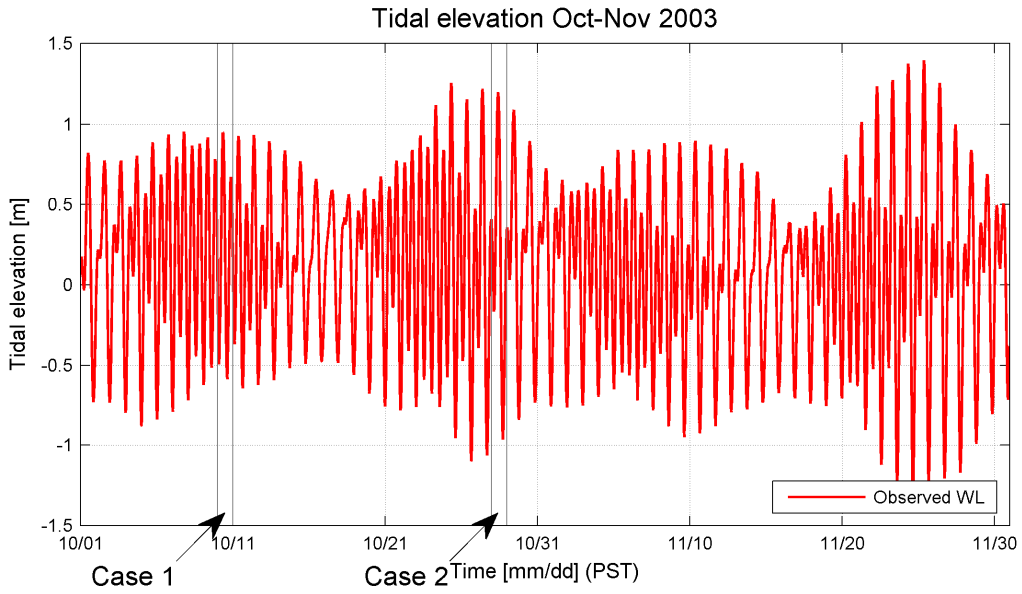

Figure 2.8 Observed tidal elevation relative to MSL for October and November 2003
[Id: 9410230, La Jolla, CA, TidesandcurrentsNOAA.gov, 2003]

The mean tidal elevations are shown in Table 2.2. These elevations are relative to mean sea level, which is determined from measurements between 1983 and 2003. Further, tidal elevations described in this report refer to this datum.

Datum	Water level [m]	Description
MHHW	0.792	Mean Higher-High Water
MHW	0.570	Mean High Water
DTL	-0.200	Mean Diurnal Tide Level
MTL	0.007	Mean Tide Level
MSL	0.000	Mean Sea Level
MLW	-0.556	Mean Low Water
MLLW	-0.832	Mean Lower-Low Water
GT	-0.539	Great Diurnal Range
MN	-1.037	Mean Range of Tide
DHQ	-1.941	Mean Diurnal High Water Inequality
DLQ	-1.887	Mean Diurnal Low Water Inequality
NAVD	-0.774	North American Vertical Datum

Table 2.2 Tidal water level elevation
[http://tidesandcurrents.noaa.gov]

Below the tidal elevation of the two considered cases are summarized. Both days show a daily inequality. The water level on October 10 varies between -0.59m and 0.95m, and on October 28 the water level varies between -0.97m and 1.20m.

As described in Chapter 2.2.3, pressure sensors and current-meters are deployed at the 1m water depth. During low tide these instruments come above the water surface and do not record. Therefore, time-series for these instruments sometimes show gaps in information.

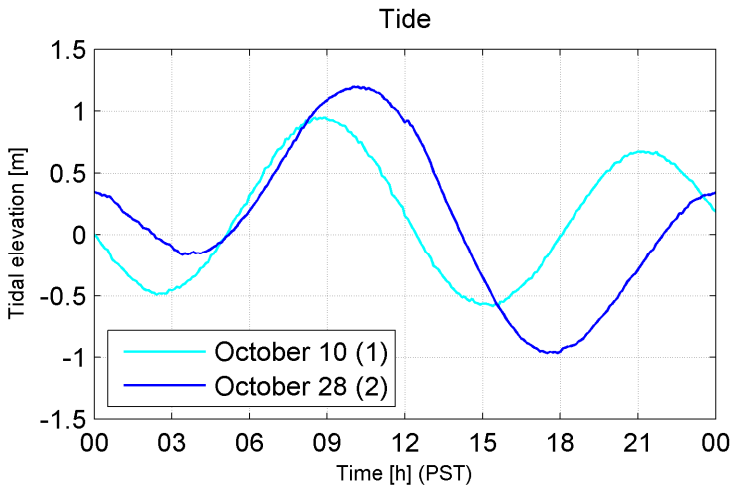

Figure 2.9 Tidal elevation during both cases (rel. to MSL)

October 10 (1)	October 28 (2)
First low 02:24 -0.49m	First low 03:24 -0.16m
First high 08:30 0.95m	First high 10:00 1.20m
Second low 15:24 -0.59m	Second low 17:30 -0.97m
Second high 21:00 0.67m	Second high 00:00 0.34m

Table 2.3 Water levels during considered cases

2.3.2 Waves

Convergence and divergence of waves, while propagating over the steep irregular bathymetry, cause an irregular wavefield. A description is given of the waves from offshore towards the coast.

First, observations of the Torrey Pine wave buoy deployed 11km offshore are described. This is considered as the offshore boundary of the project site in the numerical model. Then the wave characteristics around Scripps Canyon are described and finally in the surfzone.

2.3.2.1 Torry Pines wave buoy

Wave rose

The wave rose in Figure 2.10 describes the wave height and peak direction of the wave observations of the Torrey Pines wave buoy. During October and November of 2003, the dominant peak wave direction (41.8%) was between 270 and 300˚ relative to the north. This direction also contains the waves with the largest heights. Spectra of this wave buoy often show a bimodal energy distribution, which means that wave energy is not necessarily coming from one direction.

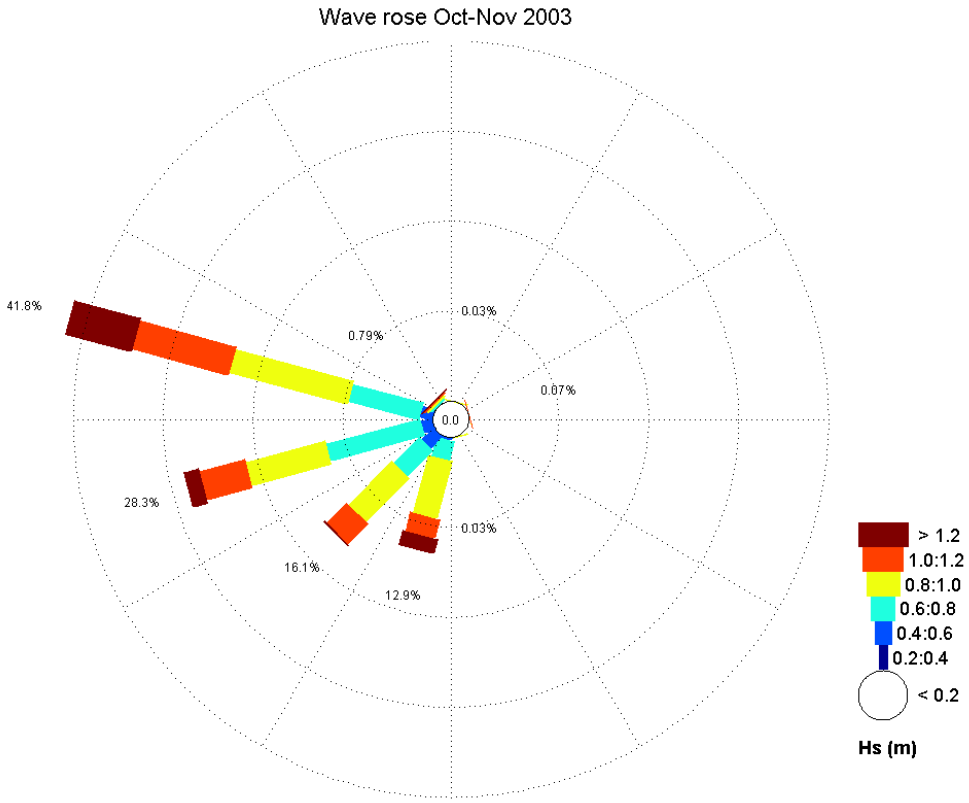

Figure 2.10 Wave rose of Torrey Pines Wave Buoy (WB100)

Represents significant wave height and peak direction at 550m water depth during NCEX

Time-series

Throughout the measurement campaign, the offshore-observed significant wave height roughly varies between 0.5 and 1.5m (Figure 2.11). The seasonal storm events on October 10 and October 22, with wave heights of respectively 1.7 and 1.9m are an exception on that. Both storms have a northwestern peak direction and a mean wave period of about 8 seconds.

Looking at the time-series of the mean wave period, October 27 and 28 are two days greatly exceeding above the average (Figure 2.11). On these days, swell waves with a period of about 14 seconds were observed with a southwestern peak direction and a wave height of about 0.9m.

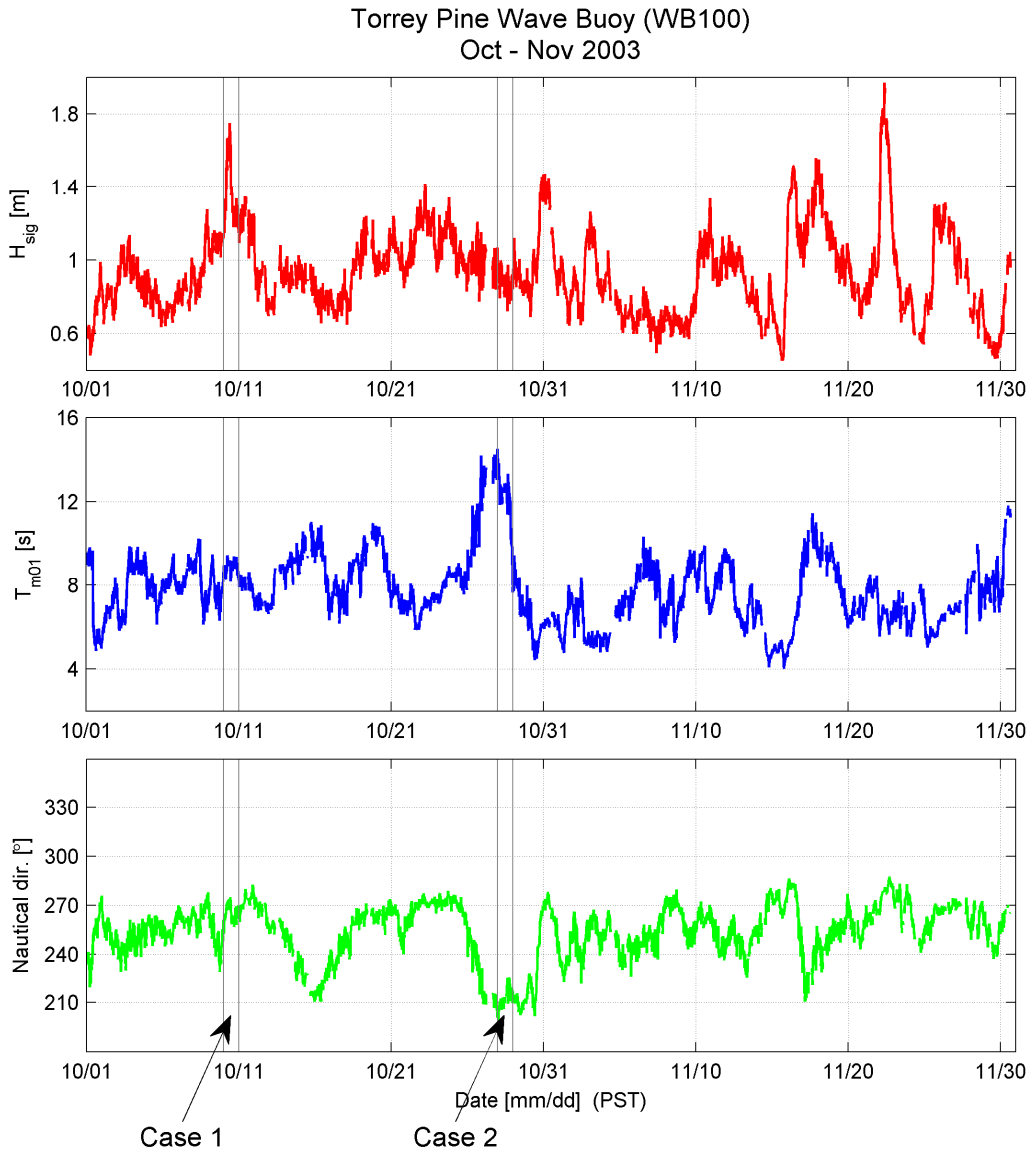

Figure 2.11 Observed wave conditions Torrey Pines Wave Buoy (H_{sig}, T_{m01} and mean dir.)

Time-series of the mean wave direction (Figure 2.11) show that the dominant mean direction was between 240 and 270˚ relative to the north. This is in contradiction to dominant peak direction, which was predominantly between 270 and 300˚. This is caused by energy distributed over frequencies other than the peak frequency, which comes from a more southern direction. This shows that energy distribution is not always narrow banded in direction.

Two-dimensional spectra of the Torrey Pines wave buoy (not presented) show that on October 10 energy comes from two directions. The two energy peaks lay between 180 and 210˚ and between 270 and 300˚ relative to the north. On October 28 spectra are narrow banded and show one energy peak between 180 and 210˚.

2.3.2.2 *Wave buoys deployed around Scripps Canyon*

In Figure 2.12, two wave roses of the buoys at 35m water depth are presented. As the figure displays 98% of the observed wave spectra have a peak direction between 240 – 300˚. Wave spectra with a peak direction between 180 and 240˚ do not even represent 1% of the observations.

Comparing this with the peak wave direction observed by the Torrey Pines buoy, indicated at Figure 2.10, the waves are clearly rotated. At the Torrey Pines wave buoy, only 70% of the waves had a peak direction between 240 – 300˚ and about 18% comes from a direction of 180 – 240˚ relative to the North.

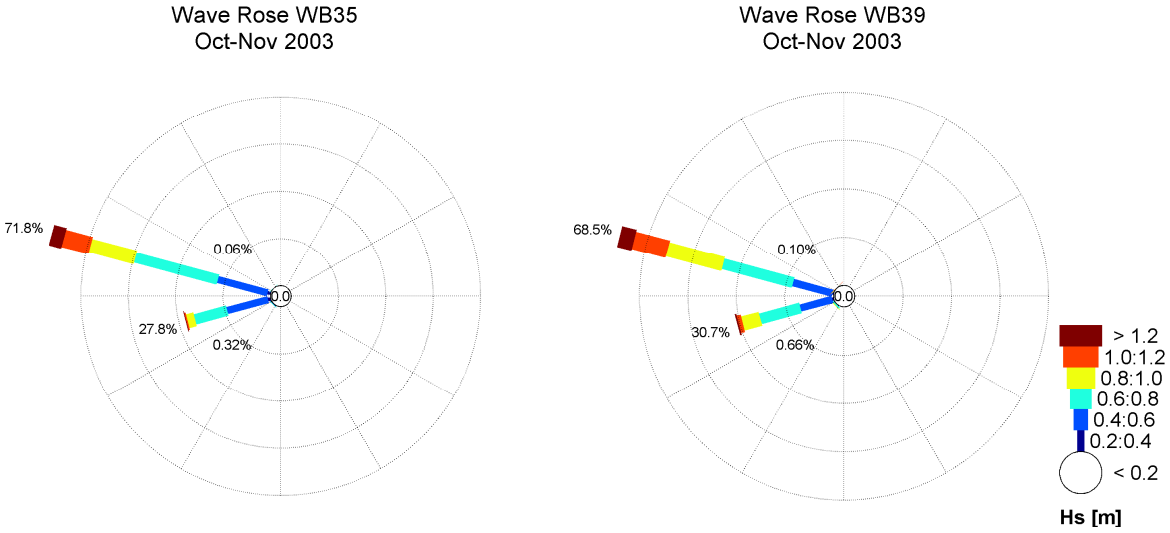

Figure 2.12 Wave roses of respectively wave buoy 35 and 39
Represent significant wave height and peak period at about 35m water depth during NCEX

In Figure 2.13, the wave roses of the wave buoys around Scripps Canyon are plotted on a map showing the canyon contours. Although the wave buoy positions are relatively close to each other, the wave roses differ significantly. The wave buoys at the northern rim of the canyon, respectively WB33 and WB34, clearly measure waves coming in from a southwestern direction. These wave buoys experience both waves coming in directly from the ocean and waves coming from the south. The observed significant wave height is predominantly larger than 0.8m (=yellow bar).

The wave buoys on top and just south of the canyon, respectively WB36, WB32 and WB37, only experience waves that were able to cross the canyon. This means that only a part of the energy is crossing the canyon and subsequently the wave height should be reduced. This is illustrated by the wave roses of the buoys south of the canyon in Figure 2.13. Observations demonstrate that significant wave heights smaller than 0.8m (=cyan bar) are common relative to all wave observations.

Thomson et al. [2007] and Magne [2007] investigate the effect of the canyon on the wavefield in the vicinity of the submarine canyon. Both found that the refraction and reflection caused the irregular propagation of wave energy shoreward.

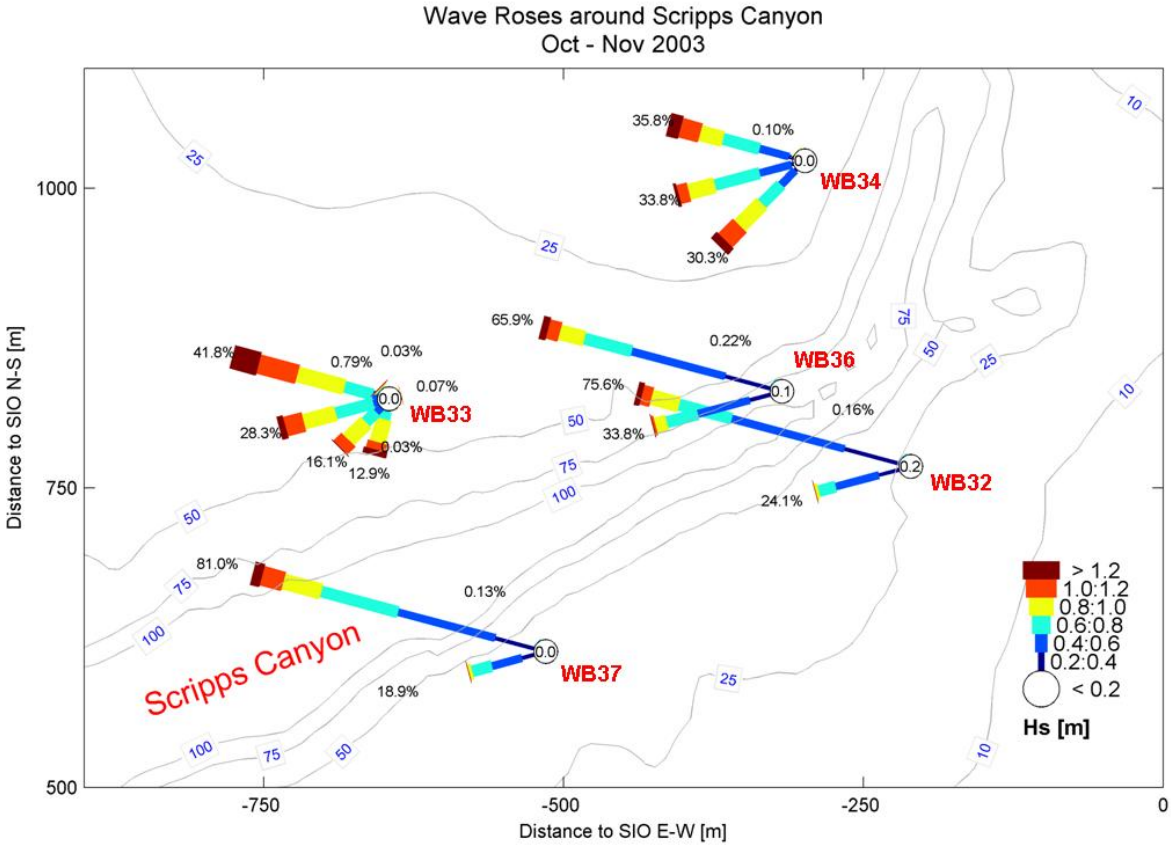

Figure 2.13 Wave roses of wave buoys deployed around Scripps Canyon

To illustrate the effect of the canyon, spectra have been compared for wave buoy 33 and wave buoy 32, respectively offshore and onshore of Scripps Canyon. On October 10 when the wave height was higher than on October 28 and the mean wave period was smaller, a relatively larger amount of energy was observed south of the canyon.

The following table represents significant wave height, mean wave period and the relative amount of energy onshore of the canyon.

Case	H_{sig} WB33 [m]	H_{sig} WB32 [m]	T_{M01} WB33 [s]	T_{M01} WB32 [s]	Energy on-/ offshore [%]
October 10, 10:00 (PST)	1.52	0.99	9.2	7.5	42.3%
October 28, 16:00 (PST)	0.48	0.23	10.1	5.7	22.9%

Table 2.4 Spectra comparison on- and offshore Scripps Canyon

The spectra of these moments in time are shown in Figure 2.14 and Figure 2.15. These figures demonstrate that predominantly energy distributed over frequencies lower than 0.1Hz deviate from each other. Although, the offshore mean wave direction differs in both cases, it can be stated that in both cases the longer waves were more influenced.

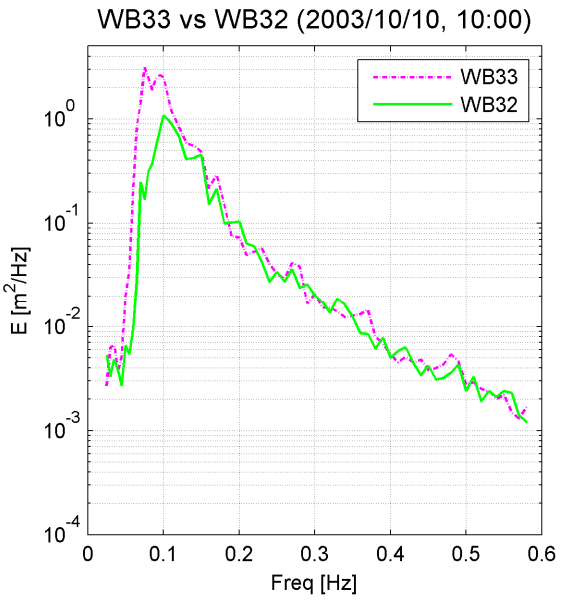

Figure 2.14 Spectra comparison 2003/10/10, 10:00

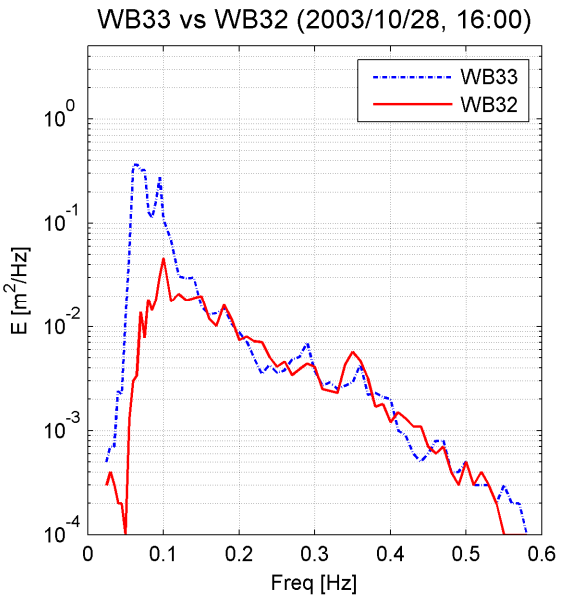

Figure 2.15 Spectra comparison 2003/10/28, 16:00

2.3.2.3 Surfzone

Finally, the waves were recorded nearshore in front of Black's Beach in respectively 5, 2.5 and 1m water depth. As the irregular bathymetry caused a lot of refraction and reflection of waves offshore, the wave heights and direction along the shore vary substantially. In section 2.1 it was explained that a so-called "focus zone" and "shadow zone" arise, indicating that at some parts along the beach high wave height develop and at some parts the wave heights remain relatively small.

To illustrate the differences in wave conditions along the shore, time-series of the significant wave height are given on Ray 1000, 1149, 1450, 1911 and 2450 at 2.5m water depth in Figure 2.16. This figure is subdivided into time-series for October 10 and 28, 2003, displaying both the significant wave heights and the mean wave direction. The wave directions are the mean incident wave angles relative to local shore normal. Positive angles ($\theta>0$) correspond to waves from the south.

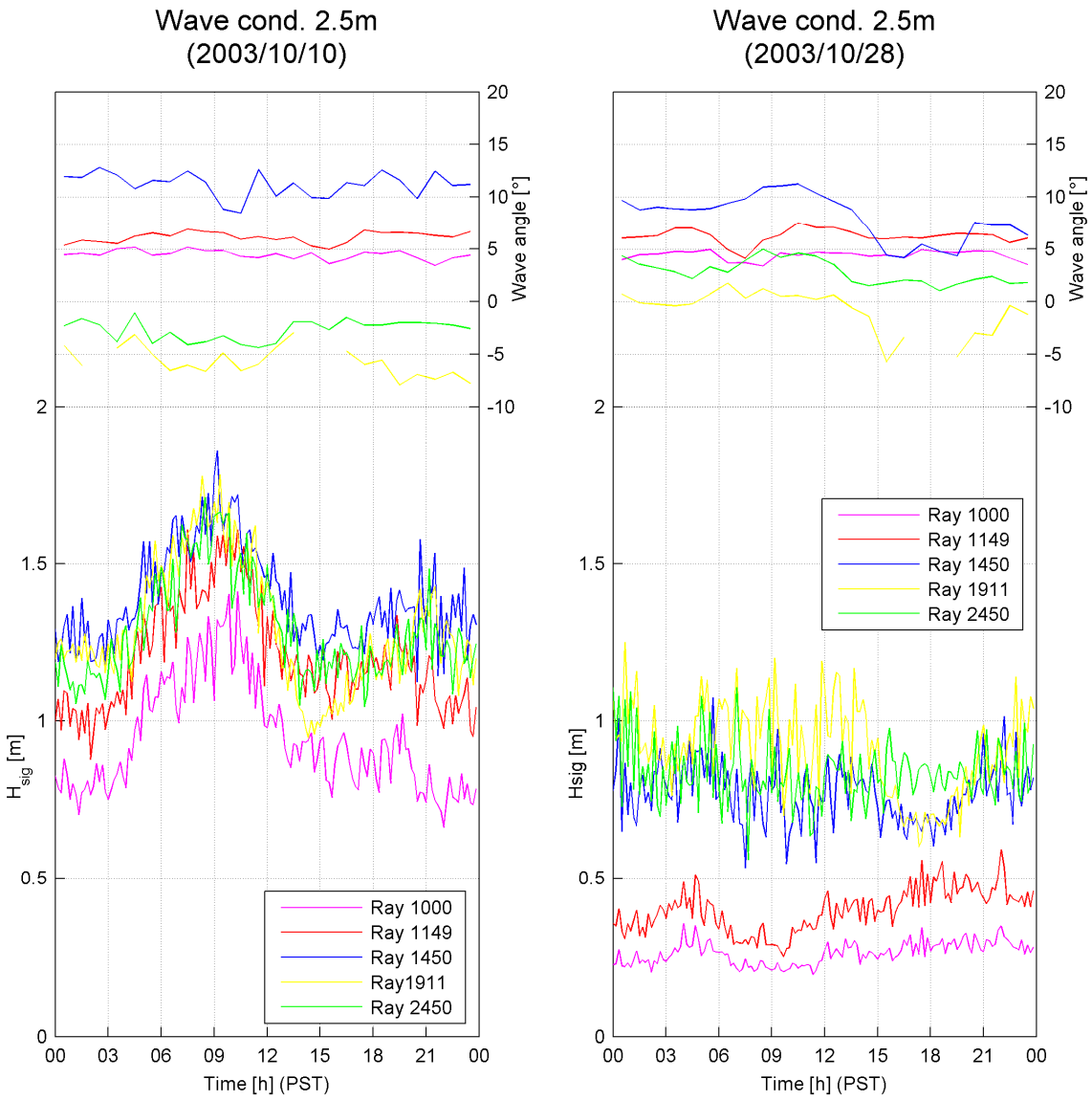

Figure 2.16 Time-series of significant wave height and mean wave direction

October 10

On this day, the wave mean wave direction was converging toward the focus zone. Observations at Ray 1911 and Ray 2450 depict that waves propagate from the north relative to shore normal. Conversely, at Ray 1000, 1149 and 1450 observations show that waves approach the coast from the south.

Considering the wave height, the smallest waves were observed at Ray 1000, onshore of Scripps Canyon. This supports the theory that a significant amount of wave energy refracts over the canyon. Moving north, towards the focus zone, wave height increases until Ray 1911, then moving farther north, heights at Ray 2450.

The highest waves are observed from 06.00 until 12.00 hours. This is consistent with the offshore observations, which showed maximum wave height of 1.7m. In addition, due to high tide (at around 09.00 hrs) the pressure sensors are in deeper water during the morning. Due to deeper water, the waves have not broken yet and not much energy has dissipated.

October 28
On the 28th of October, the wave directions at all locations are predominantly from the south. However, refraction owing to the canyon is still clearly noticeable. At the rays farthest north from the canyon, the angle of incidence is almost perpendicular to the coast. Wave angles at rays onshore of the canyon and in the focus zone are larger, meaning that waves come from the south.

Although the average significant wave height on October 28 is smaller than on October 10, an even more substantial difference develops between observed wave heights onshore of the canyon and in the focus zone.

The wave heights at 1 and 5m water depth (not shown) show the same trends along the shore as at 2.5m water depth. However, the waves at 5m water depth are higher by about 10cm compared to those in 2.5m water depth, since no breaking has influenced the waves yet. Significant waves heights in 1m water depth have decreased another 20cm compared to the waves at the 2.5m isobath.

The time-series of both days display a lot of scatter. Differences are recorded of about 0.5m between two consecutive significant wave heights. The large differences in significant wave height are realistic, since it is determined on 8.5-min records, which is too short to average through the effect of wave groups.

2.3.3 Currents

In paragraph 2.3.2, it was explained that October 10 and October 28 of 2003 were two interesting days for further investigation, because of the wave conditions. This section focuses on those cases using time-series to describe the nearshore currents.

2.3.3.1 Alongshore currents

Alongshore currents exist in the nearshore and are generated by waves approaching the beach at an angle. Inside the breaker zone a gradient in the radiation stress (S_{xy}) develops as wave energy dissipates due to wave-breaking. The radiation stress imbalance forces the alongshore flow. This alongshore flow leads to a bottom shear stress, which counteracts the wave-driven flow. When the bottom shear stress equals the cross-shore radiation stress gradient an equilibrium is reached.

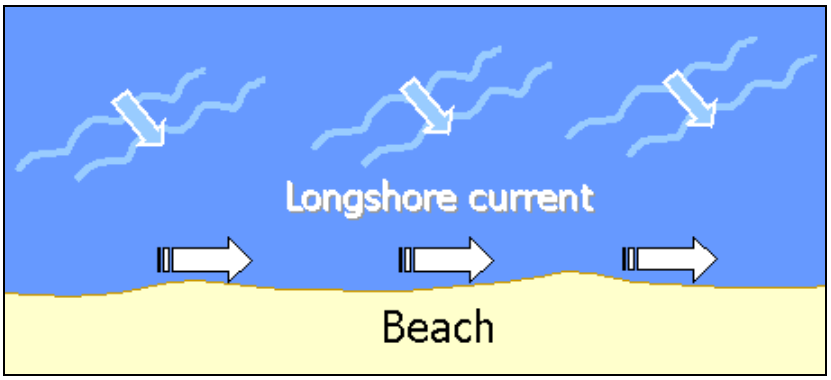

Figure 2.17 Alongshore current generated by waves
[source: http://lighthouse.tamucc.edu/Waves/NextPage1]

October 10

According to observations, alongshore currents were converging towards the focus zone on October 10. Figure 2.18 shows that southward flows are observed north of the focus zone at Ray 1911 and 2450. Conversely, south of the focus zone at Ray 1450 and 1149 the flow is northward. The current velocities are higher near the focus zone, as is the angle of incidence relative to the shoreline.

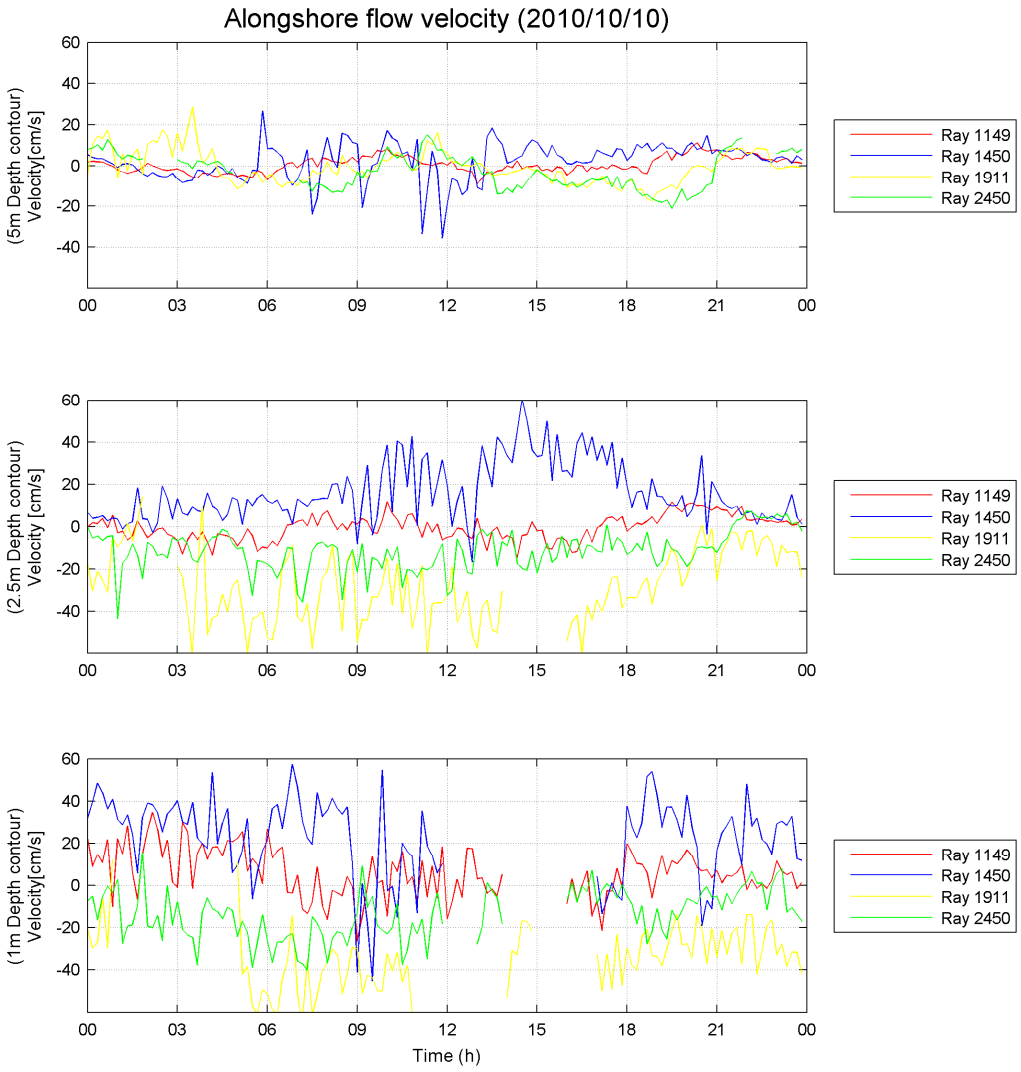

Figure 2.18 Alongshore flow velocities 30-60cm above the bed (Positive northward)

Furthermore, the alongshore flows are stronger in shallower water owing to wave breaking. More wave energy dissipates in the shallower water, which creates a larger radiation stress gradient. Considering the 1 and 2.5m depth contours flow velocities are observed up to 60cm/s. At 5m water depth the alongshore currents are close to zero except for some peaks between 6 and 12 am, when the wave conditions were severest.

October 28

The alongshore observed flow direction on October 28 diverges near the focus zone. Figure 2.19 indicate a southward flow south of the focus zone versus a northward flow north of the focus zone. The magnitudes of flow velocity are comparable to the other case. However, the flows south of the focus zone are not wave-driven. South of the focus zone the waves came from the south, which creates a northward forcing.

Furthermore, in this case you see the influence of the tidal elevation. During low tide, alongshore flow velocities are significantly larger than during high tide. When the water level falls, the current meters are situated closer to the shoreline. This indicates a non-uniform alongshore flow in cross-shore direction of the surfzone.

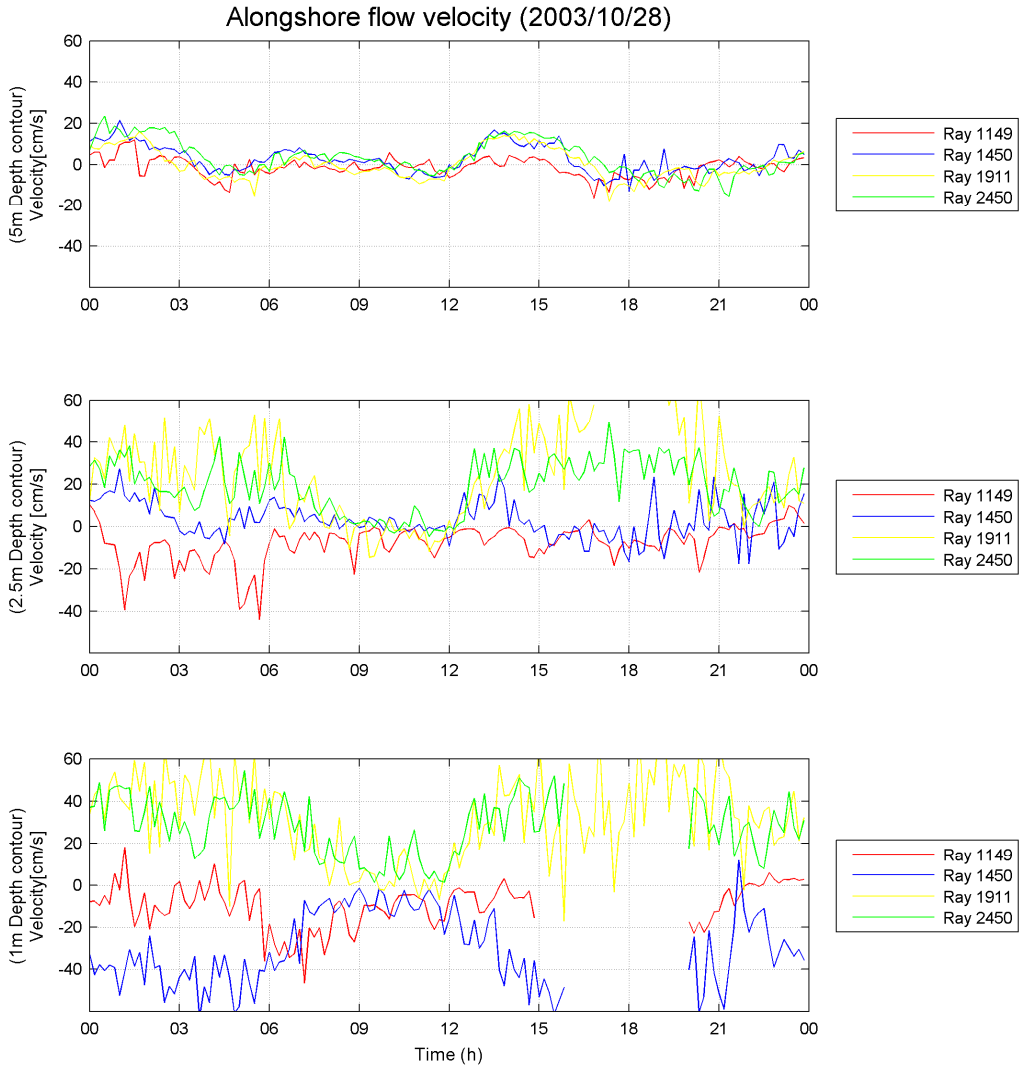

Figure 2.19 Alongshore flow velocities 30-60cm above the bed (Positive northward)

Since the wavefield at the project site is complex, set-up gradients can develop, which also force alongshore flows. The set-up gradient can both enforce and counteract the wave forcing. Which forcing mechanism is dominant differs from time to time. For this reason, alongshore currents in both directions are observed along Black's Beach.

2.3.3.2 Cross-shore currents

Cross-shore currents exist in the form of an undertow or a rip-current. Unlike alongshore flows, cross-shore currents may vary strongly in the vertical and can even change sign over the water column (Figure 2.20).

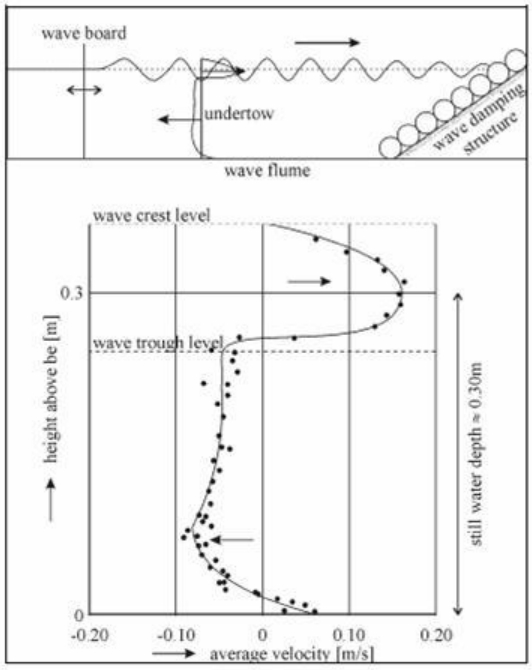

Figure 2.20 Velocities under a propagating wave
[source: lecture notes coastal morphology]

The observations of the cross-shore currents were done at 30-60cm above the bed, and therefore can not represent the flow velocity throughout the water column. Time-series of the cross-shore flow velocities

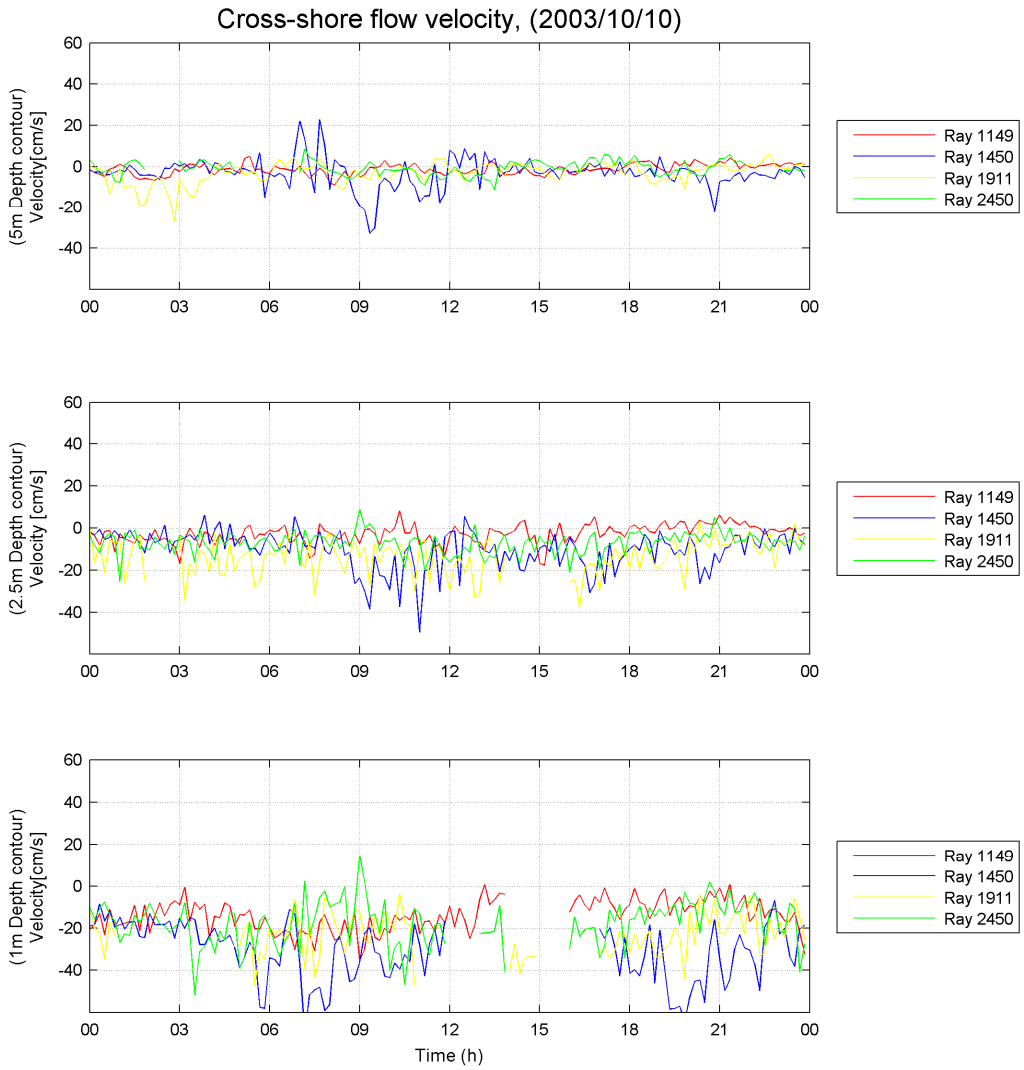

Figure 2.21 Cross-shore flow velocities 30-60cm above the bed (Positive eastward)

<u>October 10</u>

Figure 2.21 represents observed cross-shore currents on October 10. At 1 and 2.5m water depth, most of the observed velocities have a negative flow velocity, which means that the flow velocity 30-60cm from the bed is offshore directed. In addition, higher flow velocities are observed during high tide.

Except for Ray 1450, the time-series of cross-shore flow velocity at 5m water depth shows an overall velocity close to zero. Ray 1450 lies close to the focus zone where the alongshore currents converge.

October 28

Observed flow velocities on October 28, 2003 are depicted in Figure 2.22. The highest flow velocities, which were offshore directed, are observed in 1m water depth. In addition, the tide gives a clear signal in the observation at 1m water depth. During high tide, velocities up to 60cm/s develop versus velocities of about 20cm/s during low tide. Overall, the cross-shore flow velocities are small and even zero throughout the day at 2.5 and 5m water depth.

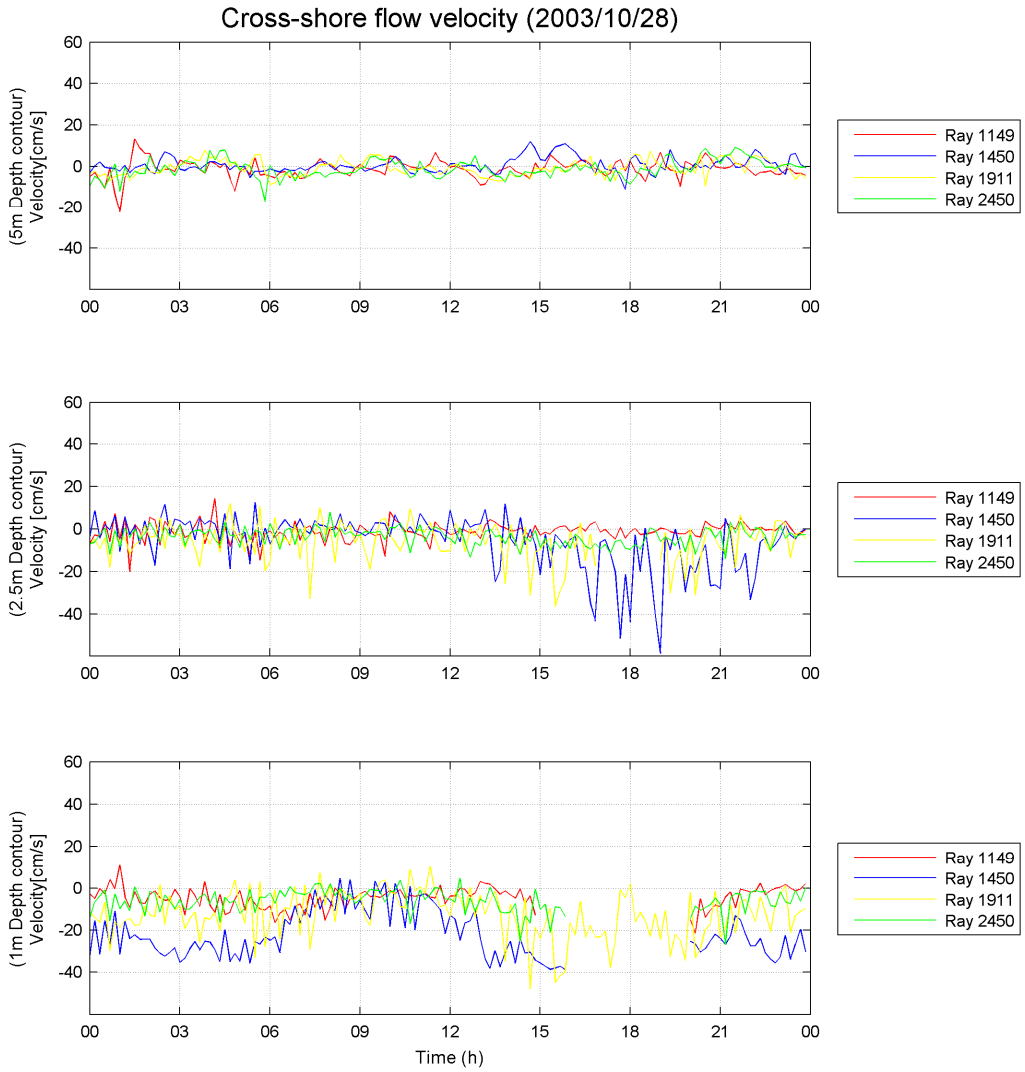

Figure 2.22 Cross-shore flow velocities 30-60cm above the bed (Positive Eastward)

2.3.4 Bathymetry

The results of the depth soundings over the Canyons executed in 2001 were expected to be still valid during the experiment. Morphological changes in those water depths are negligible and do not influence the nearshore hydrodynamics strongly. The morphological changes from the shoreline, through the surfzone, and out to 6m water depth were updated weekly, since the hydrodynamic and morphological interaction is not negligible there.

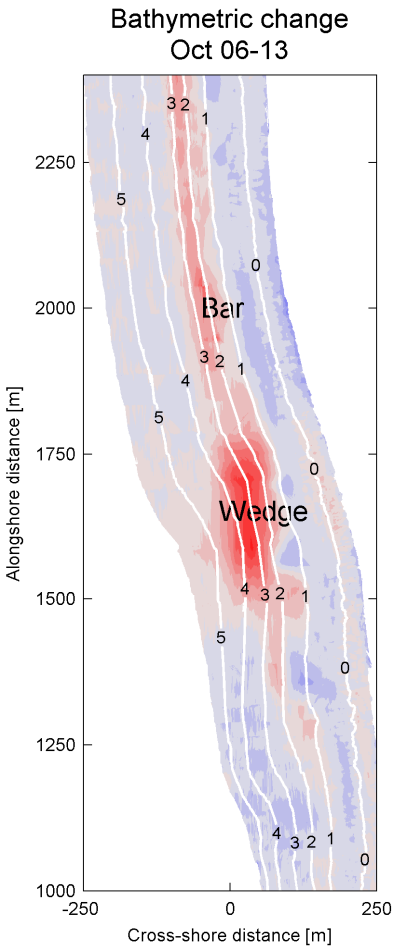

Figure 2.23 Bathymetric change between October 06 and 13, 2003

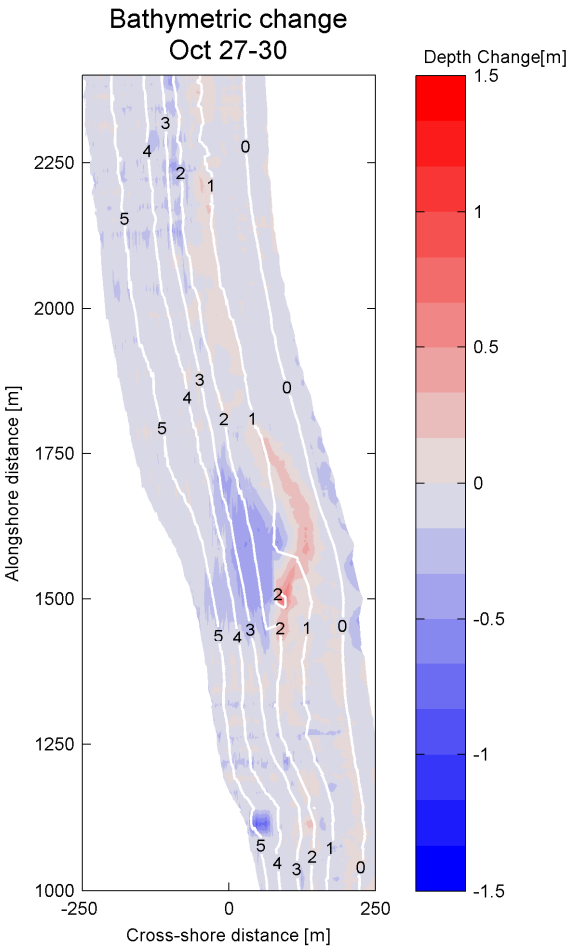

Figure 2.24 Bathymetric change between October 27 and 30, 2003

Subtracting the observed bed levels of two succeeding surveys indicate net morphological changes over the intermediate period. The net change of the bathymetry during the week with the first seasonal storm on October 10 shows a substantial morphological change (see Figure 2.23). An accumulation of sand formed what is referred to as “the wedge” close to the 3m depth contour from 1500 until 1750m north of the SIO pier. Northward the sand accreted forming a bar following the 2m depth contour.

From October 27 until October 30, the bed was also changing, as depicted in Figure 2.24. At about 1500m, locally 0.5m of sand was flushed away at 3m water depth and accumulated closer to the shoreline.

2.3.5 Wind

The distribution of wind speed and directions during October and November in 2003 is presented by the wind rose in Figure 2.25. Throughout the period, the wind is blowing from all directions with speeds rarely reaching 6m/s.

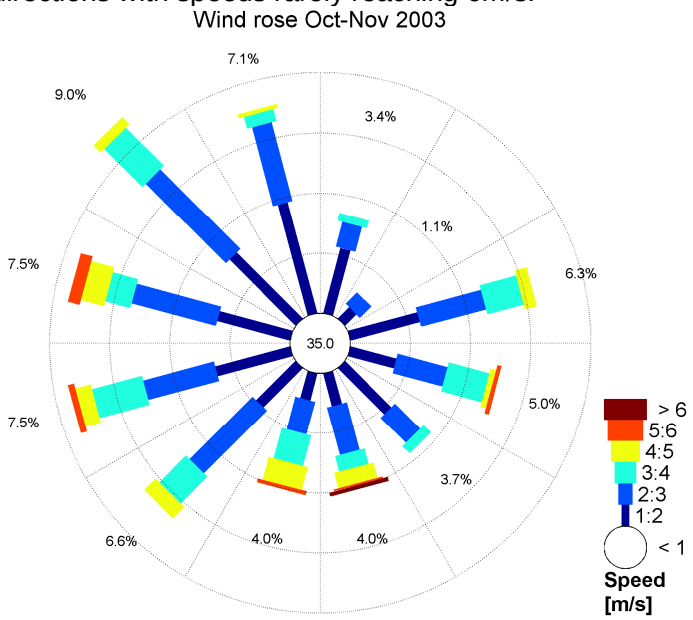

Figure 2.25 Distribution wind speed and direction in October and November 2003.

During October 9 and 10, a southern wind was blowing with a peak velocity up to 9.1m/s, as illustrated in Figure 2.26. The wind velocity during October 27 and 28 is negligible during the day. During the evening, the wind increased to 4.3m/s on average with a peak velocity of 7.4m/s.

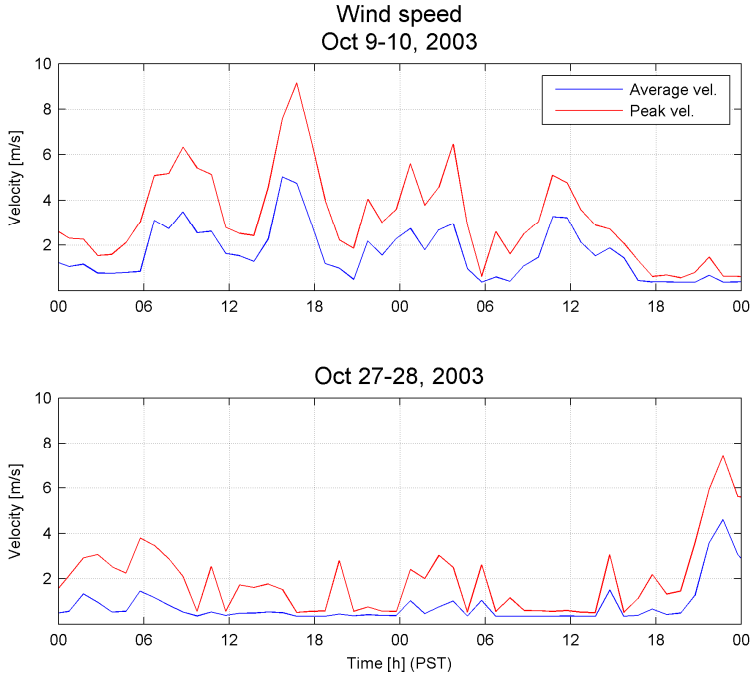

Figure 2.26 Time-series of wind velocity on October 9-10 and 27-28, 2003.

2.3.6 Summary

Data for two case studies were shown in this section. The first case study considers a day with relatively large wave heights and short periods, which originate from wind sea. Converging alongshore flows in front of Black's Beach developed and a rip current was visually observed.

On October 28, swell waves were observed offshore. At the same time a diverging alongshore flow developed in the surfzone of Black's Beach. In addition, the alongshore flow south of the focus zone opposed the direction of the wave forcing, possibly the set-up gradient could be dominant to the wave forcing.

	Case 1	**Case 2**
Date	October 10, 2003	October 28, 2003
Tidal elevation	Range from -0.59m to 0.95m relative to MSL	Range from -0.97m to 1.21m relative to MSL
Wave type	Wind sea	Swell
Max offshore H_{sig}	1.7m	0.9m
Offshore T_{M01}	8-9 seconds	10-14 seconds
Alongshore current	Converging towards focus zone	Diverging converging from focus zone
Bathymetry	A wedge was formed	Sand migration
Wind	Up to 3m/s	<1m/s during the day; picked up to 4.3m/s during the evening

Table 2.5 Summary of physical conditions for case studies

2.4 Related literature

This paragraph gives an overview of several other studies related to this research. Findings, which are relevant or even essential for the analysis of this research, are described. These studies also made use of the NCEX field data to investigate the behaviour of waves and currents in the vicinity of the steep bathymetry of the canyons.

The first section describes literature considering wave propagation adjacent to the canyon. Section two includes a description of literature dealing with the currents in the surfzone.

2.4.1 Waves

In Chapter 2.3.2 time-series of wave observations demonstrate a varying wavefield over the project site. Important processes to define these irregularities are refraction and reflection. Thomson et al. [2005; 2007] and Magne et al. [2007] studied these processes around the canyons.

2.4.1.1 Thomson et al. [2005; 2007]

Thomson et al. [2005] describes reflection and transmission of ocean surface gravity waves (periods between 20 and 200 sec) from the steep-walled Scripps Canyon. Field observations offshore and onshore of La Jolla Canyon were used to test the reflection and transmission formula of Kirby and Dalrymple [1983] for a rectangular submarine canyon.

Thomson et al. [2005] decomposed observations of pressure and velocity to distinguish the waves from distant sources, waves reflected by the canyon, and waves transmitted across the canyon. It was found that for waves approaching the canyon normal to its axis 60% of the energy reflects, and that no energy reflects at all for waves twice as long as the canyon's width. For oblique incident waves the model predictions underestimate energy reflection compared to the theoretical approximations. Evidently, some energy of the low frequency waves (<0.02Hz) was transmitted across the canyon. The neglected non-uniformity of the La Jolla canyon is brought up as a possible reason.

In continuation, Thomson et al. [2007] investigated the effects of refraction and reflection on the propagation of surface gravity waves near the submarine canyons. For this research a wave propagation model was used that accounts for conservation of energy flux during both refraction over smooth bathymetry and partial reflection from the canyons. Comparisons with field observations of the refraction-only model seemed to give poor results compared to the refraction-reflection model. Wave predictions within a few wavelengths from the canyon of the refraction only model have a significant deviation corresponding to observations. The model for both refraction and reflection gives accurate results both far and close to the canyons.

2.4.1.2 Magne et al. [2007]

Magne et al. [2007] examined the effect of a submarine canyon on swell waves with a three-dimensional coupled-mode model for wave propagation. This model predicts a more gradual transition with partial reflection/transmission compared to a classical geometrical optics approximation. Wave observations showed a decay of height by about a factor 5 over a distance shorter than a wavelength. The classical geometrical optics approximation predicts a lowering of wave height up to a factor 10. This is because oblique incident low-frequency waves cannot cross the canyon at all within this model. An abrupt transition between complete transmission at small incidence angles to no transmission at large angles.

2.4.1.3 Conclusion

Both Thomson et al. [2005; 2007] and Magne et al. [2007] used a model to investigate the effect of refraction and reflection over the canyon on surface gravity waves. All three studies demonstrated that energy carried by infragravity waves, either reflects from or refracts over the canyon, which clarifies the alongshore variations in the incident wavefield.

Figure 2.27 represents an illustration made by Magne et al. [2007] of the wave rays for a swell case (T_p=14,5-s, θ=272°) of November 30, 2003. This figure shows propagation of waves crossing the northern shelf of the canyon where the waves gradually bend towards the shore. Rays that reach the canyon's northern wall (zone 1 in Figure 2.27) are trapped on the shelf and reach the shore in a focusing region north of the canyon (zone2 in Figure 2.27).

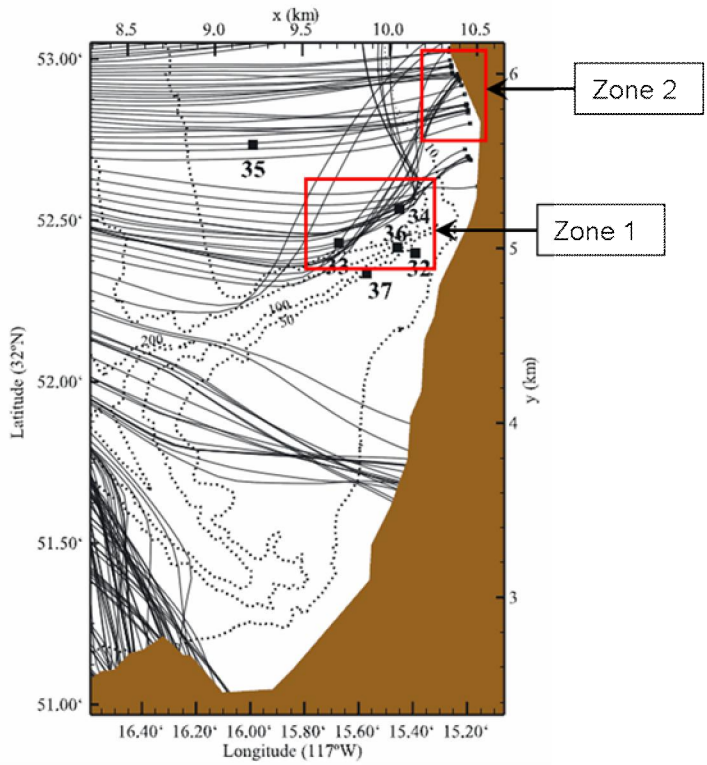

Figure 2.27 Gradual bending of wave Rays (Magne et al., 2007). Creating a focussing region in front North of Scripps Canyon

2.4.2 Currents

Long and Özkan-Haller [2005] investigated development of rip currents resulting from wave height variations associated with undulations in the canyon contours. Apotsos et al. [2008] investigated the development of alongshore currents driven by cross-shore radiation stress gradients and alongshore set-up gradients. Both studies define processes that help to explain the observed currents in the surfzone.

2.4.2.1 Long and Özkan-Haller [2005]

Argus video data of the Coastal Imaging Laboratory at Oregon State University showed rip currents in front of Black's Beach on October 10, 2003 to October 12, 2003 and on October 31, 2003. Long and Özkan-Haller [2005] used SWAN for wave simulation and a circulation model of Ozkan-Haller and Kirby [1997, 1999] to investigate the development of these rip currents. Idealized cases with specific site characteristics were considered, including a curved shoreline, an offshore submarine canyon and undulations in the canyon wall for a variety of incident wave conditions.

Long and Özkan-Haller [2005] found that undulating bathymetry at the rim of the canyon was more important than the presence of the canyon itself for development of rip currents. Due to the undulations an irregular refraction pattern exists, which causes a varying nearshore wavefield. Also period and direction of the waves play an important role.

With regard to the offshore wave conditions, Long and Özkan-Haller [2005] state that incident waves with relatively short periods are unaffected by the presence of the canyon and rip

currents do not form. In addition, waves approaching with a large angle of incidence create strong alongshore currents hindering rip current development.

Analysis by Long and Özkan-Haller [2005] of the alongshore momentum balances showed the usual equilibrium between the incident wave forcing and the water level gradient, outside of the surfzone, and an equilibrium between incident wave forcing and competing bottom friction inside of the surfzone. However, at locations where rip currents were present the advective terms seemed to be dominant, both inside and outside of the surfzone. The advective acceleration terms are balanced by the alongshore pressure gradient and bottom friction. This equilibrium of forcing terms in the alongshore momentum balance point out the importance of the inertia.

2.4.2.2 Apotsos et al. [2008]

Apotsos et al. [2008] examined the effect of alongshore variations in the incident wavefield on set-up and on alongshore flows inside of the surfzone. Due to the breaking effect in the surfzone, waves lose shoreward momentum. As result of this energy dissipation, an increase of the water level relative to mean sea level develops to create momentum balance in cross-shore direction, generating the familiar wave-induced seup.

Alongshore wave observations at Black's Beach display a varying wavefield associated with set-up variations up to 0.1m. Apotsos et al. [2008] solved simplified one- and two-dimensional momentum balance equations for the time-averaged wave set-up. The alongshore momentum balance equation includes bottom stress estimated with a quadratic bottom friction formulations. Hence, the momentum balance equations are:

Cross-shore momentum balance eq.: $-\rho g h \frac{\delta}{\delta x}\bar{\eta} = \frac{\delta}{\delta x} S_{xx} + \frac{\delta}{\delta y} S_{xy} + \tau_b$

Alongshore momentum balance eq.: $-\rho c_d \left\langle \left|\vec{u}\right| v \right\rangle = \rho g h \frac{\delta}{\delta y}\bar{\eta} + \frac{\delta}{\delta x} S_{xy} + \frac{\delta}{\delta y} S_{yy}$

Apotsos et al. [2008] applied these equations in a case study using observations of October 27, 2003, a day with constant wave conditions. Apotsos et al. [2008] describes that the cross-shore gradient of S_{xy} is more important in the outer-surfzone ($h=H_{rms,avg}/0.42>1.3$) and close to the focus zone (Ray 1450) than it is further onshore or farther north (Ray 2321). In the middle- and inner-surfzone ($h= H_{rms,avg}/0.42<1.2$), the set-up gradients becomes relatively more important as set-up increases shoreward, while $\delta S_{xy} / \delta x$ decreases shoreward, resulting in $\left|(\rho g h)\delta\bar{\eta} / \delta y\right| > \left|\delta S_{xy} / \delta x\right|$.

Apotsos et al. [2008] found that although wave forcing would create a northward current alongshore, the set-up induced pressure gradient could be dominant near the focus zone (Ray 1450) and create an opposite current southward.

2.4.2.3 Conclusion

The studies of Long and Özkan-Haller [2005] and Apotsos et al. [2008] focus on the currents in the surfzone during the NCEX measurement campaign.

Long and Özkan-Haller [2005] found that the undulations in the canyon wall caused an irregular wave refraction pattern, which is important for the development of rip currents. However, rip current did not develop when the wave period is short or the wave angle relative to the shore was large. Short waves are less affected by the presence of the canyon, therefore variations in the wavefield were too small. A large wave angle caused strong alongshore currents that inhibited rip current formation.

Apotsos et al. [2008] examined the development of the alongshore pressure gradient caused by an alongshore wave set-up gradient. It was found that in the inner surfzone, the set-up gradient was dominant to the wave forcing. This drove the alongshore current in the investigated cases opposite to the direction of wave forcing.

3 Model construction

The numerical model Delft3D has been used for this study. To understand the model set up, first an introduction is presented to Delft3D and the applications used in this study. In section two, the grids are presented on which Delft3D executes its computations. The third section describes the bathymetry determined from datasets. Model settings as time step boundary conditions and wave computation mode are described in section four. Remaining model settings are listed in Appendix B.

3.1 Introduction Delft3D

Delft3D is a multi-dimensional, process based, hydrodynamic simulation program developed by Deltares. The program is applicable for simulations of flows, waves, sediment transport, water quality, morphological developments and ecology.

Delft3D offers five options to schematise the dimensions of the area of interest. The following options are available, summarized in range of costly to fast computation time:

- 3D schematization, which is most accurate
- Quasi-3D, this model computes the vertical velocity distribution at every grid point accounting for tidal forcing, wave breaking, wind and dissipation due to bottom friction
- 2D schematization by averaging the width (2DV) or height (2DH)
- 1D schematization, which is the least accurate because of averaging in all dimensions

Two applications have been applied in this study, the module Flow and the module Wave. Both modules used a 2DH schematization.

3.1.1 Delft3D-Online

Delft3D-Online is a simulations approach in which applications communicate with each other. In this study, the modules Delft3D-Flow and Delft3D-Wave have been applied and were coupled using the online method. The simulations of both modules influence each other by computations at each time step. By coupling the modules, a dynamic two-way wave-current interaction is established.

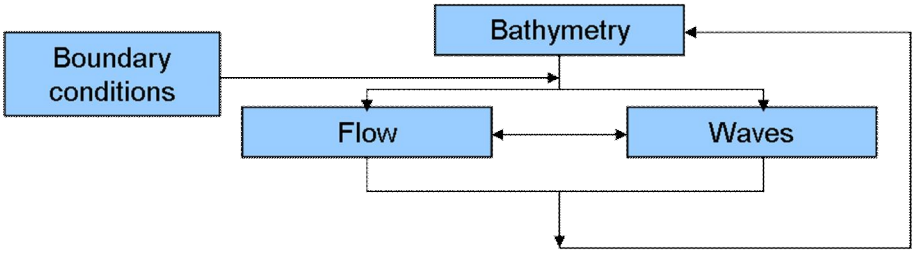

Figure 3.1 Schematic overview of processes

Figure 3.1 gives a schematic overview of the processes during a Flow-Wave interaction interval with Delft3D-Online. The model runs over a bathymetric grid with depth values on each grid point. The user can define the bathymetry by using datasets or by using output from previous model runs. Together with the initial wave and flow boundary conditions, the bathymetry provides the starting conditions of the model runs.

The flows are calculated for the specified bathymetry using the wave and flow boundary conditions. Different modules can be active during the same time step. For this study a wave field was calculated frequently. The effects of waves on flow (via forcing due to breaking, enhanced turbulence and bed shear stress) and the effects of flow on waves (via set-up, current refraction and enhanced bottom friction) are accounted for in an online coupling approach of Delft3D-Flow and Delft3D-Wave.

The communication interval of the flow and wave modules should be carefully considered since changes in the water level, bathymetry and flow field do affect the waves and vice versa.

3.1.2 Delft3D-Flow

In this research Delft3D-Flow version 3.60.00.7112 has been used. Deflt3D-Flow solves the non-linear shallow water equations. These are derived from the three dimensional Navier Stokes equations for incompressible free surface flow, in two (depth-averaged) or three dimensions.

The system of equations consists of the horizontal momentum equations, the continuity equation and the sediment transport equations. While the water depth is assumed much smaller than the horizontal length scale, the shallow water assumption is valid. Under this assumption, the vertical momentum equation can be reduced to the hydrostatic pressure equation. The vertical accelerations are assumed small compared to the gravitational acceleration and therefore not taken into account.

3.1.3 Delft3D-Wave

Delft3D-Wave performs the wave simulation by using the 3rd generation SWAN model (Booij et al., 1999), version 40.72AB. The SWAN (Simulating WAves Nearshore) model computes the evolution of short waves in coastal regions. SWAN is based on the discrete spectral balance of action density and driven by boundary conditions and winds. Random wave fields propagating from different directions can be simulated simultaneously.

The results of the wave simulation (significant wave height, peak spectral period, wave direction, mass fluxes, etc.) are included in the flow calculations through additional driving terms. In simulations where during the flow simulation the water level, bathymetry or flow velocity field changes significantly, it is desirable to update the wave simulations periodically. The wave field can thereby be updated accounting for the changing water depths and flow velocities.

3.2 Computational grids

Both modules flow and wave were set up with their own grid. Wave calculations are executed on multiple 2D grids obtained from Gorrell [2010]. The flow calculations are performed on a single 2D grid.

The grid is set up relative to a local coordinate system, of which the origin is located at the third pillar of the SIO pier. This local system is used since data of the observations is also relative to the SIO pier. In addition, if the grids were set up in a UTM11 system, the amount of digits become to large to indicate the each grid point, which make simulations inaccurate as the model rounds each location to a smaller amount of digits.

Delft3D-Wave

The wave computations are executed on three different grids (Figure 3.2). A large grid covering an area from the shore to deep water in which two smaller grids are nested. The grid spacing of the largest grid is coarse to keep calculation time small. The smaller grids gradually cover smaller areas and have a finer grid spacing to accomplish more accuracy near the field of interest.

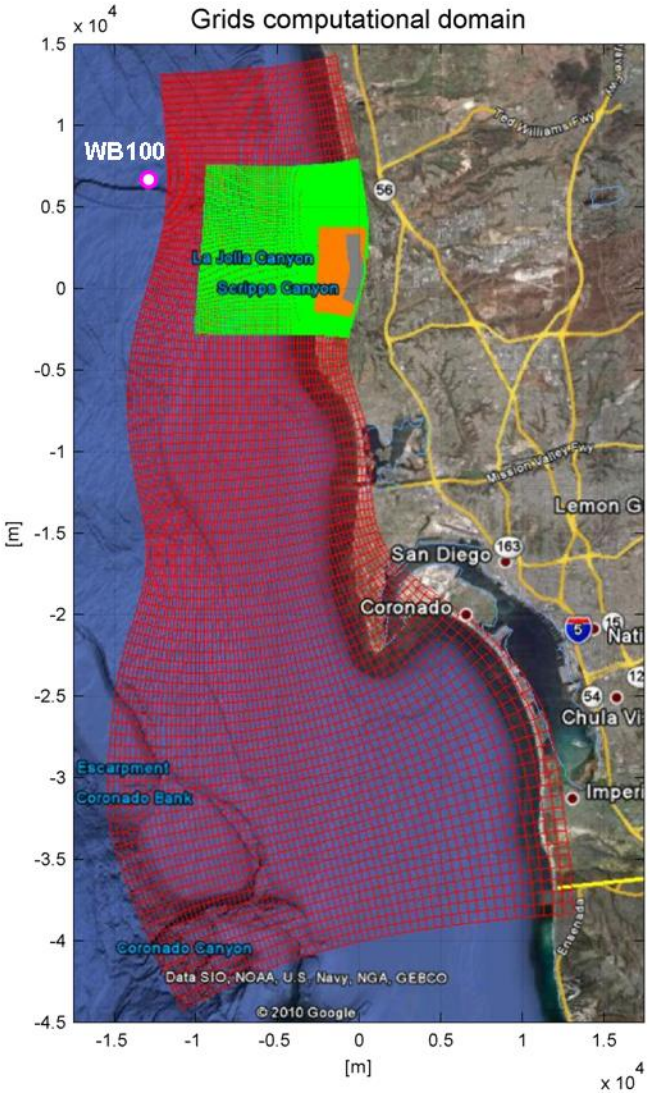

Figure 3.2 Orientation of used grids in Delft3D

The largest grid extends 13km offshore (red highlighted) so that the wave conditions observed by the offshore Torrey Pines wave buoy (WB100) deployed by NOAA can be used (see Chapter 2.3.21). The western offshore boundary of this grid is in 550m water depth. Here, refraction has not influenced the wavefield yet and the conditions can be considered spatially constant along the offshore boundary. The wave conditions along this boundary are considered to be similar to the observations.

To compute realistic wave conditions in the NCEX project site, a relatively large grid was made that extends 14km north and even 45km south from the area of interest. In this way the offshore wave conditions can also be imposed on the lateral boundaries. Constraining the

lateral boundaries with the offshore conditions is physically incorrect, but numerical refraction will rotate wave energy from the lateral boundaries shoreward where it will dissipate. Consequently, a realistic boundary condition develops along the boundary of the intermediate (green highlighted) nested grid. As in some cases swell wave come from the south, the grid has to extend further in southward direction.

The intermediate wave grid covers a domain of about 10x10km over Scripps and La Jolla canyon. This grid uses results from the largest grid to determine its boundary conditions. Finer grid spacing varying from 200x130m to 60x85m is applied to calculate wave propagation over the steep slopes of the canyons.

The smallest wave grid is the most highly resolved of all wave grids. It uses output from the intermediate grid, in which it is nested to form its boundaries. The grid spacing varies from 25x40m offshore to 7x17m along the shore.

Delft3D-Flow

Delft3D-Flow is running with a single grid, which extends about 750m in cross-shore direction and 3.5km in alongshore direction. The grid spacing offshore is about 27x12m decreasing to 5x12m at the shoreline.

The offshore boundary is situated at about 15m water depth. At this depth are rip currents expected to be dampened out. In this way no velocity gradients develops along the boundary, which would cause numerical instabilities.

3.3 Bathymetry

For each grid used in this research an accompanying bathymetry file is created. As the grids get finer spacing towards the zone of interest, the bathymetry is described more accurately. The matching bathymetry for the largest and coarsest wave grid is created with depth soundings of the National Ocean Survey (NOS) in 1932 and in 1972.

The bathymetry for the intermediate wave grid covering the canyon is made with swath sonar data from WHOI in 2001. The canyon was mapped accurately using Swat sonar technology. Since bathymetric changes in deep water (>10m water depth) are expected to be negligible, a single depth file for simulations of different days of the fieldwork is sufficient for the deep parts.

Nearshore and especially in the surfzone, interaction between bathymetry, currents, and waves becomes more important. Therefore, depth soundings were collected weekly. This makes it possible to attach a very accurate bathymetry to the simulation of the nearshore area. Both the smallest wave grid and the flow grid use observations from swath (2001) over the canyon and weekly updated depth soundings in the surfzone.

3.4 Parameter settings

The time step, the boundary conditions and the wave computation mode is described in this paragraph. A complete overview of the remainder model settings used in this study is given in Appendix B.

3.4.1 Flow module

Hydrodynamic time step

A model is set up for two specific days, October 10, 2003 and October 28, 2003, as was described in Chapter 2.3. Both model runs have to spin-up before results can be considered accurate. To allow spin-up time the simulation starts six hours before the day of interest. The length of spin-up time has been determined by trial and error.

The time step of Delft3D-Flow controls both numerical stability and the accuracy of flow results. To determine the time step a Courant number can be calculated which should not exceed a value of ten. However, this value is a rough estimate and can be taken substantially larger. The value of the courant number is calculated with the following equation (Delft3D-Flow manual, 2010):

$$CFL = \frac{\Delta t \sqrt{gh}}{\{\Delta x, \Delta y\}}$$

Where t is the time step [sec], g is acceleration of gravity [m^2/s], h is the water depth [m], and {Δx, Δy} is a characteristic value of grid spacing [m] in either direction.

According to the Delft3D-Flow manual, Courant numbers may be taken substantially larger for small variations in both time and space. If a time step of 3 seconds is applied, the courant number in front of Black's Beach is 6.68. Above the canyon this number increases significantly to even 26.58.

Although, this run seemed to be stable, a time step of just 0.3 seconds was tried as well. This gives Courant number smaller than 10 above the canyon, but flow results did not change noticeable.

For initial simulations Delft3D-Flow performed computations with a time step of 3 seconds, however time steps up to 15 seconds are tested in order to minimize computation time. These runs also still seem to be have good results. Nonetheless, this change did not give a significant decrease of the total simulation time as wave calculations by Delft3D-Wave take most of the time.

Boundary conditions

Three open boundaries are applied at the flow grid. The two lateral boundaries, respectively north and south are specified as Neumann boundaries (Roelvink and Walstra, 2004). The lateral boundaries specify an alongshore water level. The offshore boundary is constrained with a time varying tidal water level.

Measurements of the pressure gauge at the west end of SIO pier are used to determine the water level along the offshore boundary (see Chapter 2.3). This water level elevation is considered spatially uniform, so no gradient in the water level is caused due to tide. For that reason Neumann conditions are prescribed along the lateral boundaries, which are set to zero.

Roller model

The Roller model is an extension of Delft3D-Flow and allows modelling short waves in the Flow domain. This application to the flow model enables an accurate representation of the wave forcing to the nearshore currents. The Roller model delays the energy dissipation,

resulting in a landward shift in the cross-shore profile of alongshore velocity. The boundary conditions for the Roller model are derived from Delft3D-Wave, which imposes the wave height along the boundaries of the Flow domain. Within the Flow domain, the roller model uses the mean wave direction and wave length from Delft3D-Wave.

The Roller model can only be applied in cases where the wave spectrum is narrow-banded both with respect to frequency as with respect to direction. Given these limitations, it is possible to determine a dominant frequency (the mean frequency) and a dominant direction from the wave field information. The mean wave direction field along which wave energy and roller energy are transported is not predicted by the Roller model but used from the Delft3D-Wave module.

3.4.2 Wave module

Coupling interval

For both the October 10 and October 28 simulations, the model is running for 30 hours including 6 hours of spin-up time. Measured wave conditions from the Torrey Pine buoy are used. For this simulation, new wave conditions are computed after each coupling interval of 20 minutes.

The length of the coupling interval of the Flow and Wave modules should not be chosen too large since changes in the water level, and flow field affect the wave conditions and vice versa. To save computation time this interval should be kept as large as possible. However, to achieve more accuracy the interval should be small (van Rijn and Walstra, 2003).

New wave conditions are calculated every 20-minutes. The input parameters the wave model accounts for are:

- Wave spectra along the offshore and lateral boundaries
- Water level from the flow module, which is used and extended into the domain of the wave module
- Wind conditions from the flow module, which is also used and extended into the domain of the wave module

Wave computations in the nearshore do not account for refraction owing to currents. The currents are not taken account for since it caused an imbalance in the flow computations.

Flow computations are performed during the interval of two succeeding wave computations. The input parameter the flow model accounts for are:

- Wave conditions
- Water level (updated every minute)
- Wind

Boundary conditions

The wave model is constraint with 1-dimensional wave spectra files at the northern, eastern, and southern boundary of the largest wave grid. The boundary spectra files contain information of energy, mean direction and spreading per frequency bin. These spectra files are formed using data of the Torrey Pines wave buoy deployed in deep water 11km offshore (observations of this wave buoy are described in 2.3.2.1). This buoy provides spectra every half hour, containing energy, and coefficients of directional Fourier series over frequency bins from 0.025 until 0.58Hz.

The 1-D spectra files use the energy distribution over the frequency bins. Mean direction and spreading for each frequency bin is calculated using the Fourier coefficients. The spectra file of the wave buoy provides four coefficients, respectively A1, B1, A2, and B2, which are described by Kuik et al. [1988]. Kuik et al. [1988] describes how direction and spreading are calculated out of those coefficients. He found that mean direction and spreading calculated with coefficients A2, B2 handle reflected waves much better than the mean direction and spreading calculated with coefficients A1 and B1. As the model is set up covering a coastal region, reflected waves from the beaches have to be taken into account, therefore A2 and B2 are used to define mean direction and spreading in the 1-D boundary file. Hence the equations used are:

Mean direction: $\theta = \arctan(B_2 / A_2) / 2$

Spreading: $\sigma = \sqrt{\left|0.5 - 0.5 * \left(A_2 * \cos(2\theta) + B_2 * \cos(2\theta) \right)\right|}$

The medium size wave grid is nested in the largest wave grid, which defines the wave conditions at the boundary of the intermediate wave grid. The same procedure is valid for the smallest wave grid, which uses results from the intermediate wave grid to define its boundaries

Stationary mode

Wave computations can be performed in either the stationary or the non-stationary mode. Under the stationary assumption, the time component in the action balance equation is not taken into account, implying instantaneous wave propagation throughout the domain.

In the present study, wave computations in Delft3D-Wave are performed in stationary mode. This is done because fairly local information is used from the Torrey Pines wave buoy along all boundaries. In a non-stationary set up, waves coming from the south would be over delayed. Waves coming in from the south start at a wave grid boundary that is relatively far from the NCEX surfzone. E.g. in a bi-directional wave case, the waves from the west would not be delayed as much, while the waves from the south would be.

4 Offshore wave calibration

As described in Chapter 2.3, two specific cases are considered, (1) wind sea on October 10 and (2) swell waves on October 28. This chapter describes the calibration of the wave model by comparing the Delft3D-Wave predictions with the wave buoy records.

Delft3D-Wave calculates the wave propagation from the offshore boundary to the shoreline through the three nested wave grids. As consistency check, wave results from Delft3D-Wave are compared with spectra of the buoy data. The wave comparison is examined as a function of wave propagation direction. Chapter 2.2.2 describes the wave buoys that are deployed north of and close to Scripps canyon (Figure 2.5).

First, the wave conditions at the offshore boundary are validated by comparing model result near the boundary with data from the Torrey Pine wave buoy (WB100 indicated in Figure 3.2). Secondly, data from wave buoy 35 deployed in about 35m water depth 400m north of the canyon is compared with model results.

The significant wave height, mean wave period and mean direction are calculated from the 30-min period spectra to compare with model results throughout the experiment. Spectra plots are shown for moments in time where time-series show a significant difference.

Three calibration steps are considered in this paragraph:

A. Reference case
B. Modification directional bins
C. Inclusion of wind growth

A. Reference case

The reference case for the simulation of the two cases is described in Chapter 3. The settings in this model set up are default settings based on expert judgement to perform a reasonable simulation. However, comparison of the output of this simulation with the observations show deviations to adjust modifies the set up. These modifications are introduced in the succeeding simulations.

B. Modification directional bins

In the second simulation, the accuracy of the wave model has been increased by modifying the directional bins. The width of the directional bins was decreased from 10˚ to 4˚ in this calibration step.

C. Inclusion of wind growth

In the third calibration step, wind has been added to the model. Delft3D-Wave also automatically accounts for quadruplets when wind is added to the model. Quadruplets is wave-wave interactions and distributes energy from the mid to the high frequencies.

4.1 Case 1: Wind sea (Oct 10)

This case simulates the wave conditions of October 10. The wave conditions on this day at the offshore boundary were as follows:

- Significant wave height about 1.5m
- Mean wave period about 8 to 9 seconds
- Mean wave direction: West
- Peak direction: Northwest

4.1.1 Reference case (1A)

Large wave grid (1A)

Figure 4.1 and Figure 4.2 illustrate the significant wave height and mean wave period in the domain of the largest wave grid of reference case 1A. The mean western wave direction at the offshore boundary slightly refracts to shore normal while propagating into shallower areas. Near the headlands 5 and 25km south from SIO, the Figure 4.2 shows yellow areas, representing a local increase of the mean wave period. Wave refraction towards these headlands appears to affect the longer periods more.

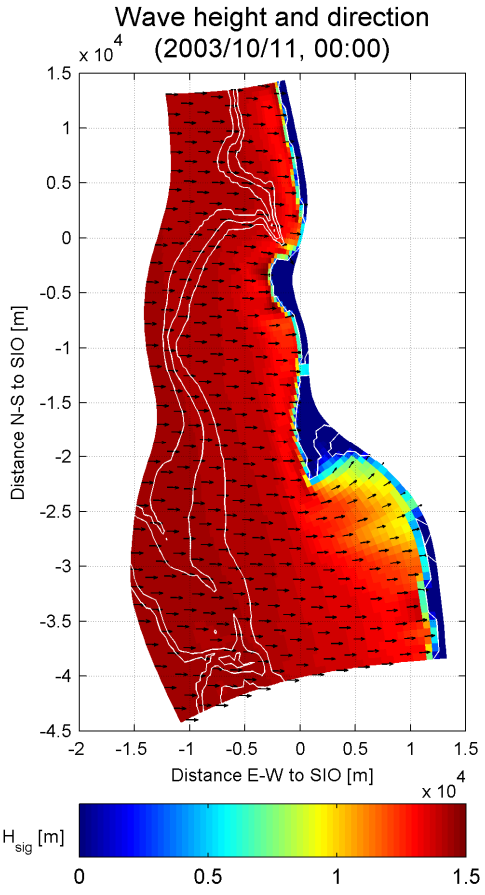

Figure 4.1 H_{sig} and mean wave direction large wave grid

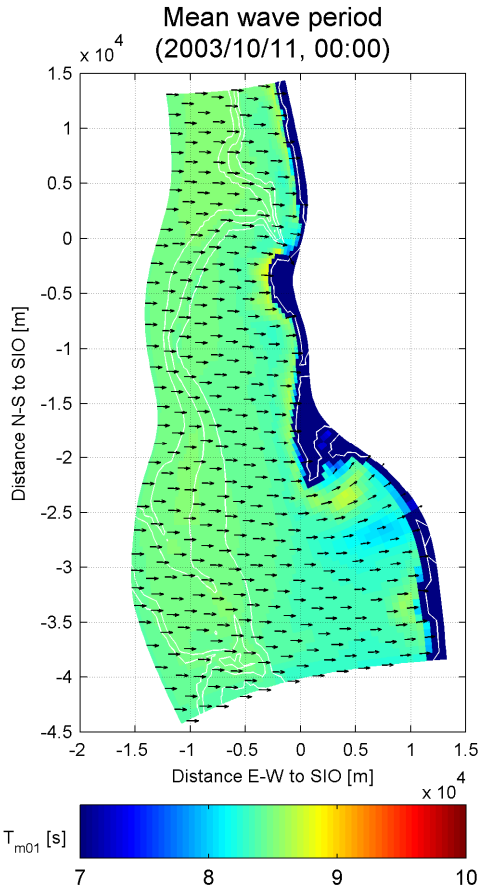

Figure 4.2 T_{m01} and mean wave direction large wave grid

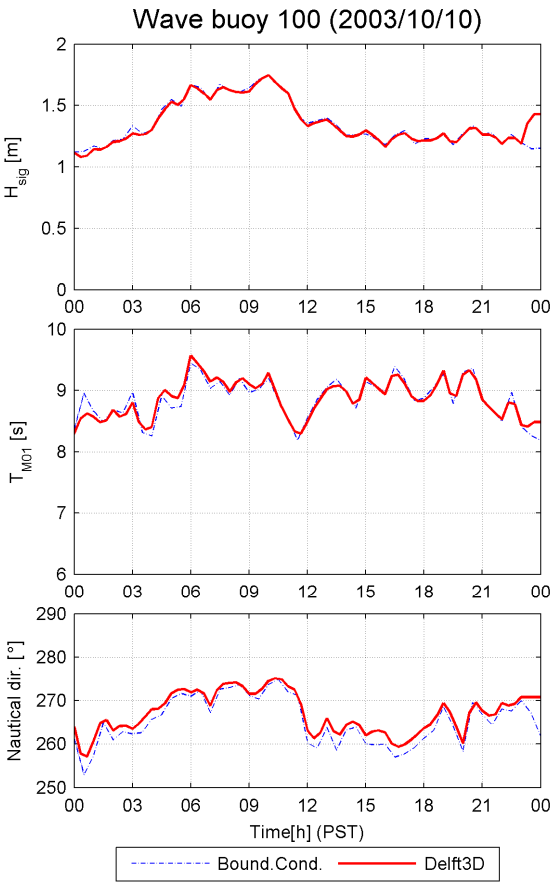

Figure 4.3 H_{sig}, T_{m01} and Nautical dir. of wave buoy 100 (2003/10/10)

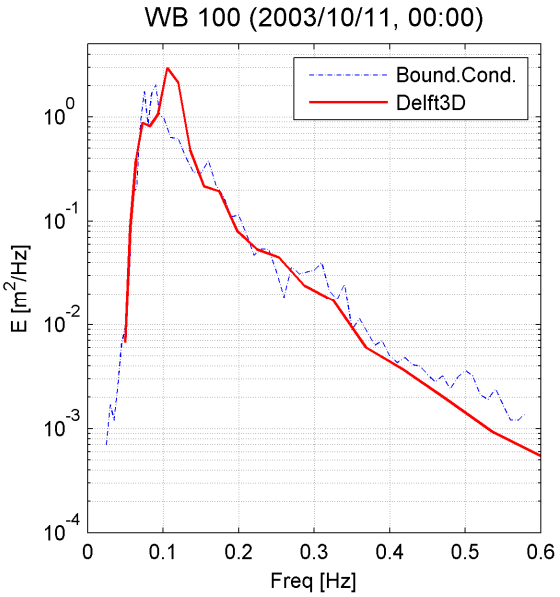

Figure 4.4 Energy spectrum WB100 (2003/10/11, 00:00)

Figure 4.3 represents the comparison of wave conditions just inside the domain of Deflt3D-Wave with time-series for wave buoy 100 (indicated in Figure 3.2). This comparison shows whether the boundary conditions of the wave model are used correctly. Time-series of significant wave height, mean wave period and nautical direction agree reasonably well over the first 23 hours. However, predictions of all three quantities deviate from the observations during the last hour. The significant wave height is overpredicted by about 0.3m, the mean wave period by about 0.5s and the mean direction by almost 10˚.

The observed spectrum of that moment is shown next to the spectrum computed by Delft3D-Wave (Figure 4.4). The figure shows that energy is overestimated between 0.10-0.15Hz (period of 7 to 10 seconds), over which relatively a lot of energy is distributed. Furthermore, the energy over the frequencies between 0.06 and 0.10Hz (period of 10 to 17 seconds) is underestimated.

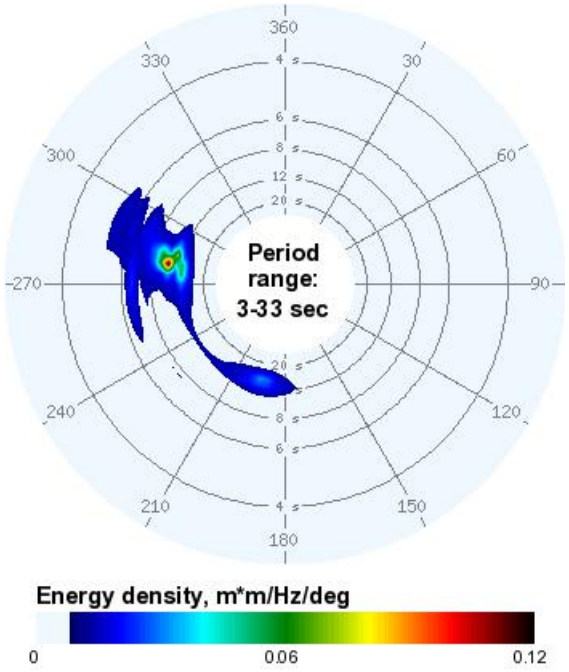

Figure 4.5 2-dimensional energy spectrum WB100 (2003/10/11, 00:00) [http://cdip.ucsd.edu]

The 2-dimensional wave spectrum from the Torrey Pine wave buoy (Figure 4.5) shows a bimodal spectrum at the end of the day. The energy is distributed over two energy peaks. One energy peak has a peak direction of 285˚ relative to north and one energy peak (at relatively lower frequencies) has a peak direction of 190˚ relative to the north. The energy from the south represents swell waves propagating to the NCEX project site from the south.

According to the Delft3D-Wave manual, for swell waves a directional bin width has to be applied of 3˚ to 5˚. However, within the reference case (1A), 10˚ bins were applied. The results of the modification of the bin width is shown in the next calibration step.

Small wave grid (1A)

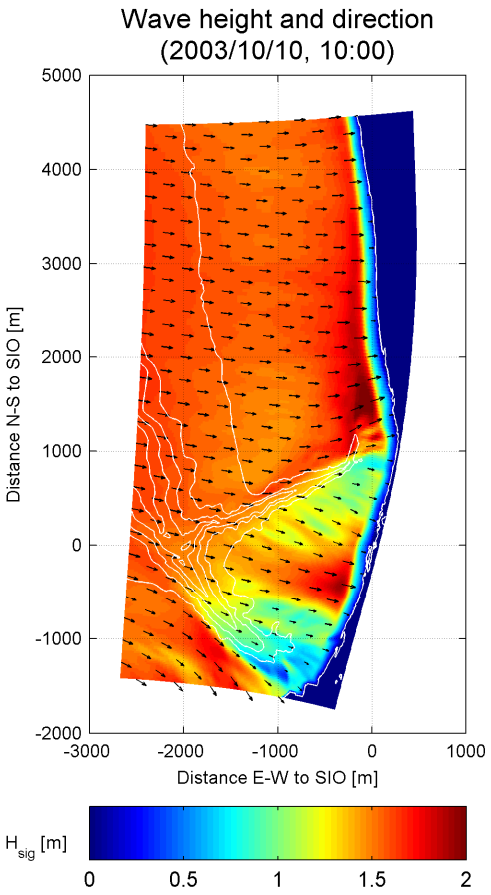

Figure 4.6 H_{sig} and mean wave direction small wave grid

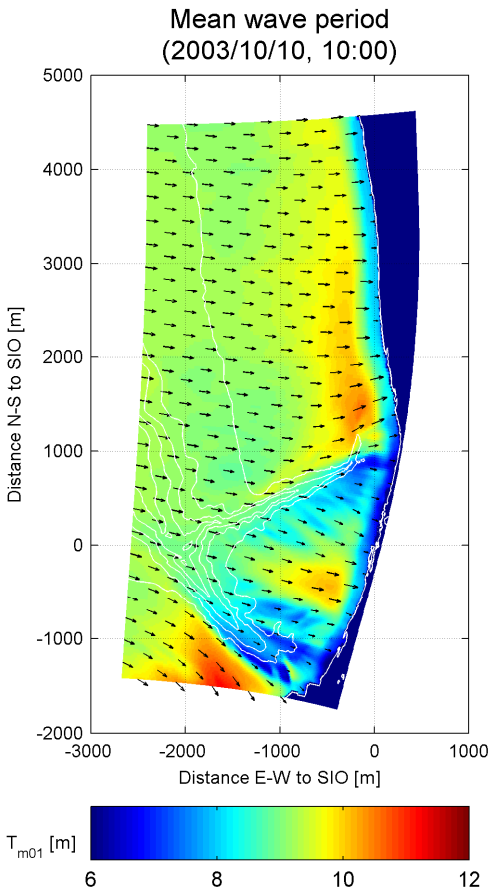

Figure 4.7 T_{m01} and mean wave direction small wave grid

Figure 4.6 and Figure 4.7 illustrate the significant wave height and mean wave period in the domain of the small wave grid. These figures clearly show the refraction over the canyons. The direction of wave propagation rotates away from the canyon, which cause the focussing effect north of the canyon. In addition, at the locations where the wave height is higher, also the wave period is larger. This pattern shows that predominantly wave energy over the lower frequencies refracts.

Time-series comparisons for wave buoy 35 (Figure 4.8) also show deviating predictions during the last hour of the model run. Wave periods are overestimated, with a peak error at 10:00 am of about 1s. The spectra comparison (Figure 4.9) of 10:00 am demonstrates an underprediction of the wave energy over high frequencies (>0.40Hz), which can be the cause of an overpredicted mean wave period.

The reason for this deviation could be that wind was neglected so far. As wind adds energy to the high frequencies, it is added to the model set up in the third calibration step.

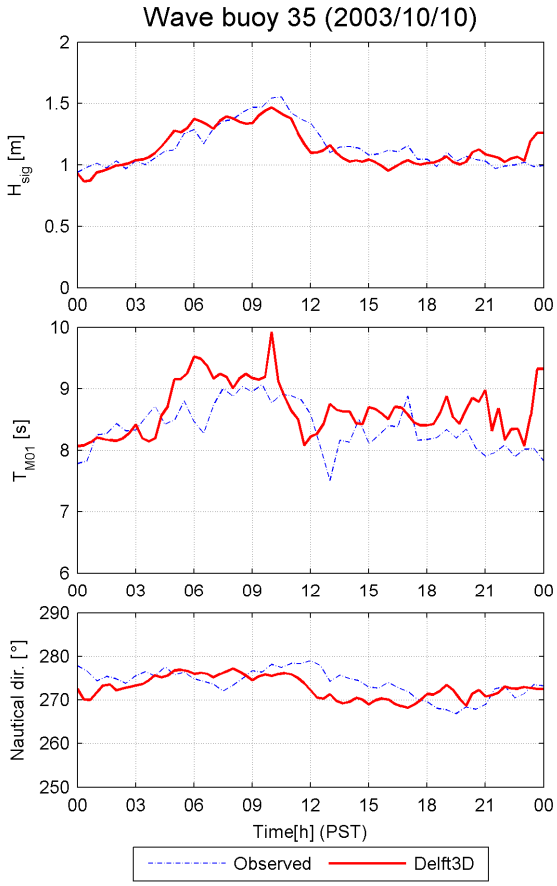

Figure 4.8 H_{sig}, T_{m01} and Nautical dir. of wave buoy 35 (2003/10/10)

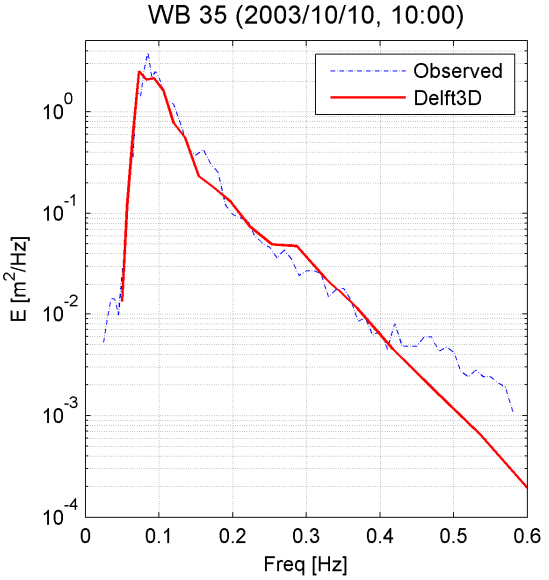

Figure 4.9 Energy spectrum WB35 (2003/10/10, 10:00)

4.1.2 Modification directional bins (1B)

In the initial run, wave conditions were computed using 10˚ directional bins. The 2-dimensional wave spectrum (Figure 4.5) of the Torrey Pine buoy shows for October 10 a broad banded energy distribution. Wind sea waves came from the west and swell waves came from the south. To increase the accuracy of this wave field, the directional bin width has been decreased to 4˚.

Large wave grid (1B)

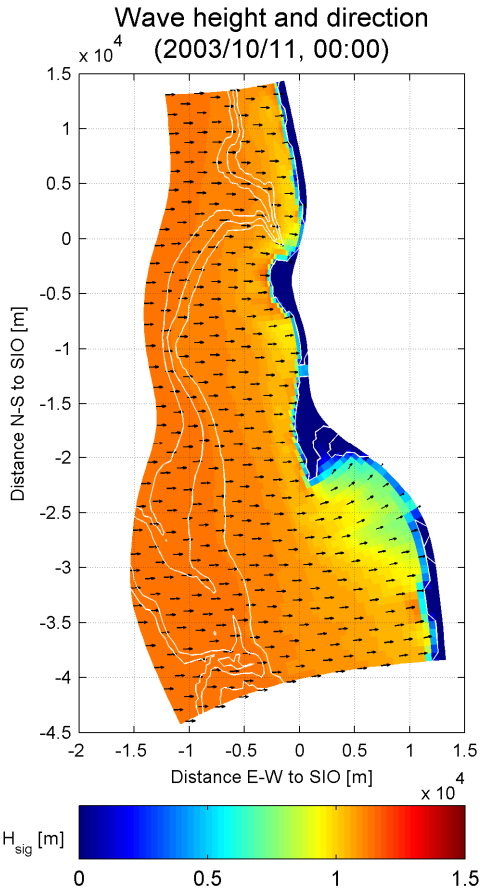

Figure 4.10 H_{sig} and mean wave direction large wave grid

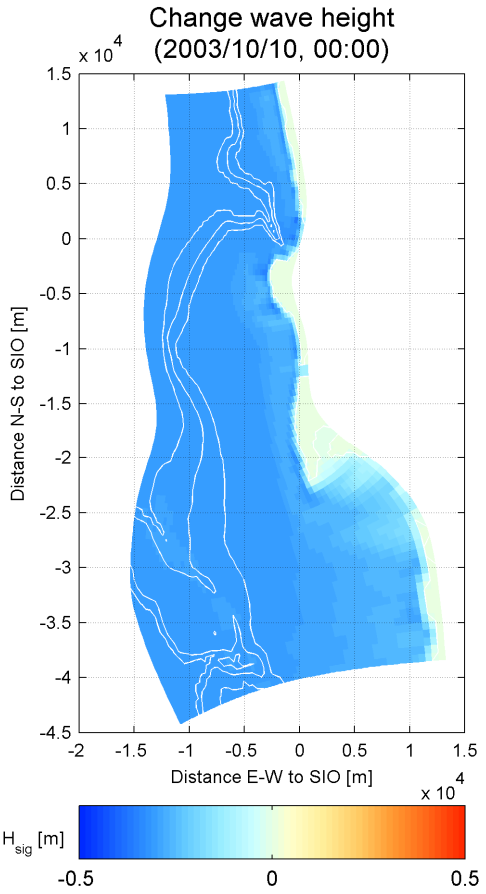

Figure 4.11 Change H_{sig} after modification dir. bins

Figure 4.10 illustrates the significant wave height and mean wave direction in the domain of the largest wave grid after modification of the directional bins (1B). The effect of this modification is represented by Figure 4.11. The significant wave height reduces by about 0.3m over the whole domain.

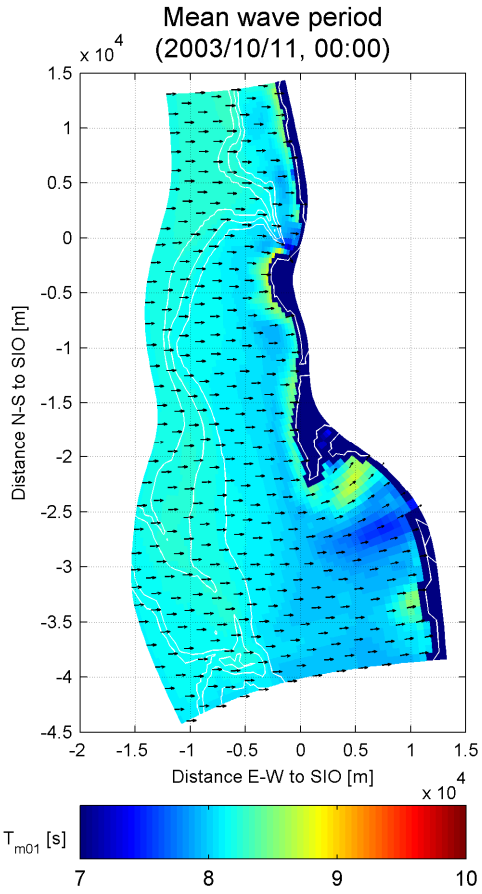

Figure 4.12 T_{m01} and mean wave direction large wave grid

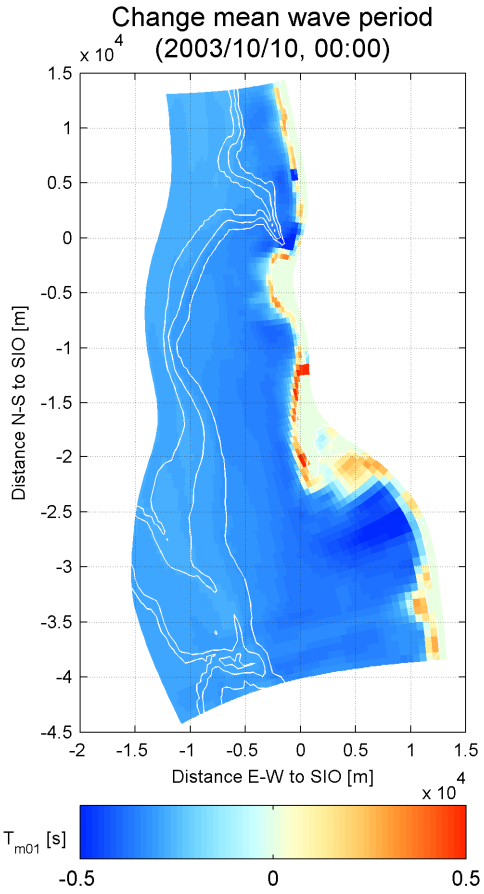

Figure 4.13 Change T_{m01} after modification dir. bins

Figure 4.12 shows the mean wave period and mean wave direction after modification of the directional bins. The effect of the modification of the directional bins on the mean wave period compared to the reference case (1A) is shown in Figure 4.13. The comparison shows a reduction of the mean wave period 0.3 to 0.5 seconds.

As Delft3D-Wave is better capable to simulate the swell waves with the 4˚ directional bins, are the long southern swell waves better accounted for. Possibly this setting causes the reduction of both the significant wave height and the mean wave period.

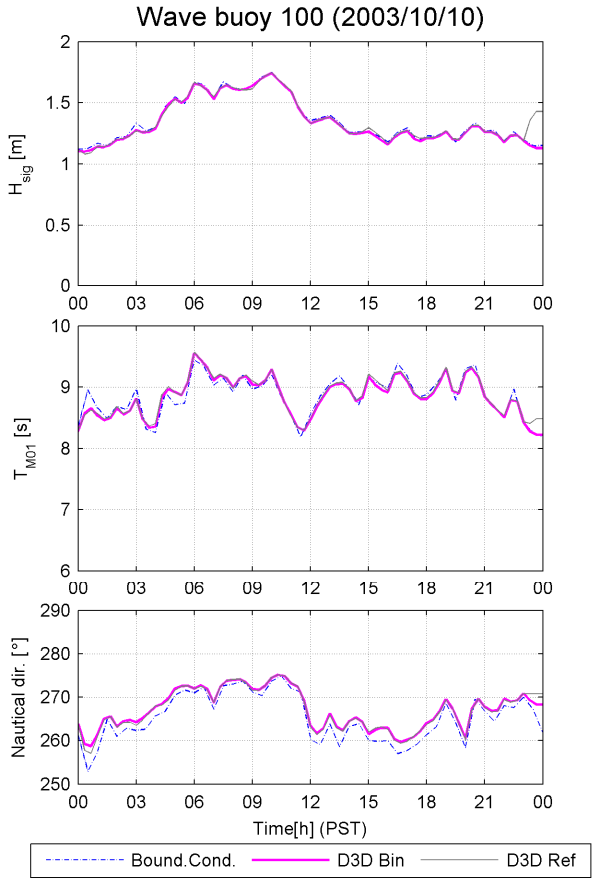

Figure 4.14 H_{sig}, T_{m01} and Nautical dir. of wave buoy 100 (2003/10/10)

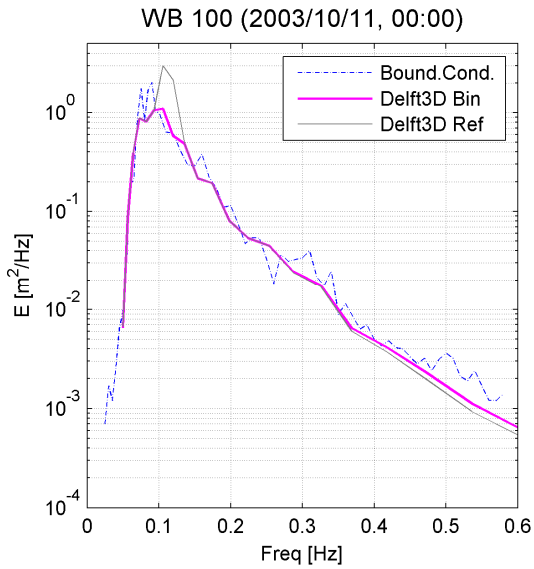

Figure 4.15 Energy spectrum WB100 (2003/10/11, 00:00)

Figure 4.14 demonstrates that modifying the directional bins to 4˚ bandwidth eliminates the overprediction of significant wave height and mean wave period during the last hour. However, mean wave direction is still slightly overpredicted during the last hour.

Figure 4.15 shows that the overprediction of energy between 0.1 and 0.15Hz is eliminated. Apparently, the model is better able to simulate the low frequencies when it is set up with a narrow directional bin of 4˚.

Small wave grid (1B)

The significant wave height in the small nested domain for high resolution bins is represented by Figure 4.16. At this moment in time, the model gave good predictions for the significant wave height in the reference case (1A). However, looking at the differences of this run (1B) relative to the reference case small changes in significant wave height are shown (Figure 4.17), which is caused by small differences in the wave propagation direction. The small changes of wave propagation direction result in spatially alternating behaviour of slightly increased and reduced wave height. The model appears to account the effects of the bathymetry more accurate, resulting in small differences of the significant wave height.

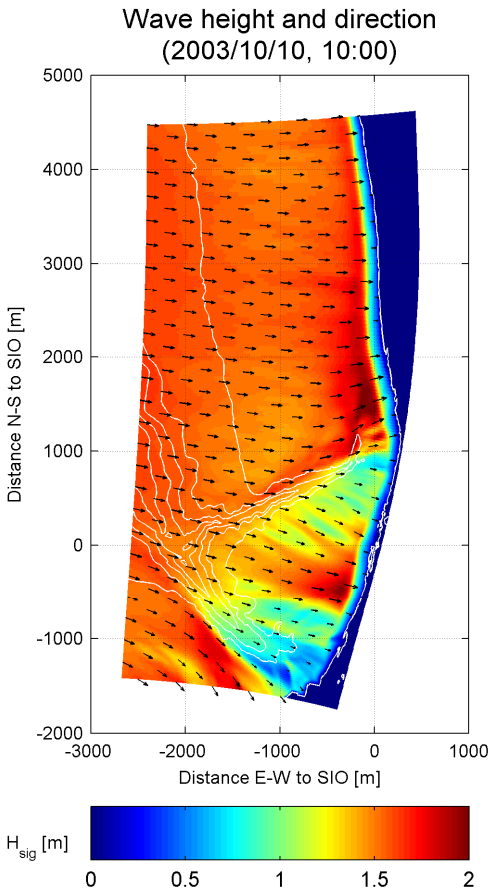

Figure 4.16 H_{sig} and mean wave direction small wave grid

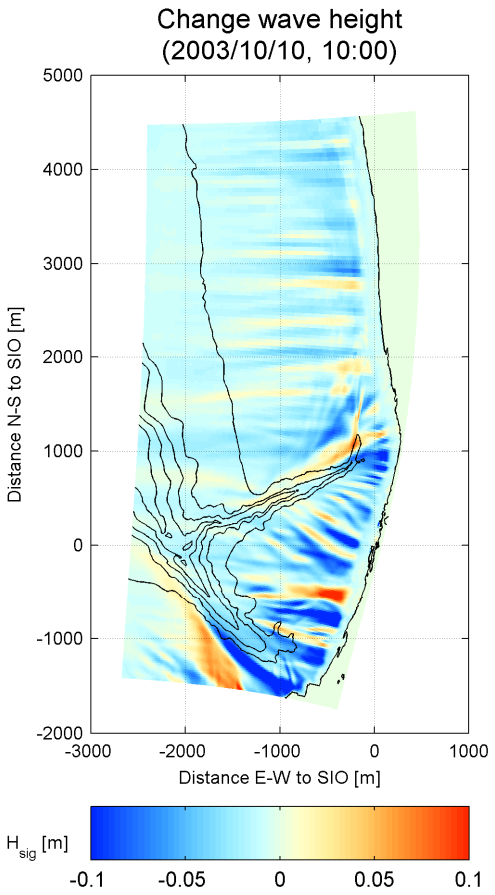

Figure 4.17 Change H_{sig} after modification dir. bins

Figure 4.18 and Figure 4.19 show the mean wave period and the change within the small nested wave grid at 10:00 am. The mean wave period north of the canyon is longer, than onshore of the canyon as in the reference case (1A). The change of the mean wave period after increasing the resolution of the bin width shows that the longer mean wave periods north of the canyon become even longer and the periods onshore of the canyon reduce. This feature implicates that the low frequency waves refract stronger relative to the reference case.

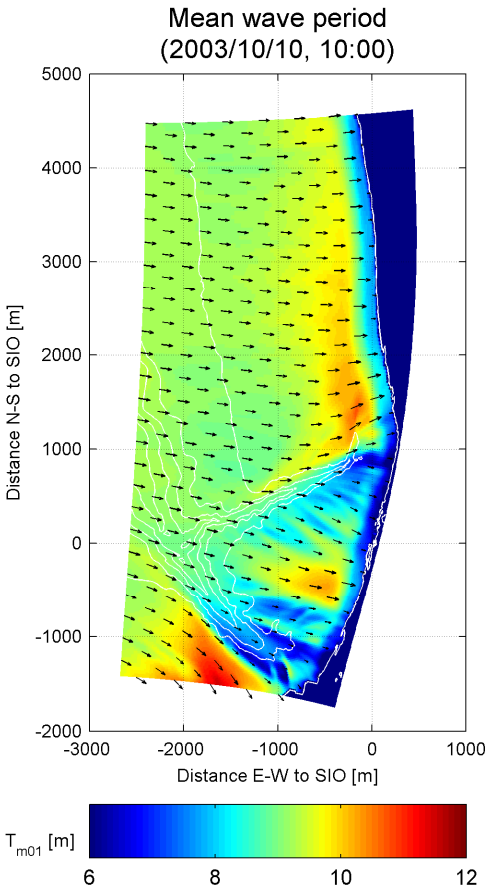

Figure 4.18 T_{m01} and mean wave direction small wave grid

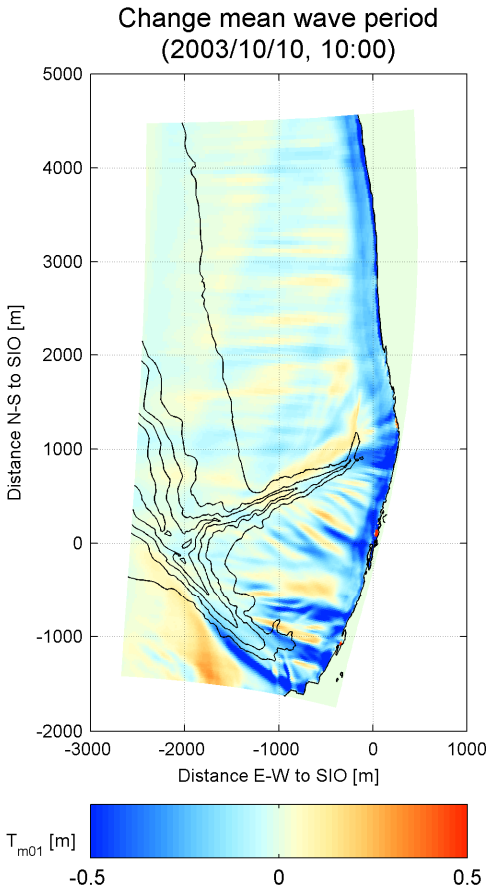

Figure 4.19 Change T_{m01} after modification dir. bins

Time-series of wave buoy 35 show that also in this second model run (1B) the mean wave period is overpredicted. The spectra comparison at 10:00 am (Figure 4.21) clearly shows an underprediction of the energy over the high frequencies, which possibly indicates the omission of wind energy.

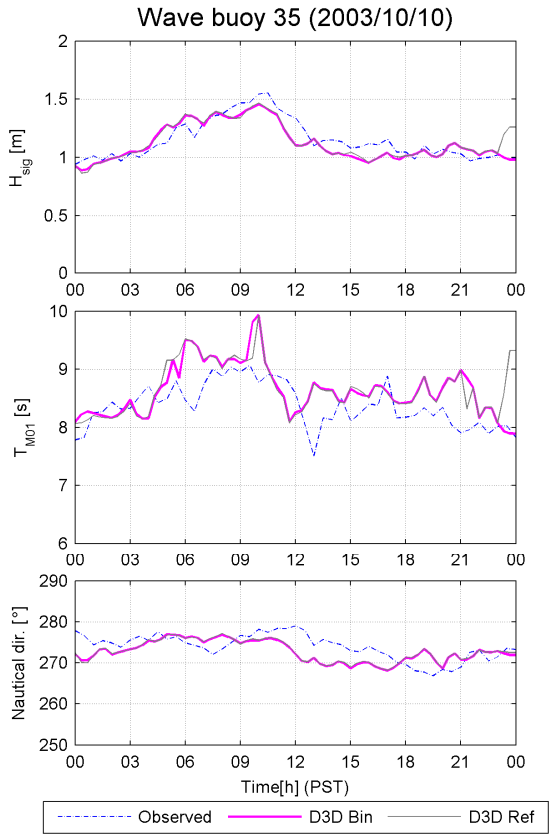

Figure 4.20 H_{sig}, T_{m01} and Nautical dir. of wave buoy 35 (2003/10/10)

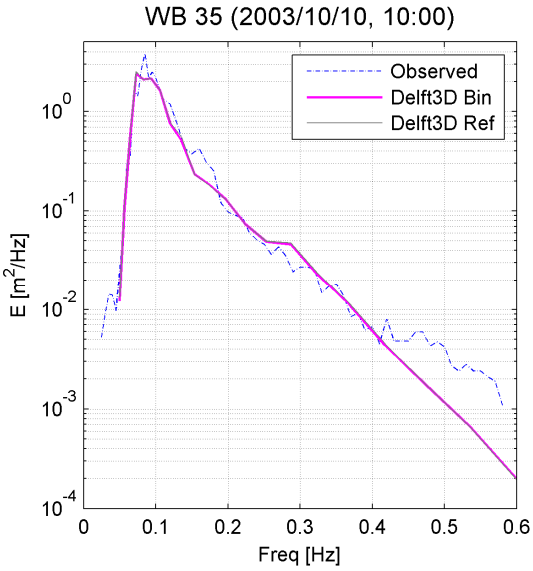

Figure 4.21 Energy spectrum WB35 (2003/10/10, 10:00)

4.1.3 Inclusion of wind growth (1C)

In the third calibration step, the physical factor wind has been added to the model. Hourly averages of wind velocity and directions are used from observations at the west end of the SIO pier. The wind is considered uniform over the computational domain and is linearly interpolated from hour to hour. In addition, the model automatically accounts for the presence of quadruplets when wind is added.

Large wave grid (1C)

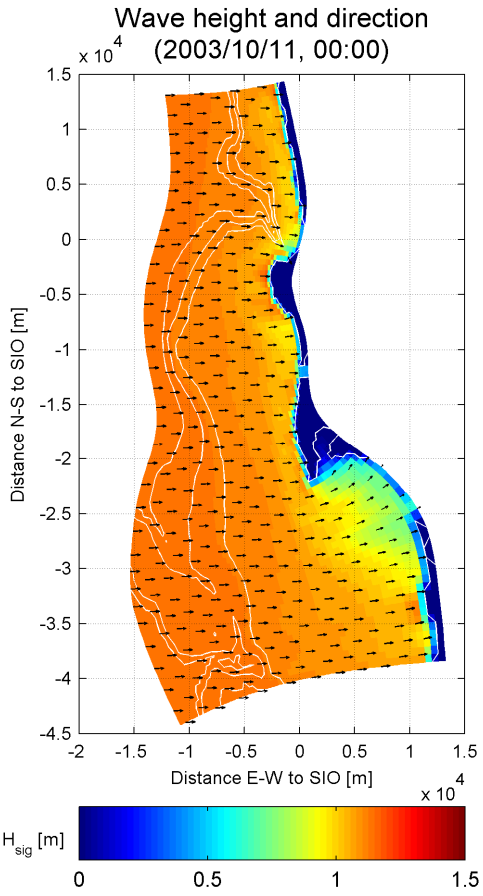

Figure 4.22 H_{sig} and mean wave direction large wave grid

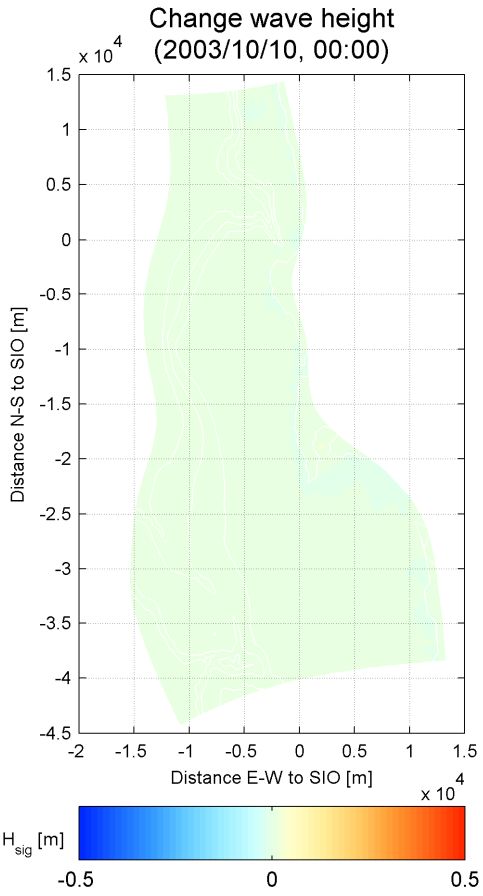

Figure 4.23 Change H_{sig} after inclusion of wind growth

Figure 4.22 represents the wave height over the large wave grid. Figure 4.23 shows that no significant change develops in the model predictions after inclusion of wind. This hardly noticeable change is expected for this moment in the day as the wind velocity was just 0.5m/s.

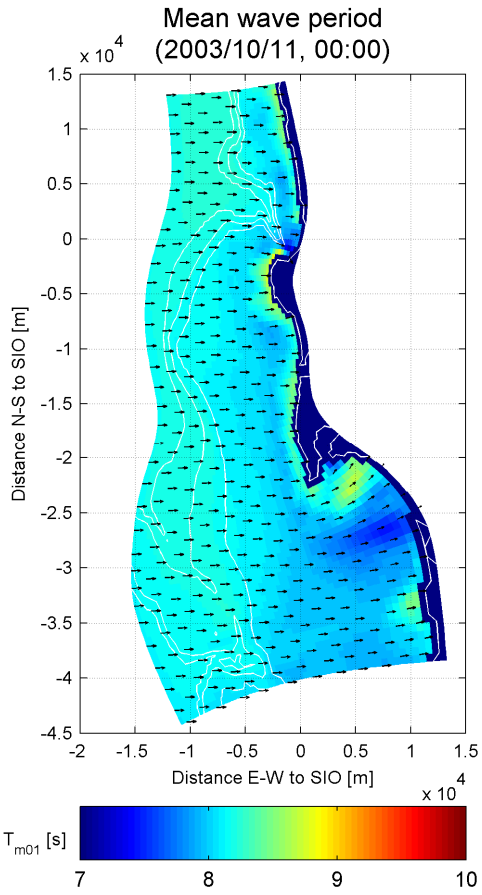

Figure 4.24 T_{m01} and mean wave direction large wave grid

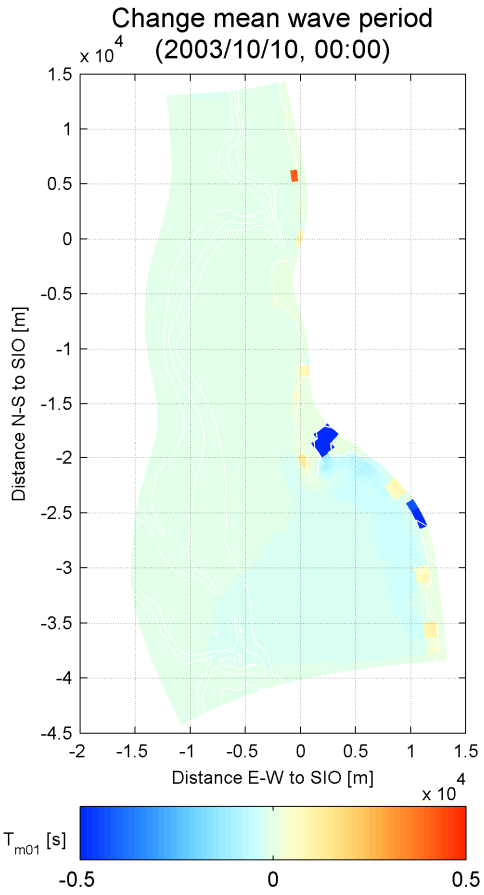

Figure 4.25 Change T_{m01} after inclusion of wind growth

Also the mean wave period is relatively unaffected after adding wind to the model (Figure 4.24 and Figure 4.25).

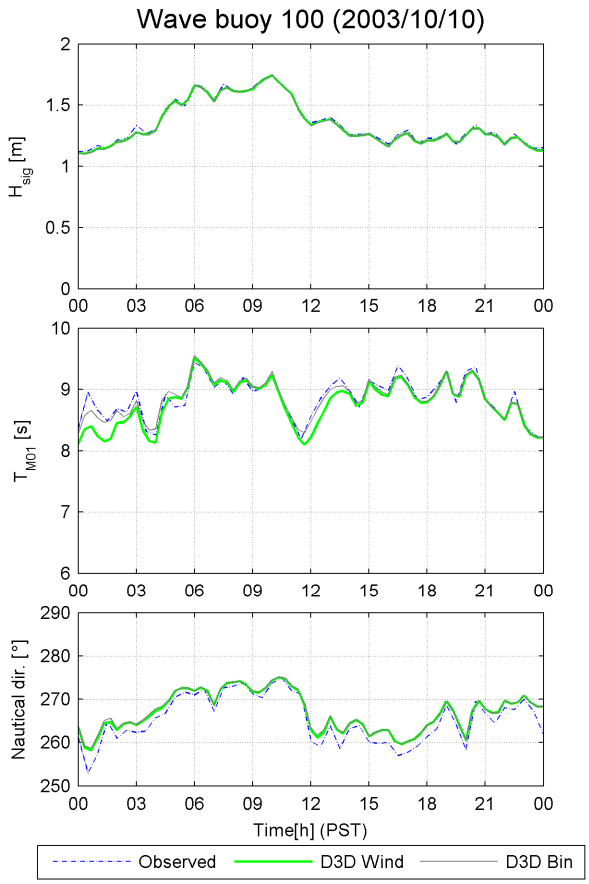

Figure 4.26 H_{sig}, T_{m01} and Nautical dir. of wave buoy 100 (2003/10/10)

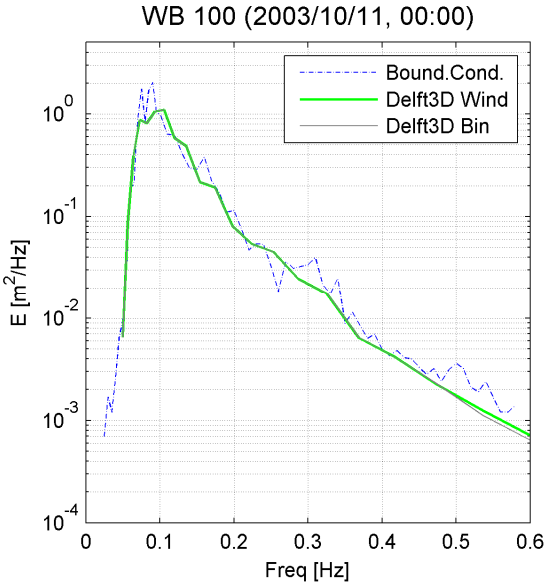

Figure 4.27 Energy spectrum WB100 (2003/10/11, 00:00)

The time-series comparisons (Figure 4.26) show a slight underprediction of the mean wave period at the offshore boundary between 00:00 and 03:00 am. During this period, mean wind velocities up to 3m/s and gusts of wind up to 6m/s were observed.

The underprediction of the mean wave period is expected since the model runs in stationary mode. The model calculates a fully developed sea state for the given wind conditions. However, in the model this observation point lies right next to the offshore boundary, which in reality would correspond to a small fetch length. No fully developed sea state could have developed and no significant influence on the mean wave period would be noticeable.

Small wave grid (1C)

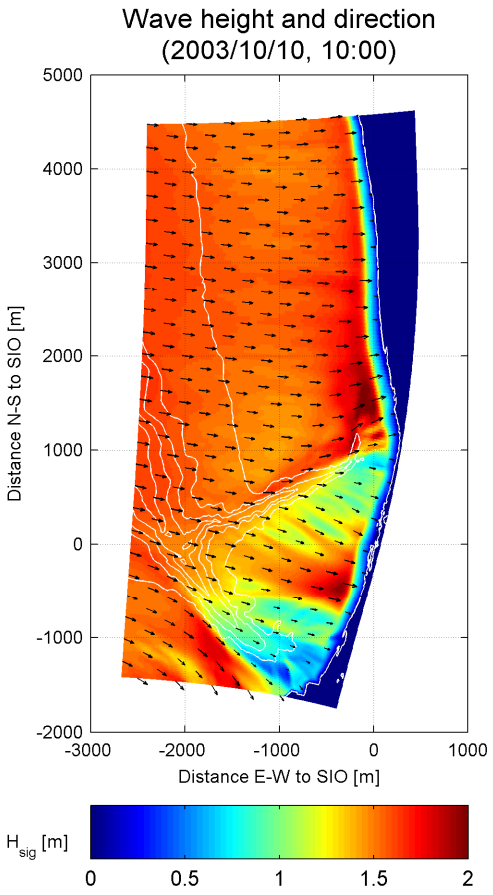

Figure 4.28 H_{sig} and mean wave direction small wave grid

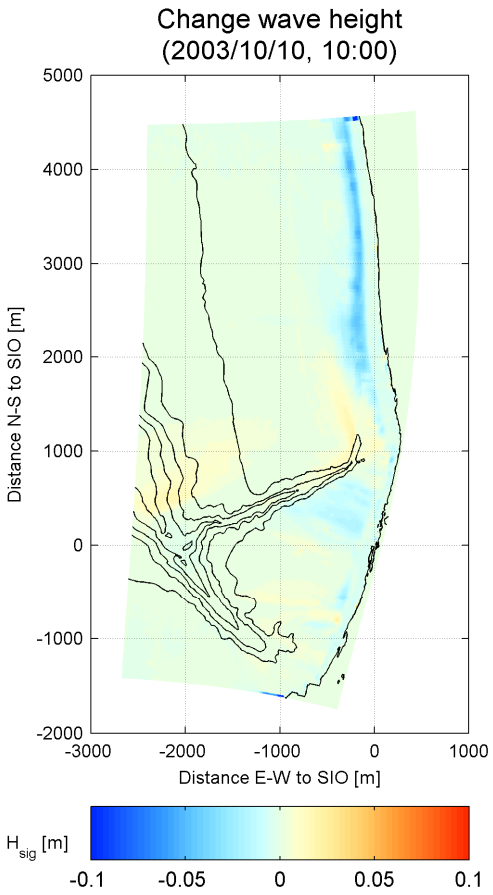

Figure 4.29 Change H_{sig} after inclusion of wind growth

Figure 4.28 and Figure 4.29 show the influence of the wind on the significant wave height at 10:00 am within the domain of the small wave grid. As the wind velocity was only 0.5m/s the change of the significant wave height only changes a few centimetres.

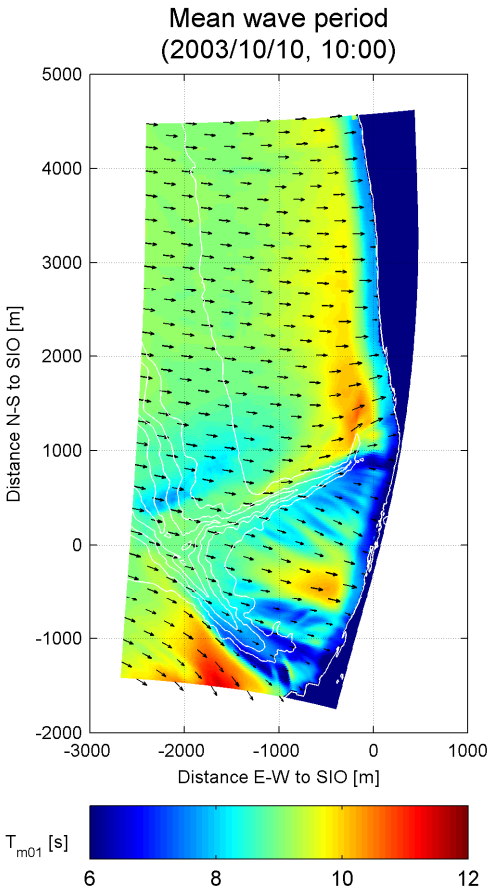

Figure 4.30 T_{m01} and mean wave direction small wave grid

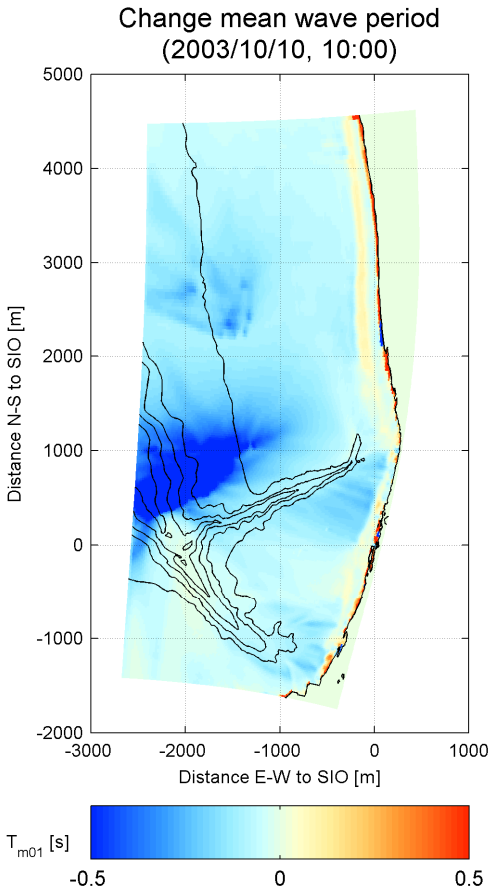

Figure 4.31 Change T_{m01} after inclusion of wind growth

The wave model shows a slight reduction of the mean wave period offshore after adding wind (Figure 4.31). The decrease of mean wave period is irregular distributed over the project site. Offshore locally the mean wave period decreases by a second.

Along the coast North of the canyon (1000m to SIO), the reduction of the mean wave period is smaller than onshore of the canyon (0m to SIO). The slightly larger reduction of the mean wave period onshore of the canyon is caused by the growth of the short high frequency waves. The high frequency waves generated by wind cross the canyon easier than the energy distributed over low frequency waves.

The offshore area where the period reduced up to 0.5 seconds is possibly caused by influence of the bathymetry. As described in Figure 4.2 low frequency waves refract towards the headland South of the NCEX project site. Therefore, the wave energy west of the NCEX project site exist out of relatively higher frequency waves. At 10:00 hours, a wind was blowing of 4m/s which created high frequency wind waves. The wind waves propagated regardless of the bathymetry, while wave energy distributed over low frequencies refracted over the shelves north and south of the canyons. Resulting in a locally relatively larger reduction of the mean wave period.

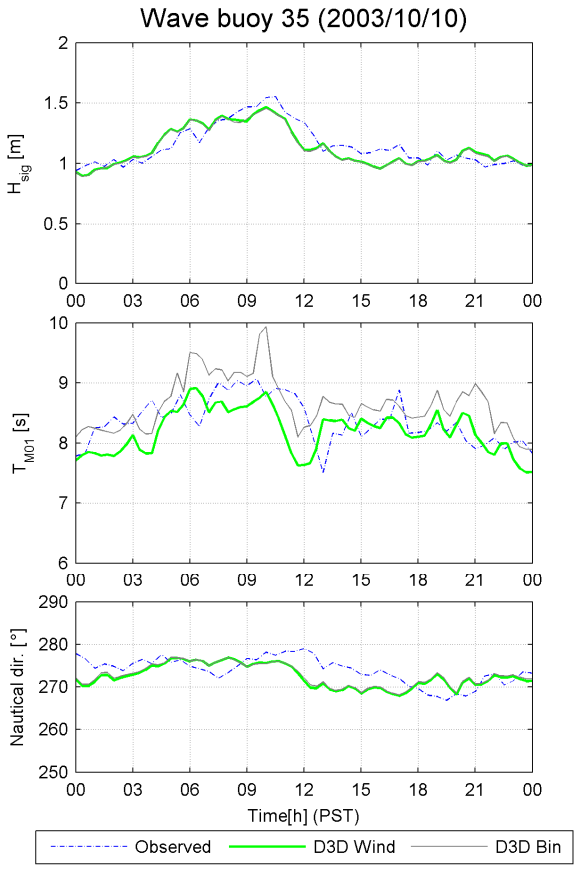

Figure 4.32 H_{sig}, T_{m01} and Nautical dir. of wave buoy 35 (2003/10/10)

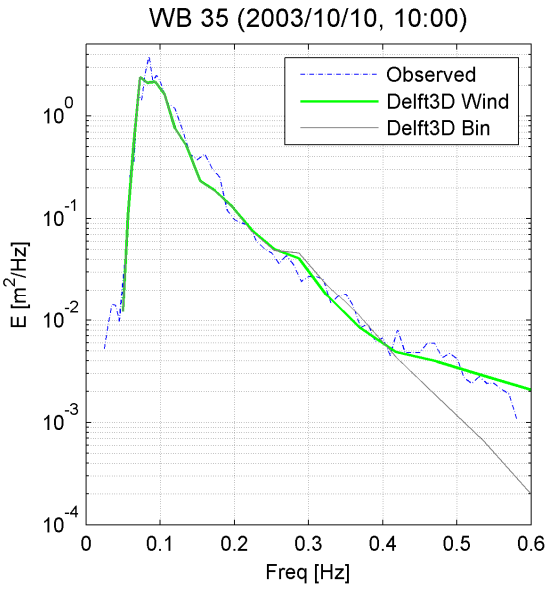

Figure 4.33 Energy spectrum WB35 (2003/10/10, 10:00)

The time-series for wave buoy 35 (Figure 4.32) demonstrate that the mean wave period is no longer consistently underpredicted. In addition, the spectra comparison shows better agreement at the frequencies larger than 0.40Hz (Figure 4.33).

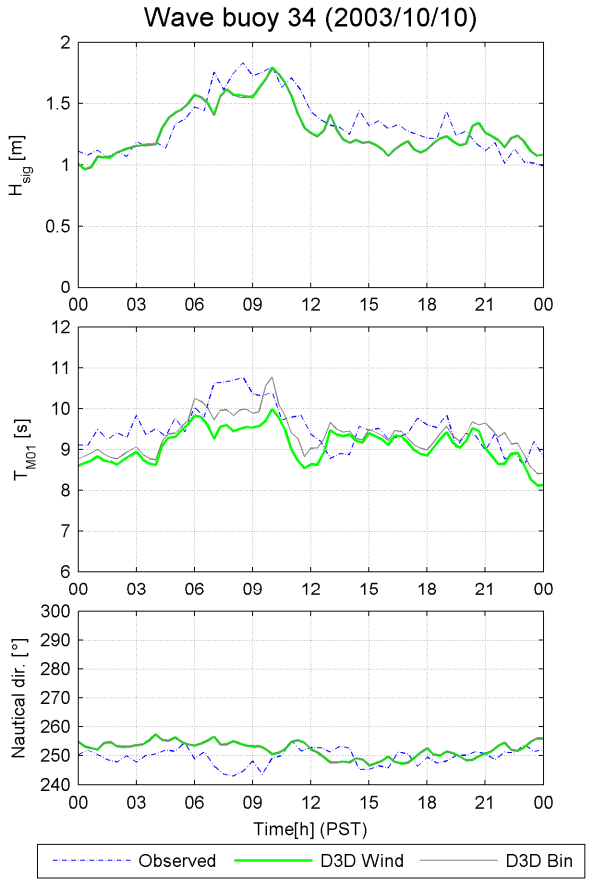

Figure 4.34 H_{sig}, T_{m01} and Nautical dir. of wave buoy 34 (2003/10/10)

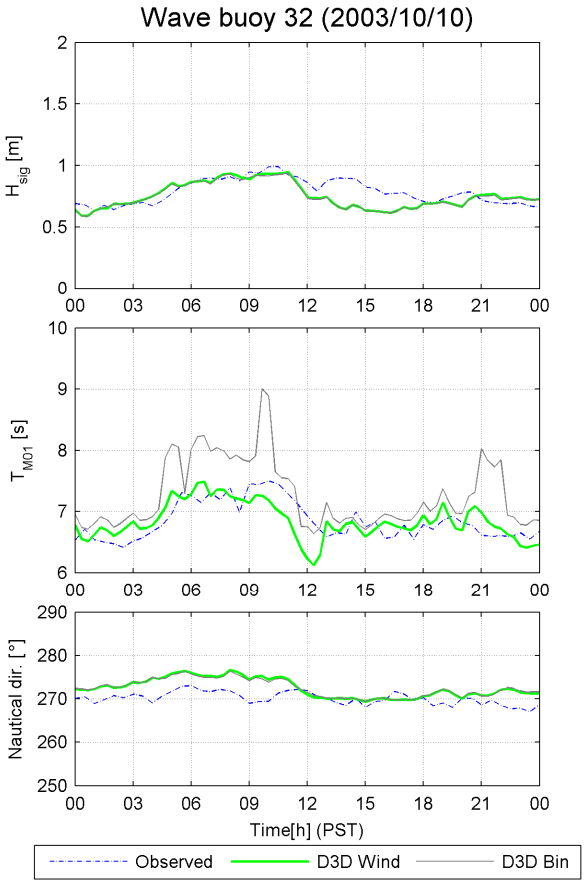

Figure 4.35 H_{sig}, T_{m01} and Nautical dir. of wave buoy 32 (2003/10/10)

The effect of the submarine canyon on the waves is represented by Figure 4.34 and Figure 4.35. Time-series for wave buoy 34 deployed north of the canyon (Figure 2.5) are depicted next to the time-series of wave buoy 32 deployed onshore of the canyon. The significant wave height onshore of the canyon is substantially smaller and has a smaller mean wave period than those alongshore of the canyon. Furthermore, do time-series of the mean wave period of wave buoy 32 show a larger improvement than time-series of wave buoy 34. The relative larger improvement is of wave buoy 32 can be addressed to the fact that relatively a larger amount of wave energy onshore of the canyon is distributed over high frequencies.

4.2 Case 2: Swell (Oct 28)

The second case simulates the wave conditions on October 28. The wave conditions on this day at the offshore boundary were as follows:

- Significant wave height about 0.8m
- Mean wave period about 12-14 sec.
- Mean wave direction: southwest
- Peak direction south-southwest

4.2.1 Reference case (2A)

Large wave grid (2A)

Figure 4.36 and Figure 4.37 illustrate the significant wave height and mean wave period in the domain of the largest wave grid of the reference case (2A) on October 28 at 21:00. The vectors show the refraction of the waves. At the southern and offshore boundary, the mean wave direction is southwest. In shallower areas near the shore, the waves rotated to the west.

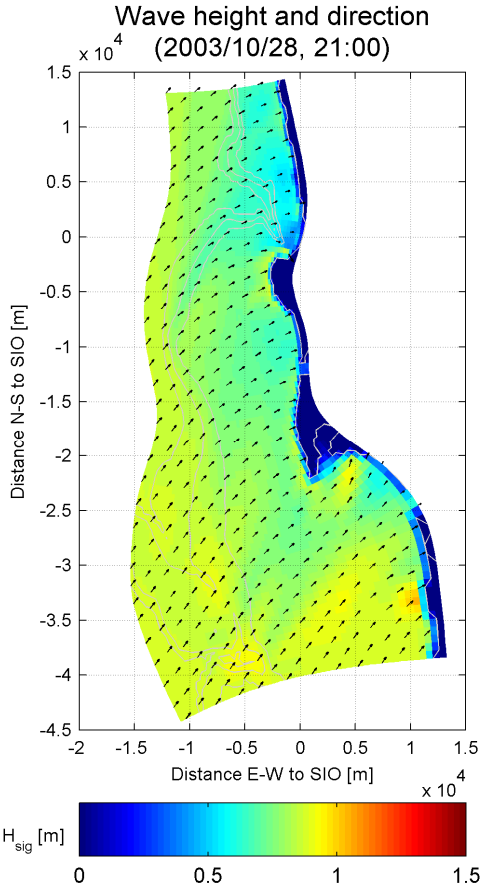

Figure 4.36 H_{sig} and mean wave direction large wave grid

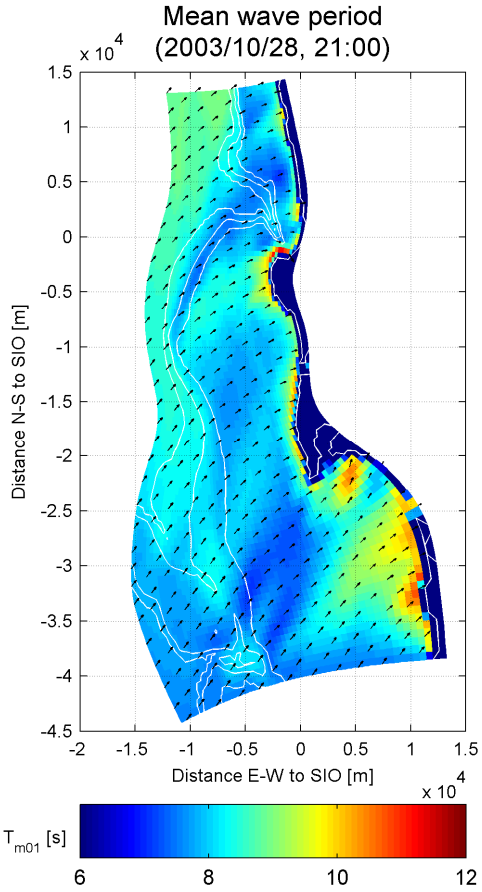

Figure 4.37 T_{m01} and mean wave direction large wave grid

In Section 3.2 was explained that the large wave grid extended far to the south to create realistic wave conditions close to the NCEX project site in case of southern swell waves. In Figure 4.37 is the effect of the extension visible along the coastal boundary between 25 and 45km south of SIO. The imposed wave conditions along the southern boundary refract towards this part of the coast creating relatively long period waves, which in reality will not be there. However, this refraction creates realistic wave conditions near the area of interest.

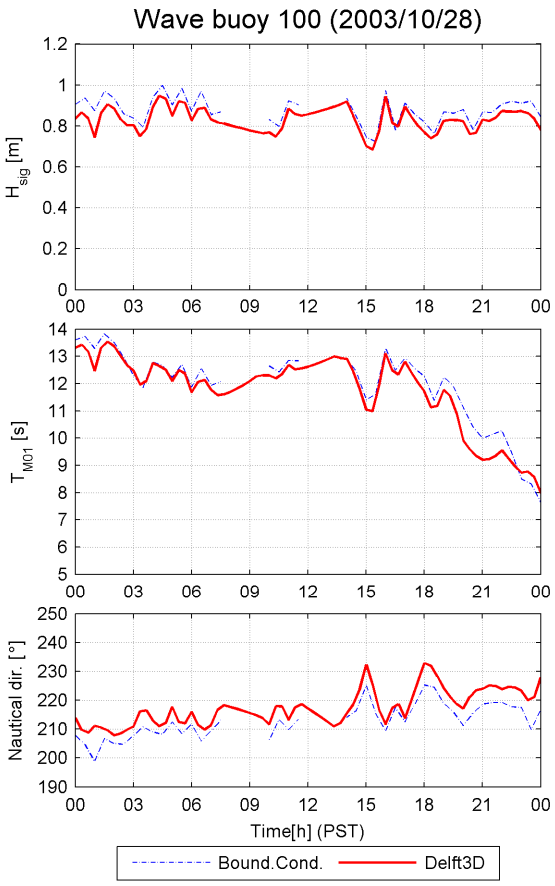

Figure 4.38 H_{sig}, T_{m01} and Nautical dir. of wave buoy 100 (2003/10/10)

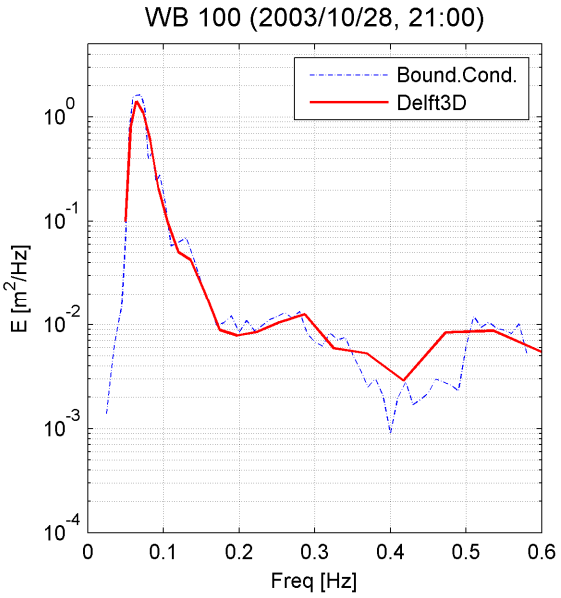

Figure 4.39 Energy spectrum WB100 (2003/10/28, 21:00)

The boundary conditions are shown in Figure 4.38. The time-series shows two gaps in the wave buoy observations, respectively between 08:00 and 09:30 am and between 12:00 and 14:00 am. The straight red lines in the time series over these periods occur because the model interpolates over these periods.

Time-series of both significant wave height and mean wave period show a slight underprediction throughout the day, while the mean wave direction is slightly overpredicted.

Small wave grid (2A)

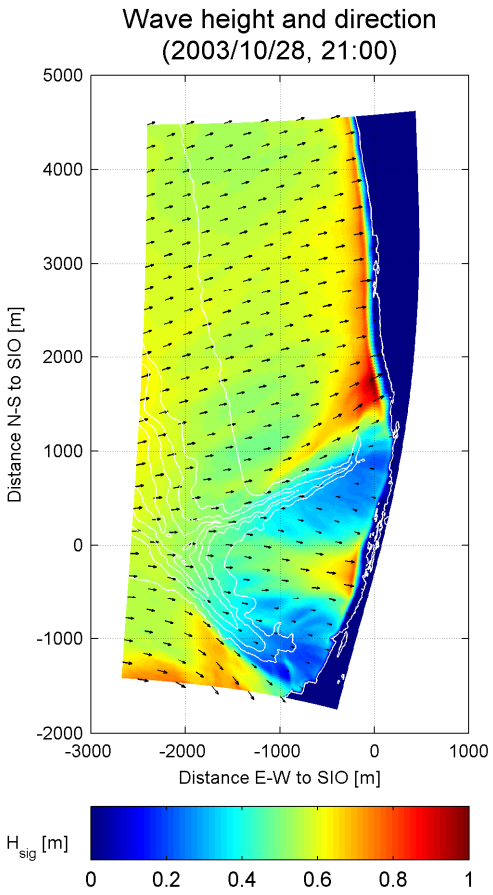

Figure 4.40 H_{sig} and mean wave direction small wave grid

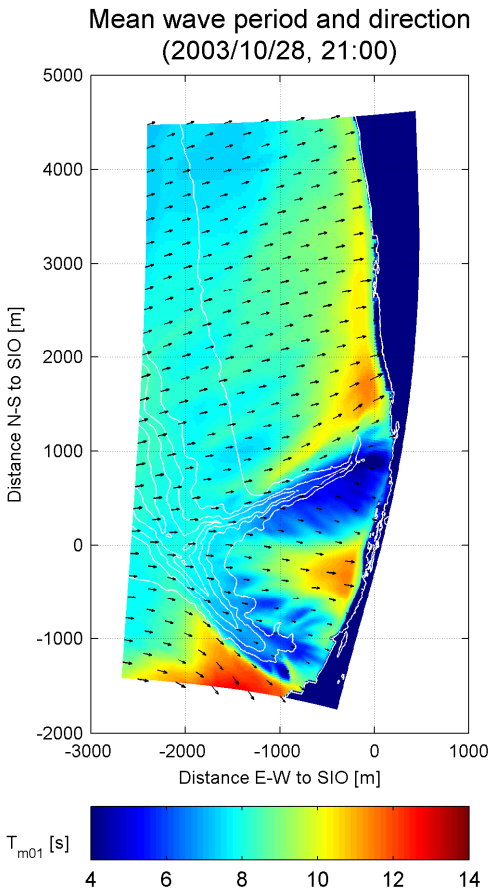

Figure 4.41 T_{m01} and mean wave direction small wave grid

Figure 4.40 and Figure 4.41 illustrate the significant wave height and mean wave period in the domain of the small wave grid. The vectors show that the mean wave direction at the offshore boundary (100m water depth) is from the southwest. These figures show the refraction over the canyons, the alongshore gradients in wave height and wave period in more detail than the large wave grid.

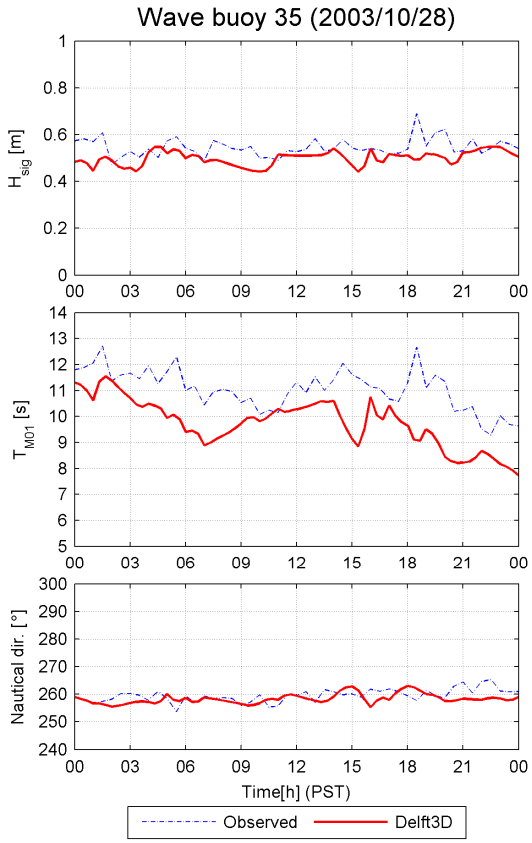

Figure 4.42 H_{sig}, T_{m01} and Nautical dir. of wave buoy 35 (2003/10/28)

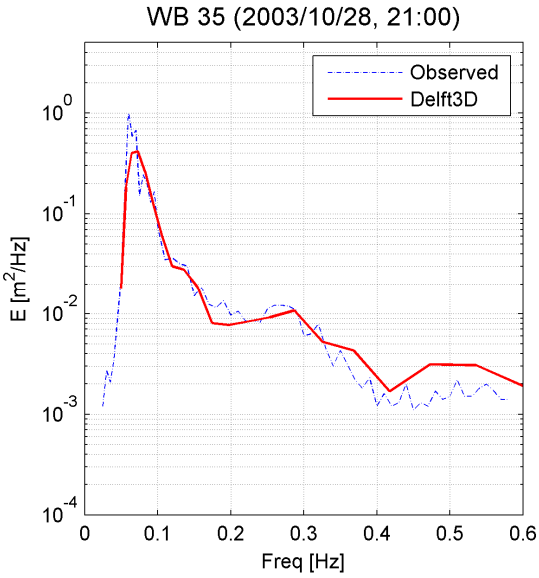

Figure 4.43 Energy spectrum WB35 (2003/10/28, 21:00)

Comparisons of model predictions with wave buoy 35 (Figure 4.42) show a constant underprediction of the period. The spectra comparison at 21:00 hours (Figure 4.43) shows that the energy is underpredicted over the lower frequencies and overpredicted over the higher frequencies.

4.2.2 Modification directional bins (2B)

In the initial run (2A), wave conditions were computed using 10˚ directional bins. 2-dimensional wave spectra of the Torrey Pine buoy show narrow banded swell wave spectra from the southwest on October 28. Following the Delft3D wave manual the resolution of the directional bins is set to 4˚.

Large wave grid (2B)

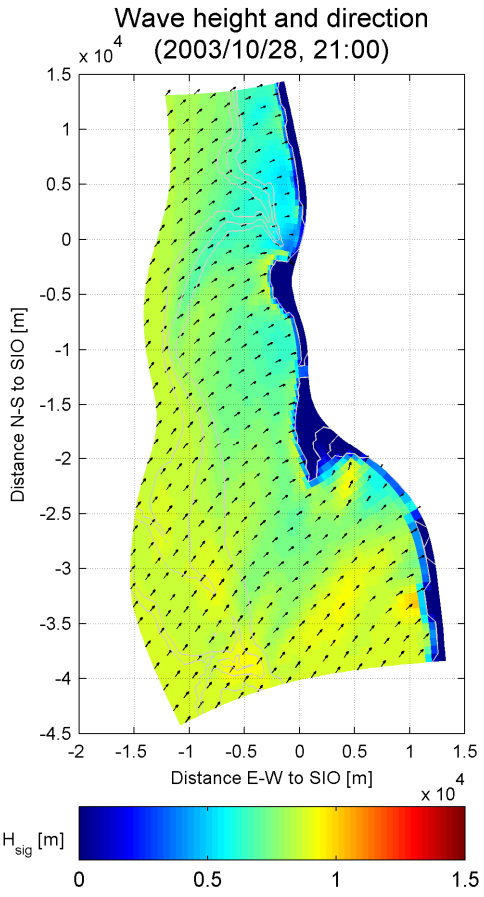

Figure 4.44 H_{sig} and mean wave direction large wave grid

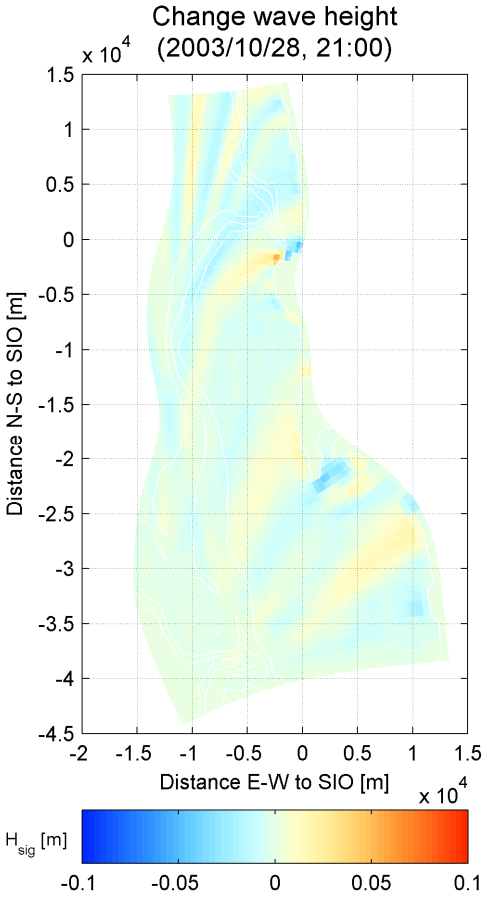

Figure 4.45 Change H_{sig} after modification dir. bins

Adjusting the directional bins to 4˚ has only small influences on the significant wave height. Figure 4.44 illustrates on first sight the same wave patterns as Figure 4.36 of model run 2A. The differences in wave height (indicated in Figure 4.45) appear to be just a few centimetres. The pattern of the differences shows gradual curves to the shore of slightly increasing and slightly decreasing wave height, implying that only a part of the energy is having an adjusted course of propagation.

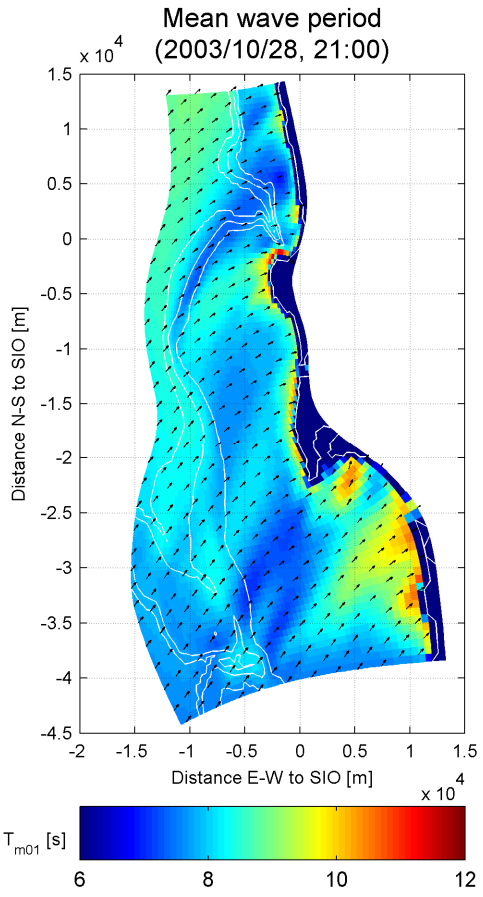

Figure 4.46 T_{m01} and mean wave direction large wave grid

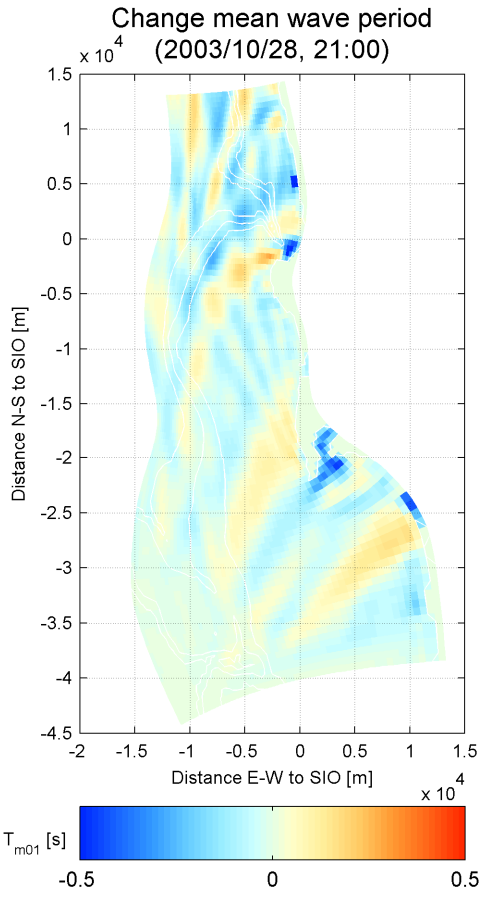

Figure 4.47 Change T_{m01} after modification dir. bins

The mean wave period (Figure 4.46) shows that along the coastal boundary between -25 and -45km a relatively high period develops. The high period is caused by to refraction of the low frequency waves from the southern boundary. The boundary conditions along the southern boundary actually represent the offshore observed wave energy. The offshore swell waves imposed on the southern boundary will refract first and therefore create an area with relatively long periods.

Also 5km south from the SIO pier an area with relatively longer periods develops. These waves seem to originate from the offshore boundary of which the low frequencies refract over the shallow areas just south of the canyons. Figure 4.47 shows that along the depth contour (100m depth, not indicated) the period decreases by about 0.2 seconds.

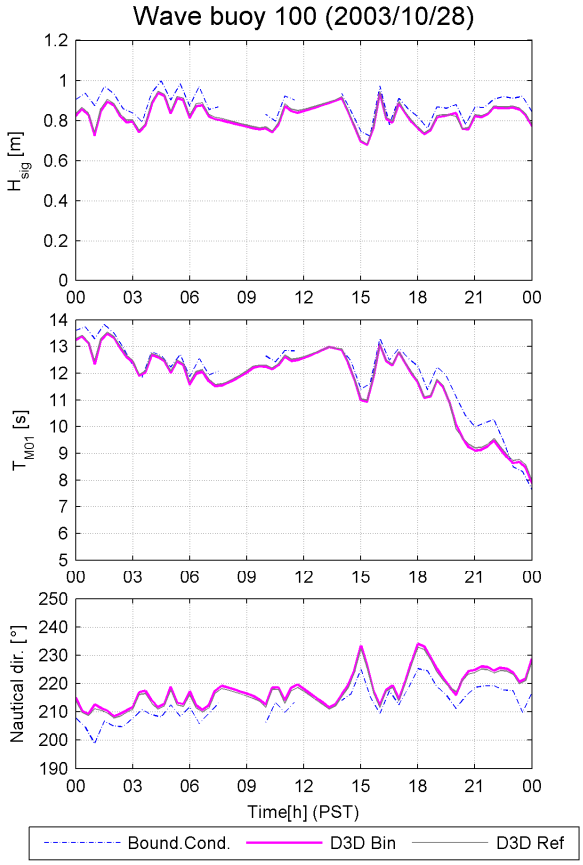

Figure 4.48 H_{sig}, T_{m01} and Nautical dir. of wave buoy 100 (2003/10/28)

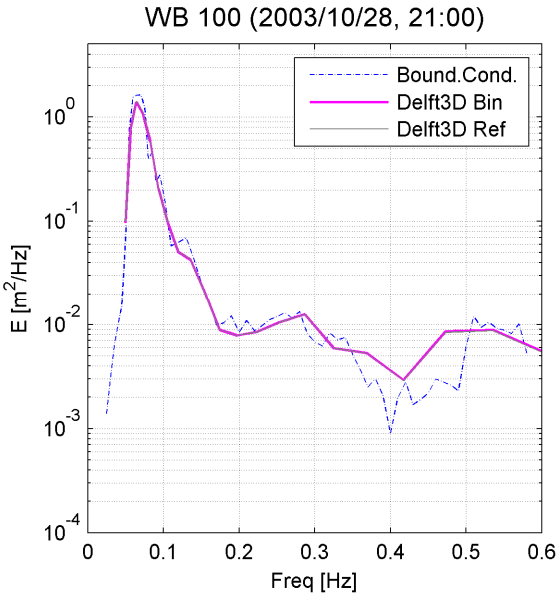

Figure 4.49 Energy spectrum WB100 (2003/10/28, 21:00)

Changing the width of the directional bins to 4˚ does not reduce the small errors in the time-series of wave buoy 100 at the offshore boundary (Figure 4.48). Significant wave height and mean wave period are still slightly underpredicted and the mean wave direction is overpredicted

Small wave grid (2B)

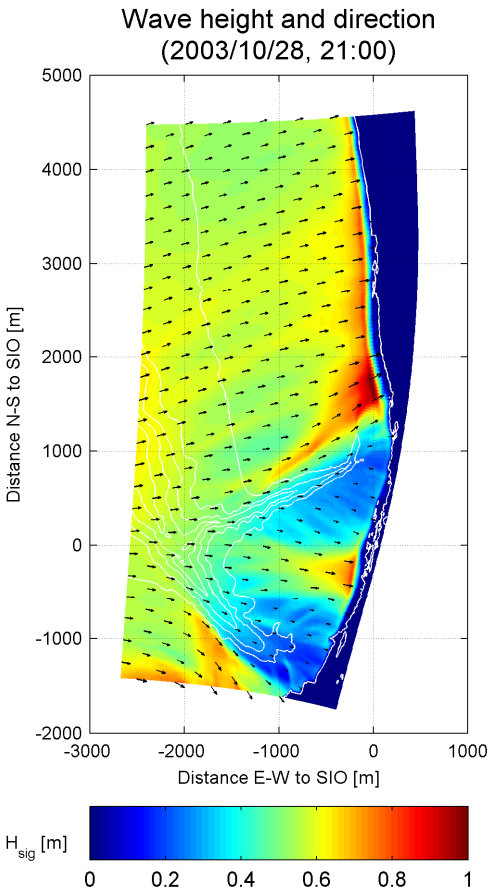

Figure 4.50 H_{sig} and mean wave direction small wave grid

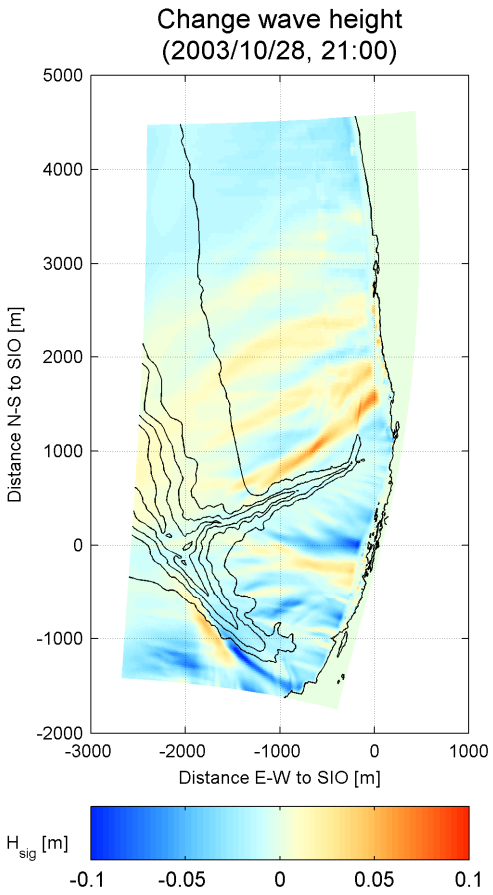

Figure 4.51 Change H_{sig} after modification dir. bins

Within the domain of the small wave grid (Figure 4.50 and Figure 4.51), the wave height has only changed order 5cm. onshore of the canyon the wave height predominantly slightly decreases and north of the canyon and in between La Jolla and Scripps canyon the wave height slightly increases. Indicating that the model takes more refraction into account.

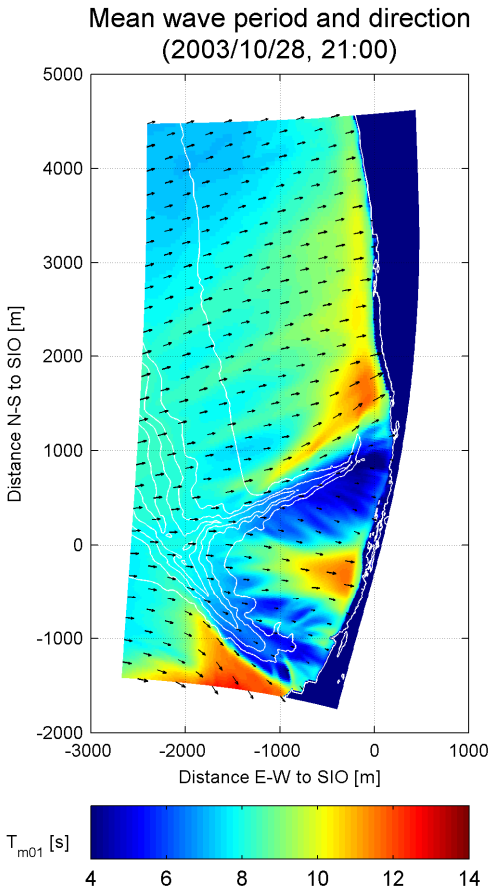

Figure 4.52 T_{m01} and mean wave direction small wave grid

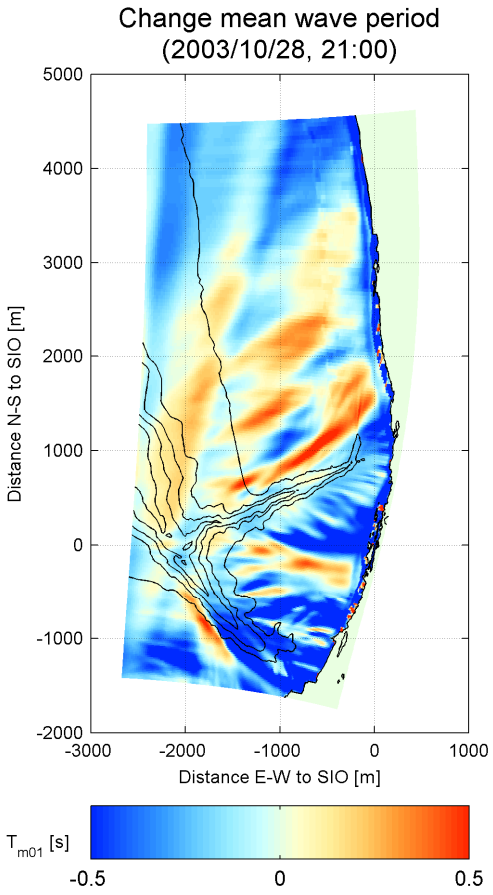

Figure 4.53 Change T_{m01} after modification dir. bins

The patterns of both the wave period (Figure 4.52) and the change of the wave period (Figure 4.53) are comparable to the patterns of change of the wave height in the domain of the small wave grid. In the areas of wave focussing, also the wave period is longer. This focussing of the longer periods pleads for the stronger effect on the long period waves.

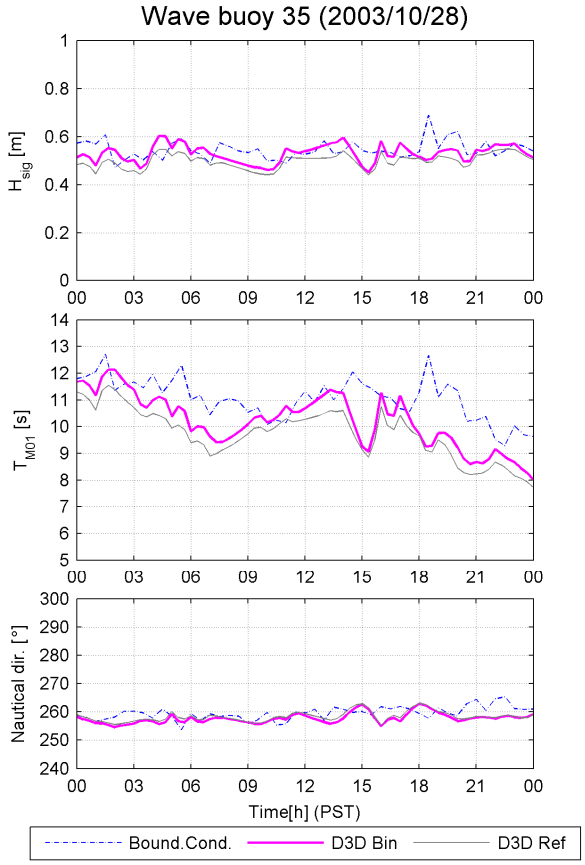

Figure 4.54 H_{sig}, T_{m01} and Nautical dir. of wave buoy 35 (2003/10/28)

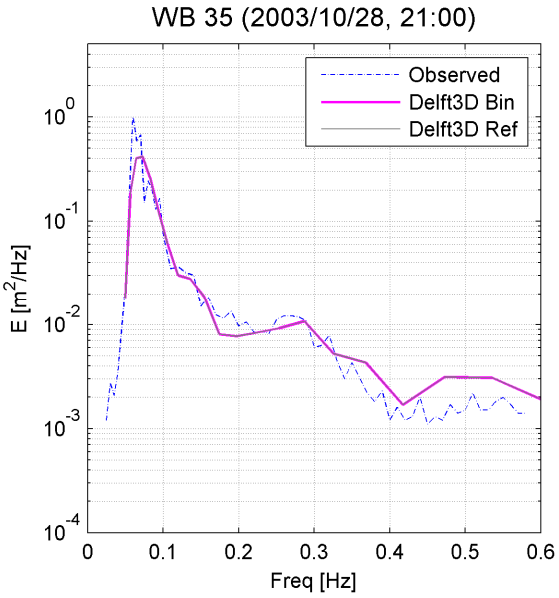

Figure 4.55 Energy spectrum WB35 (2003/10/28, 21:00)

Figure 4.55 displays a spectra comparison for wave buoy 35 at 21:00 hours. The spectrum shows an underprediction over both the low frequencies (0.05-0.1Hz) and as the high frequencies (>0.4Hz).

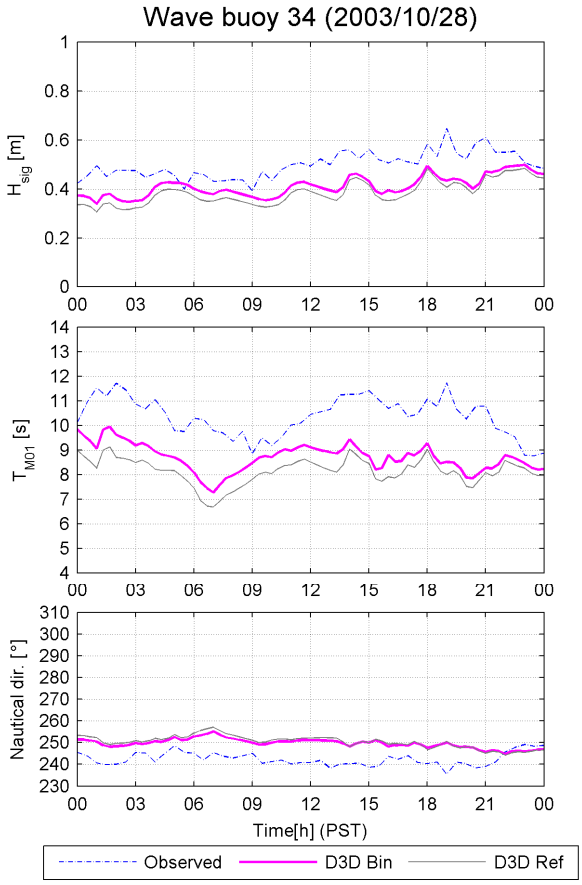

Figure 4.56 T_{m01} and Nautical dir. of wave buoy 34 (2003/10/28)

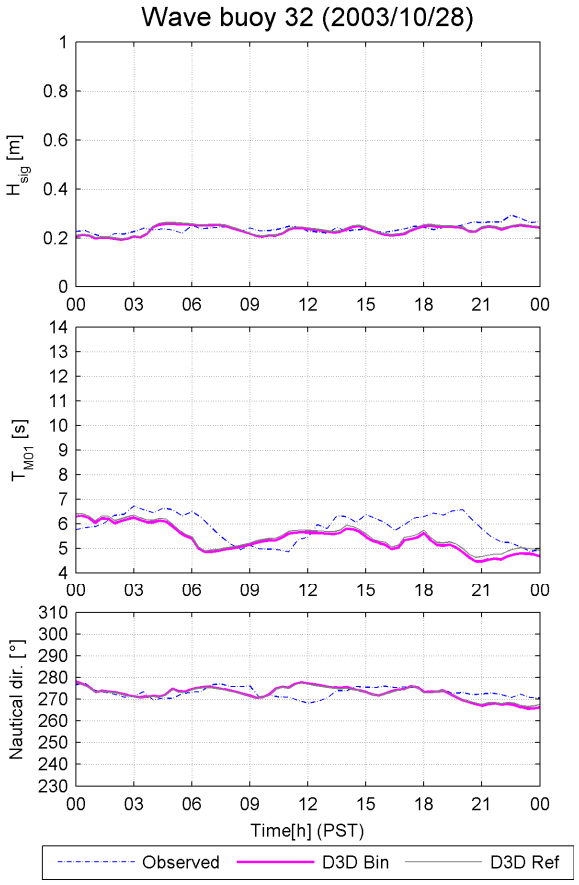

Figure 4.57 H_{sig}, T_{m01} and Nautical dir. of wave buoy 32 (2003/10/28)

Time-series for wave buoy 34 deployed north of the canyon (at the tip of the boot shape) are depicted next to the time-series for wave buoy 32 deployed onshore of the canyon. These time-series comparisons show that the predictions at the canyon tip is still deviating. Both the wave height and the wave period is underpredicted. Onshore of the canyon wave height is predicted right, but the period shows a lagging effect.

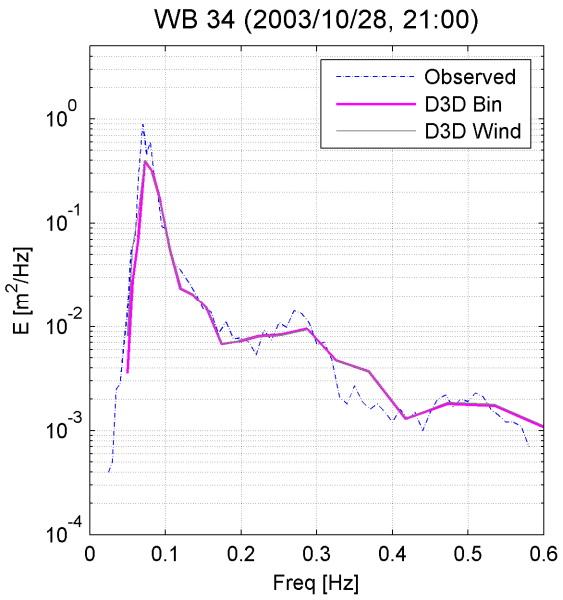

Figure 4.58 Energy spectrum WB34 (2003/10/28, 21:00)

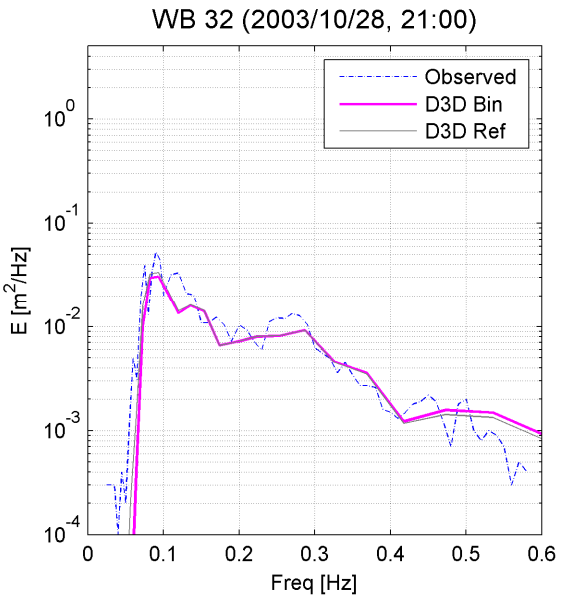

Figure 4.59 Energy spectrum WB32 (2003/10/28, 21:00)

In search for the reason of the underprediction, Figure 4.58 and Figure 4.59 are demonstrating spectra comparisons at 21:00 hours. At both buoy locations the model predicts slightly too much energy over relatively high frequencies.

4.2.3 Inclusion of wind growth (2C)

Case 2, simulating the conditions of October 28, is a day with hardly any wind during the day. However, during the evening the wind picks up to about 4m/s with peak velocities up to 7m/s. This calibration step (2C) will describe the influences of adding wind to the model. As the wind velocity is largest at 23:00 hours, vector plots are shown of that moment.

Large wave grid (2C)

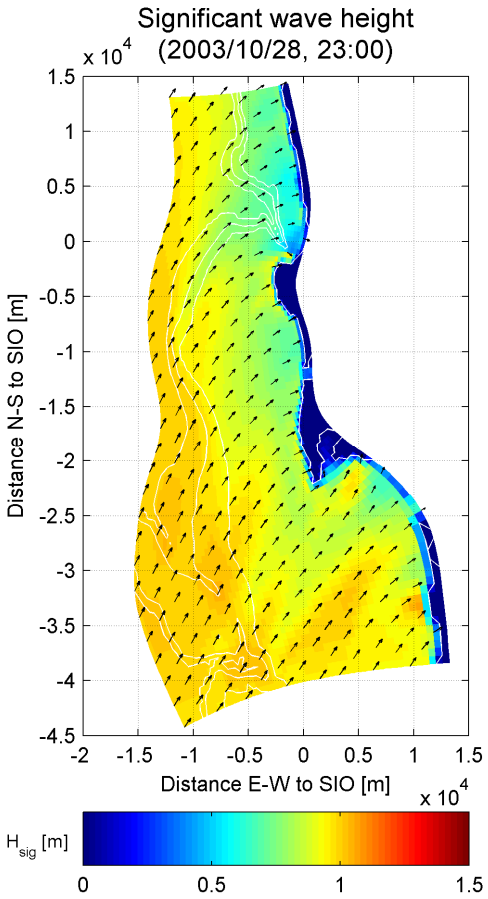

Figure 4.60 H_{sig} and mean wave direction large wave grid

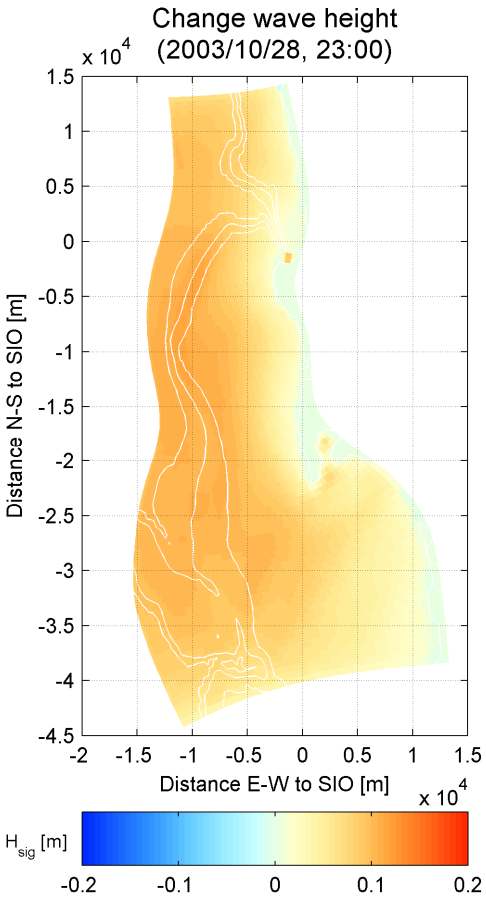

Figure 4.61 Change H_{sig} after adding wind

The influence of the wind on the significant wave height within the model is represented by Figure 4.60 and Figure 4.61. The pattern of this modification is smooth and seems to have influence over the whole domain of the large wave grid. The wave height increases by about 10cm.

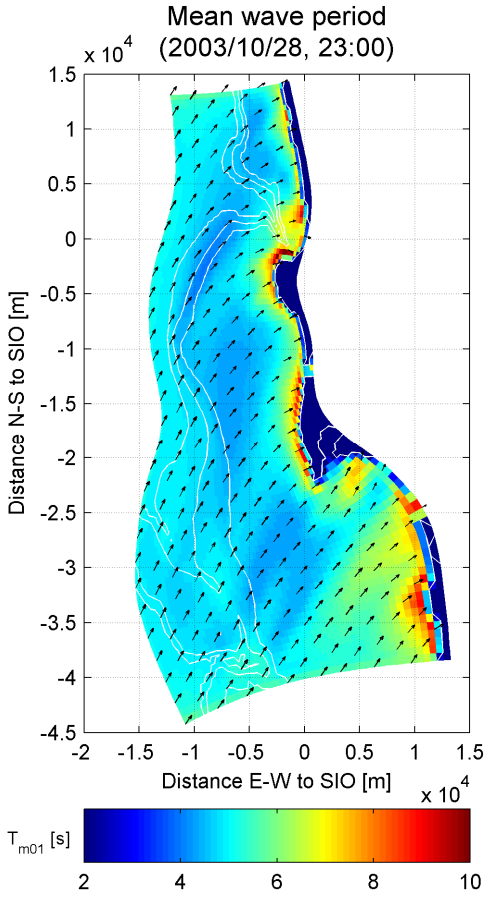

Figure 4.62 T_{m01} and mean wave direction large wave grid

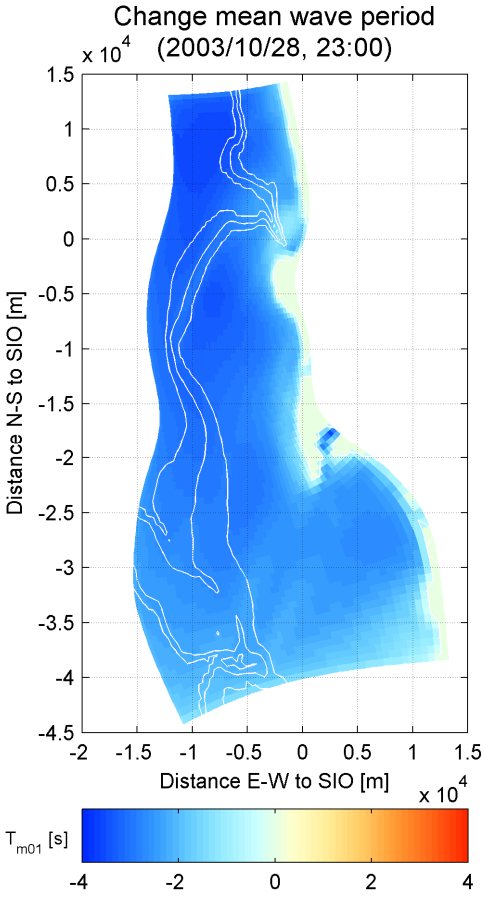

Figure 4.63 Change T_{m01} after adding wind

The influence of the wind on the wave period seems also smooth over the whole domain and decreases the mean wave period by about 3 seconds (Figure 4.63). This reduction of the wave period is caused due to the fact that wind energy adds energy to the higher frequencies.

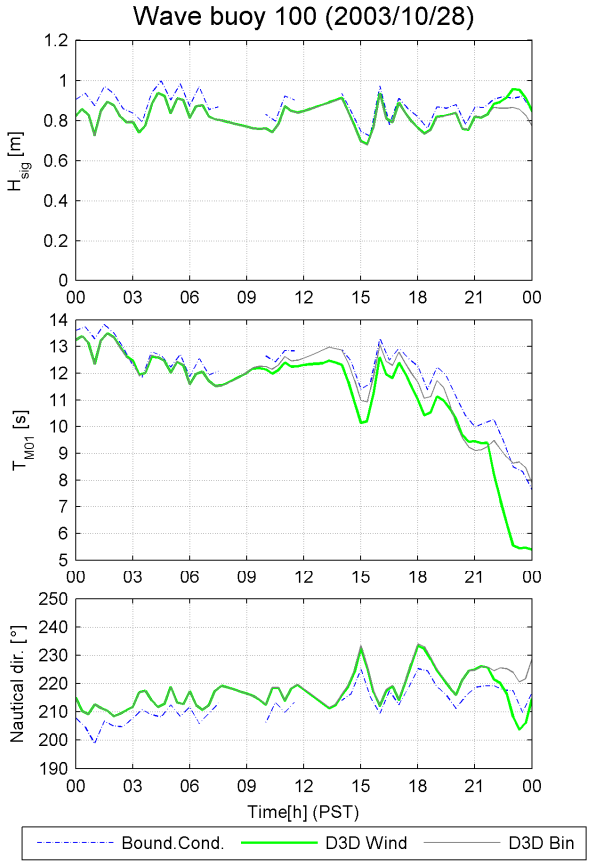

Figure 4.64 T_{m01} and Nautical dir. of wave buoy 100 (2003/10/28)

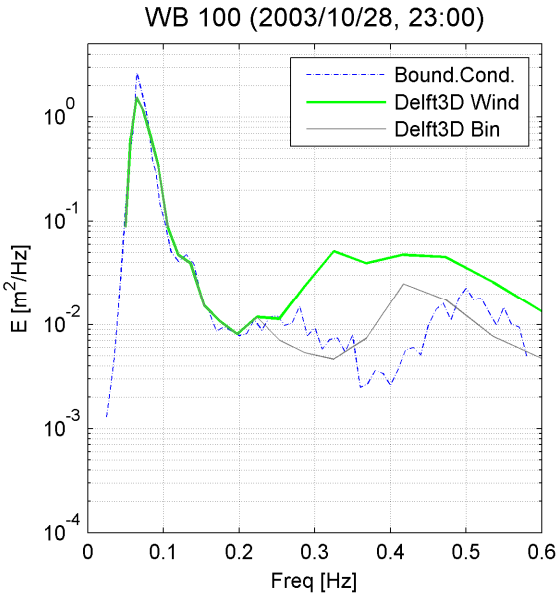

Figure 4.65 Energy spectrum WB100 (2003/10/28, 23:00)

Observations show winds were negligible during the day, but the wind picks up during the evening. This physical parameter would increase the overprediction of energy over the high frequencies. This carries-over to the mean period, which would be underestimated even more. Figure 4.64 shows that indeed only during the last few hours when the wind is significant the period significantly deviates.

Small wave grid (2C)

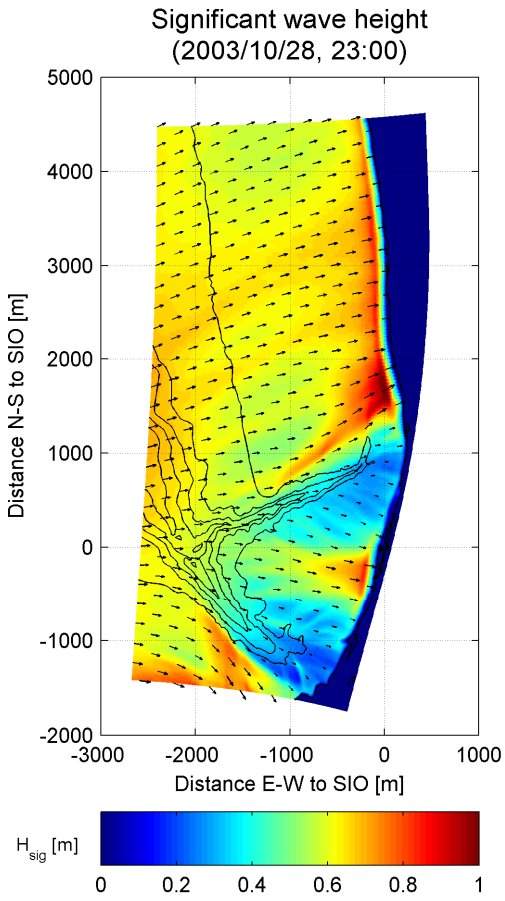

Figure 4.66 H_{sig} and mean wave direction small wave grid

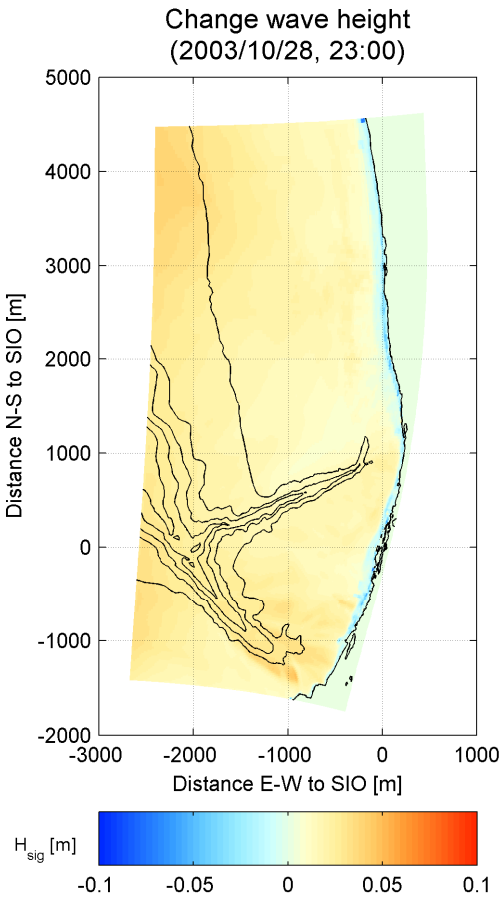

Figure 4.67 Change H_{sig} after inclusion of wind growth

Nearshore, the wind increases the significant wave height smoothly over the whole domain (Figure 4.66 and Figure 4.67). The smooth increase of wave height over the entire wavefield shows that the wind has no influence on the spatially redistribution of the wave energy.

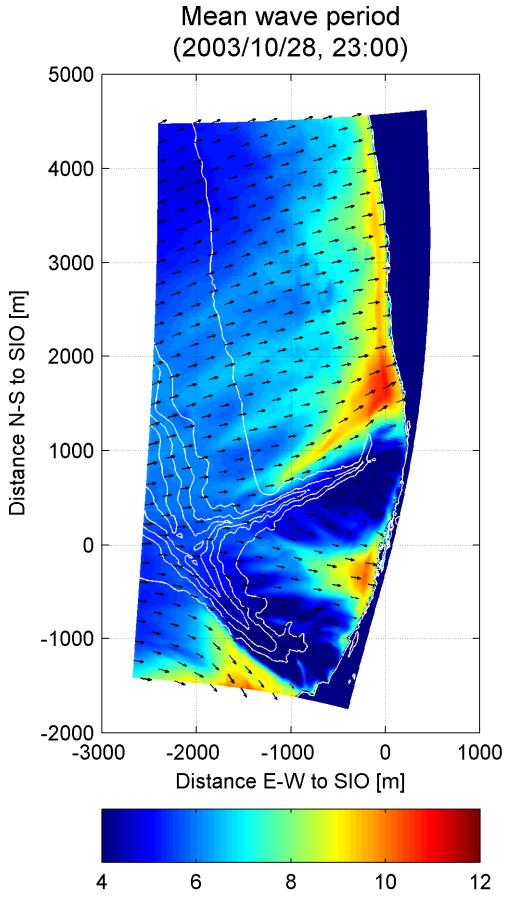

Figure 4.68 T_{m01} and mean wave direction small wave grid

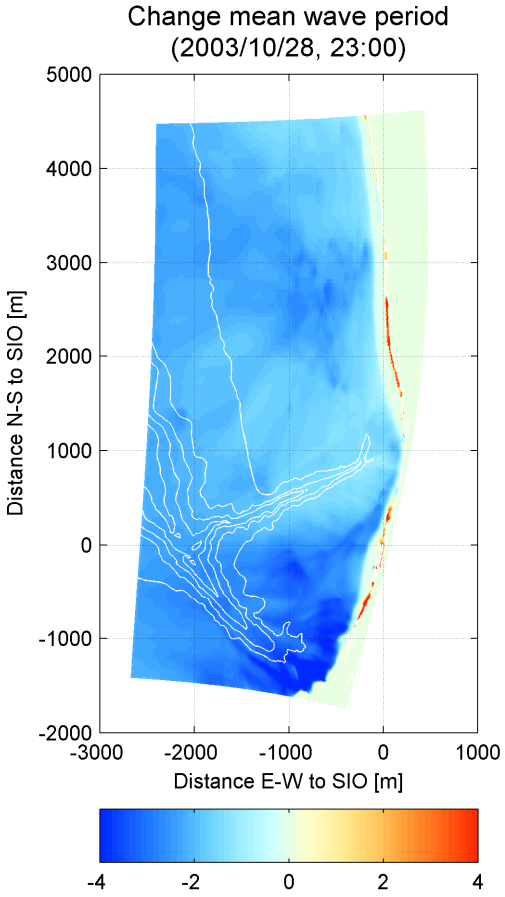

Figure 4.69 Change T_{m01} after inclusion of wind growth

Figure 4.68 Figure 4.69 show a smooth reduction of the wave period over the entire domain, in contrary to run 1C where the wave period reduction varied over the domain. A possible difference is that in this run (2C) the wind is offshore directed, which would create wind waves in offshore direction.

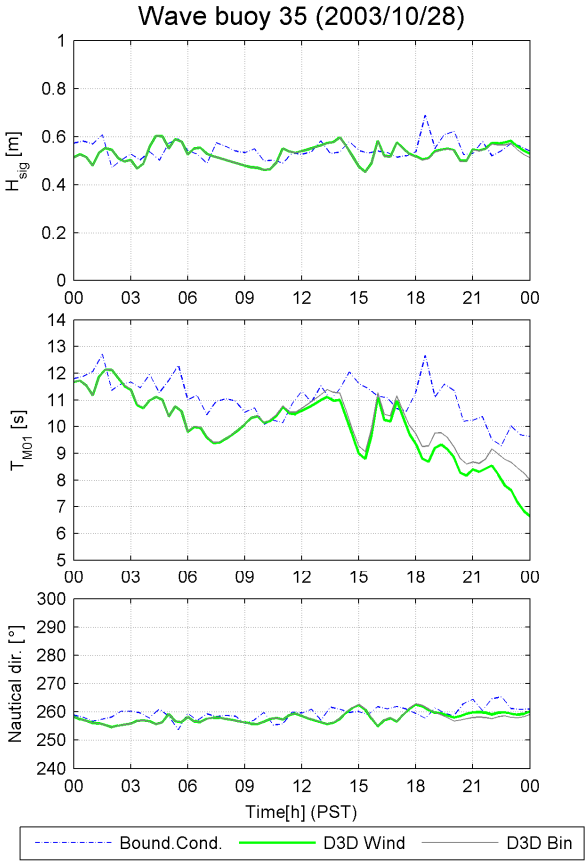

Figure 4.70 H_{sig}, T_{m01} and Nautical dir. of wave buoy 35 (2003/10/28)

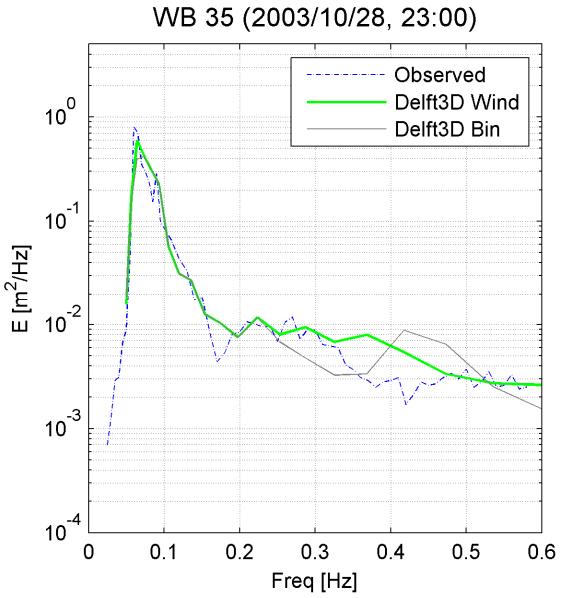

Figure 4.71 Energy spectrum WB35 (2003/10/28, 23:00)

Time-series of wave buoy 35 shows that the wave height remains unaffected in run 2C. The wave period on the other hand, deviates more during the evening than it did in run 2B (no wind). A reason for this could be that the model computes a fully developed sea state generated by the wind, which in reality is not the case. The wind picked up in a short period, which would only slightly decrease the mean wave period.

Although adding wind to this model run does not improve the wave simulations, the effects are shown. Time-series comparisons for wave buoy 100 and wave buoy 35 showed an increased model deviation of the mean wave period during the evening, when the wind velocity increased.

4.3 Conclusions

Three model runs have been examined for two cases. The results of the initial runs (1A and 2A) show the model predictions without wind and a directional bin width of 10˚. In calibration step 1B and 2B, the number of directional bins was increased to obtain better accuracy. This modification improved the model results in both cases. The Delft3D-Wave manual prescribes the use of a bin width of 3˚ to 5˚, as some swell waves were observed during the last simulation hour.

Adding wind in the third calibration step (1C and 2C) improved simulations for case 1, with relatively larger wind sea energy. Wind adds energy to the high frequencies in the spectrum, which causes a smaller mean wave period. Adding wind improved the model performance, as initially the mean period was overpredicted.

However, adding wind did not improve model run 2C. In the second case, in which longer swell waves were simulated, the mean wave period was already underpredicted during the last three hours of the simulation. Therefore, in the remaining model-data comparisons in Chapter 5, the directional bin width is set to 4˚ in both cases, but wind is only added to case 1 of October 10.

5 NCEX surfzone predictions

After calibrating the waves offshore in Chapter 4, this chapter will show the comparison of model predictions of Delft3D-Flow with the NCEX observations in the surfzone. In the first section is looked at the incident waves. The second section describes the wave set-up results, and the third section describes the comparison of flow velocities in the alongshore and cross-shore direction.

5.1 Pressure sensors

The Roller model is an extension to Delft3D-Flow, which is applied in this study, and determines the wave conditions within the Flow domain. The boundary conditions for the Roller model are derived from Delft3D-Wave, which imposes the wave height along the boundaries of the Flow domain. Within the domain, the Roller model uses the mean wave direction and wavelength from Delft3D-Wave.

The domain of Delft3D-Flow extends from the shoreline to about 15m water depth and partially covers Scripps canyon. The waves predictions are compared with measurements of the pressure sensors deployed at 1, 2.5 and 5m water depth (described in section 2.2.3).

In addition, the mean wave directions are examined since these have a substantial influence on the flows nearshore. The Roller model uses the mean wave direction from Delft3D-Wave, computed from the spectra over a range between 0.05Hz and 1.00Hz.

However, the mean observed wave direction are estimated over a frequency range between 0.05 and 0.30Hz owing to attenuation of the wave signal through the water column (in 5m water depth it is not possible to estimate directions at freq > 0.30Hz from near bed pressure sensors). Therefore, mean wave directions are also estimated over $0.05<f<0.30$Hz from Delft3D-Wave spectra.

Figures in this section show significant wave heights of six different Rays, three south and three north of the focus zone, at 2.5m water depth. Furthermore, the wave directions are shown relative to shore normal. Positive angles ($\theta>0$) indicate waves coming from the south and vice versa.

5.1.1 Case 1: Wind sea (Oct 10)

Offshore, the incident waves came from a west-northwest mean direction on October 10. Propagating shoreward, the waves are affected by the bathymetry. Close to the canyon, the waves show strong refraction. This refraction is shown in Figure 5.1 between 1000 and 1500m north of the SIO pier, which a model result of the simulation of October 10 at 10:00 hours. Further north from the canyon, the waves still propagate shoreward from a west-northwest direction. Furthermore, according to the model, the highest waves develop at about 1500m north of SIO. Also, onshore of the canyon (between 1000 and 1400m) the waves height shows spatial oscillation in alongshore direction, which is possibly caused by the undulations of the canyon wall. The undulations are illustrated by the depth contours, which are not parallel to the shoreline.

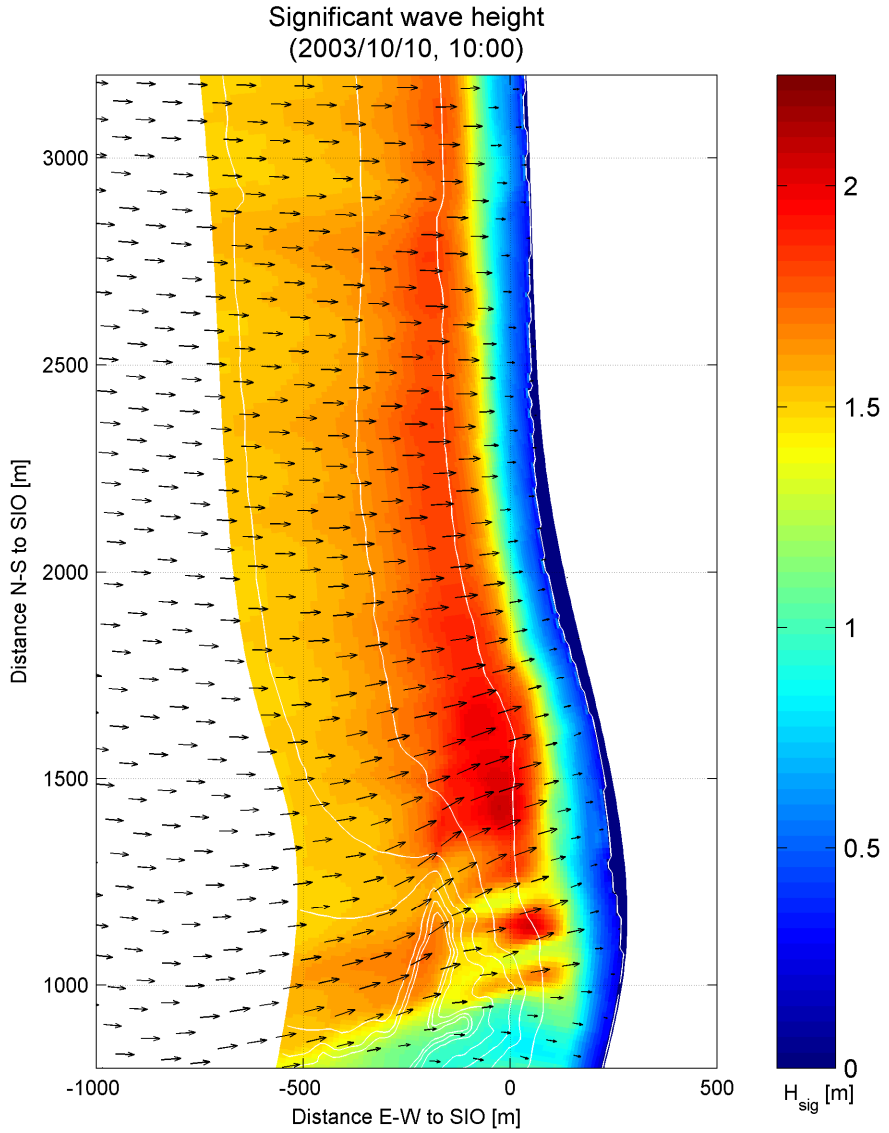

Figure 5.1 Nearshore predicted significant wave height (2003/10/10, 10:00)

Time-series of model predictions and observations are shown for Ray 1000, 1149 and 1450 in Figure 5.2. The first two of these Rays are in the shadow zone onshore of the canyon, where relatively low wave heights are observed. The wave height increases northward from the canyon until Ray 1450.

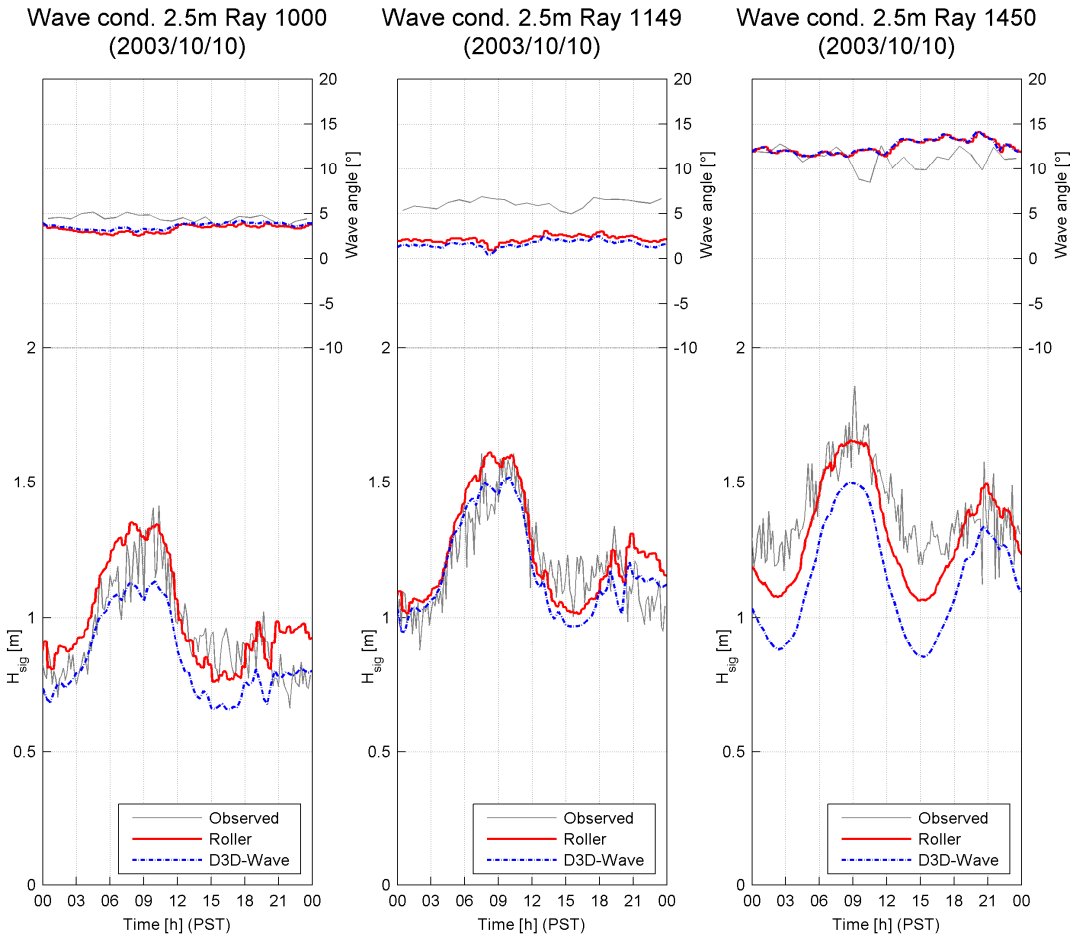

Figure 5.2 Significant wave height at 2.5m water depth at Rays south of the focus zone (2003/10/10)

The Roller model predicts the trend of increasing wave height until Ray 1450. The wave height onshore of the canyon is slightly overpredicted, whereas the wave height at Ray 1450 is underestimated, possibly due to the model transferring too much energy over the canyon. The wave heights at Ray 1000 and Ray 1149 during the last four hours of simulation are overestimated. This overestimation was already observed by the wave buoys described in sections 4.1.3.

The direction of wave propagation is underestimated at Ray 1000 and 1149 throughout the day. Waves in the model approach the shore almost perpendicular, while observations give positive oblique angles, which imply waves approach from the south.

Time-series in Figure 5.3 depict model comparisons of Rays north of the focus zone. Both modelled wave height and wave direction are close to observed values. In addition, time-series of the wave heights are shown from Delft3D-Wave. These wave heights are not used further in this research, but clearly show the difference with the Roller model results. The

Roller model gradually dissipates wave energy shorewards, conversely to Delft3D-wave. Therefore, the Roller model shifts wave energy shoreward, which explains the higher waves.

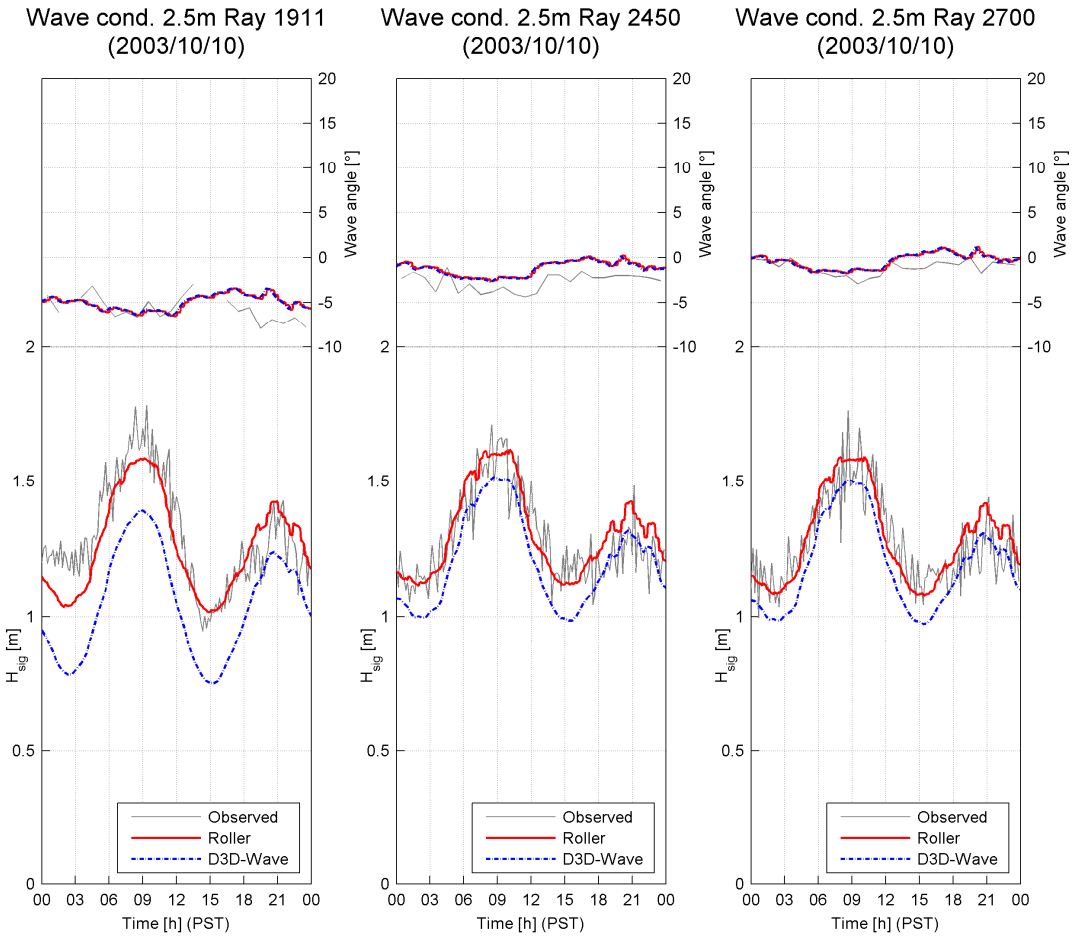

Figure 5.3 Significant wave height at 2.5m water depth at Rays North of the focus zone (2003/10/10)

Time-series of the significant wave height of Ray 1911 shows an underprediction during the first 6 hours of simulation. A similar underprediction was shown in Figure 5.2 for Ray 1450. Both Rays lie close to a point where a significant amount of sediment accretes between the two successive surveys (Figure 2.23) before and after the day of simulation. The rapid morphological change for which is not accounted for could have influence on the prediction of the significant wave height.

Mean and the root-mean-square errors for significant wave heights are summarized in Table 5.1. Wave heights onshore of the canyon are overpredicted, whereas wave heights in the focus zone are underpredicted, suggesting that not enough energy has refracted to the focus zone, which might cause the underprediction at Ray 1450 and 1911.

Ray (at 2.5m isobath)	H_{sig}-mean observed [m]	H_{sig}-mean predicted [m]	RMS-error [m]
1000	0.94	1.00	0.13
1149	1.20	1.24	0.12
1450	1.39	1.32	0.14
1911	1.30	1.26	0.11
2450	1.29	1.31	0.09
2700	1.27	1.29	0.10

Table 5.1 Predicted and observed H_{sig} at 2.5m water depth (2003/10/10)

5.1.2 Case 2: Swell (Oct 28)

On October 28, swell waves from a south-southwest mean direction were observed offshore (550 water depth). At the offshore boundary of the flow domain (about 15 water depth) the incident waves were already refracted to a southwest direction. Also within the flow domain, the waves strongly refract and show significant gradients in alongshore wave heights (see Figure 5.4).
According to the model, the highest waves develop at about 1700m north of SIO. Also, onshore of the canyon (between 1000 and 1200m) the waves height shows spatially oscillation in alongshore direction, which are probably caused by the undulations of the canyon wall relative to the shoreline.

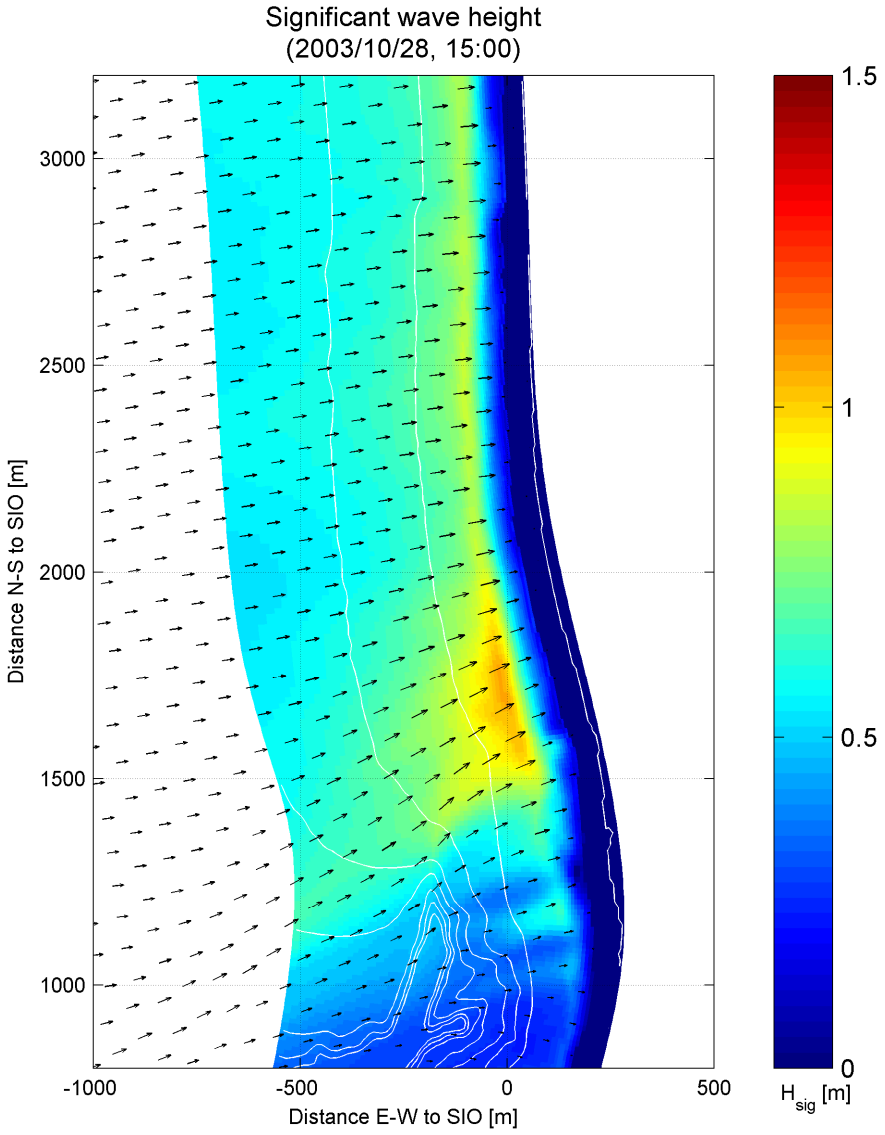

Figure 5.4 Nearshore predicted significant wave height (2003/10/28, 15:00)

Time-series comparisons for the wave buoys in 4.1.1.2 have already shown that swell waves are influenced more by the irregular steep bathymetry than wind waves. Thomson et al.

[2007] explained that a larger amount of energy refracts offshore of Scripps Canyon for low frequency waves. This stronger effect creates a steeper alongshore gradient of observed significant wave heights alongshore. Figure 5.5 depicts wave height results onshore and just north of the canyon. Wave heights at Ray 1450 are about 0.4m higher than at Ray 1000. The model predicts the wave heights reasonably well.

The predicted wave directions differ from the observations up to 10˚ for the Rays south of the focus zone. The underestimated wave direction onshore of the canyon is comparable to the simulation of wind sea waves (Oct 10). At Ray 1450, wave direction is overrated by about 10˚. Furthermore, ray 1000 and ray 1149 show a significant difference between the wave direction, which are determined from the Delft3D-Wave (0.05<f<0.30Hz) and the Roller model (0.05<f<1.00Hz). This indicates that at these rays relatively more energy is distributed over the frequencies larger than 0.30Hz.

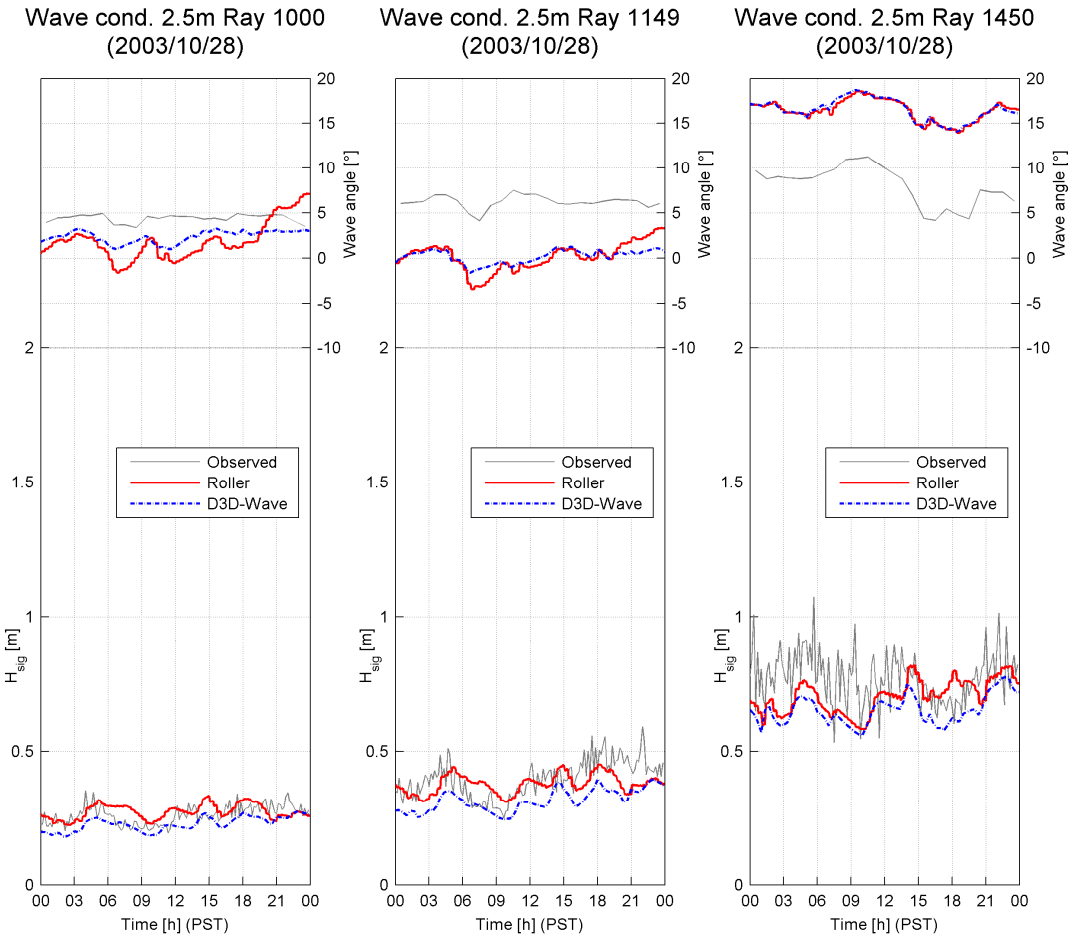

Figure 5.5 Significant wave height at 2.5m water depth at Rays South of the focus zone (2003/10/28)

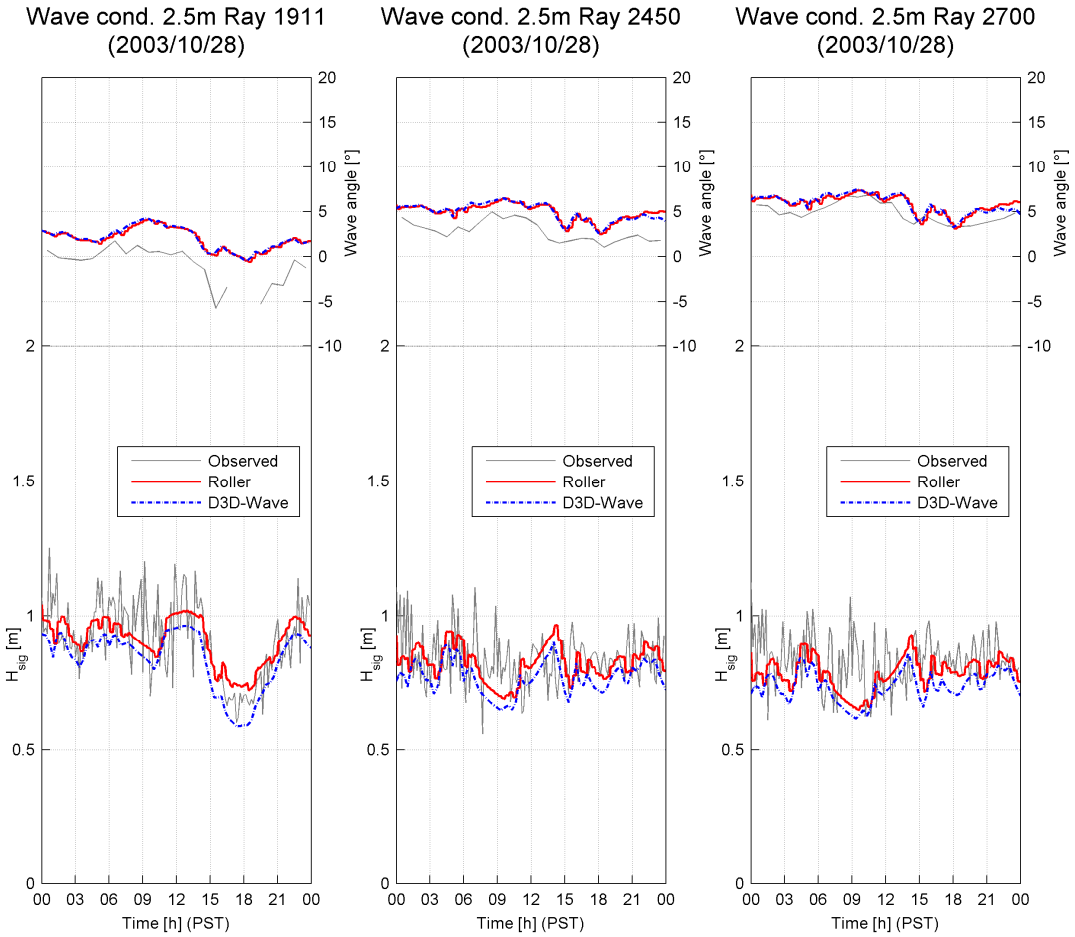

Figure 5.6 Significant wave height at 2.5m water depth at Rays North of the focus zone (2003/10/28)

Figure 5.6 depicts wave heights north of the focus zone. Wave heights are highest at Ray 1911, closest to the focus zone, and decrease northward. Wave direction is overestimated by about 3˚ at Ray 2450.

Ray (at 2.5m isobath)	H_{sig}-mean observed [m]	H_{sig}-mean predicted [m]	RMS-error [m]
1000	0.26	0.27	0.04
1149	0.40	0.38	0.07
1450	0.77	0.70	0.13
1911	0.91	0.91	0.11
2450	0.83	0.82	0.11
2700	0.83	0.78	0.12

Table 5.2 Predicted and observed H_{sig} at 2.5m water depth (2003/10/28)

5.1.3 Direction of wave propagation

In the preceding sections comparisons are shown between the observed and predicted mean direction of wave propagation in the surfzone. In particular, the comparisons of the mean directions onshore of the canyon show significant deviations. In the following, four possible clarifications are given for the deviations in the comparison of direction of wave propagation.

Frequency range of energy spectrum

The wave direction within the Roller model is used from Delft3D-Wave, which computes the mean directions from the wave spectra. The wave energy in this spectrum is distributed over a frequency range from 0.05 to 1.00Hz. Conversely, the mean observed wave direction is estimated over a frequency range between 0.05 and 0.30Hz. Observed frequencies in the surfzone higher than 0.30Hz are not accurate owing to the attenuation of the wave signal through the water column.

However, manually computing the mean directions over only the frequencies between 0.05Hz and 0.30Hz did not gave large differences overall. Only the second case showed significant differences of wave direction in the shadow zone. These deviations indicate that onshore of the canyon wave energy distributed over frequencies larger than 0.30Hz has a significant influence on the mean wave direction

Roller model

The use of the Roller model is accepted when the wave direction of propagation is narrow-banded. The reason for this is that the wave energy propagation within the Roller model propagates according to the mean direction. Nonetheless, the propagation of wave energy of each frequency bin in Delft3D-Wave is able to propagate in a different directions. The wave energy in the Roller model would therefore propagate according a mean direction, although in Delft3D-Wave this wave energy could possibly spread.

Refraction over currents

Within the surfzone an alongshore flow develops. Incident waves refract over these currents in the surfzone, which influences the direction of wave propagation. Within Delft3D-Wave it is possible to take refraction over these alongshore currents into account. However, this option has not been used since this caused instabilities in the model run.

Bathymetry

The direction of wave propagation is dependent on the bathymetry within the surfzone. As the bathymetry within the surfzone was surveyed weekly, an accurate bottom profile could be created for the model. The bathymetry within the surfzone in Delft3D was defined by the closest preceding survey.

For the simulation of October 10, survey data was used of October 6. Although, this survey seems very short to the day of simulation, it might not be accurate enough. This is based on the comparison of two successive surveys in Chapter 2.3.4. This comparison shows that a sandbar develops during the week of October 10. Locally the bathymetry elevates approximately 1.2m, which is expected to have a significant influence on the waves.

5.1.4 Conclusions

The effect of the canyon on the wave field is considered for two different types of waves, swell and wind waves. The longer swell waves experience more influence of the canyon than the shorter wind waves. Therefore, large alongshore gradient in wave height may be associated with larger period waves.

Significant wave height

To examine the model results further, root-mean-square-errors were calculated for the significant wave height for each ray. As shown in Table 5.3, rms-errors north of the canyon

are in the order of 0.1m. However, onshore of the canyon rms-errors for the wind sea case increase to 0.13m, while rms-errors decrease for the swell case to 0.04m.

Ray (at 2.5m isobath)	RMS-error [m] Oct 10	RMS-error [m] Oct 28
1000	0.13	0.04
1149	0.12	0.07
1450	0.14	0.13
1911	0.11	0.11
2450	0.09	0.11
2700	0.10	0.12

Table 5.3 RMS-error of predicted significant wave height

In addition, the time-series of the observed significant wave height show a lot of scatter due to wave groups as was explained in section 2.3.2.3. As the model predictions in this paragraph showed, this has not been simulated. Reproducing this scatter will not be possible as long for the boundary conditions offshore half-hourly wave spectra are used.

Mean wave direction

Predicted mean wave direction was compared with the observation. The observation show a mean wave direction over 0.05Hz to 0.30Hz. As the Roller model determines the mean wave direction over a frequency range between 0.05 and 1.00Hz, also the mean wave direction over the frequencies between 0.05 and 0.30Hz was determined from Delft3D-Wave.

Time-series comparisons showed that especially onshore of the canyon the mean wave direction deviate from observation.

5.2 Wave set-up

Alongshore variations in wave height causes an alongshore variable wave-induced set-up, which causes an alongshore sea-surface gradient, which drives alongshore currents. In chapter 2.4.2.1, set-up is defined as a local increase of the water level in the surfzone relative to mean sea level. In this study, the pressure sensor deployed at the 2.5m isobath 100m north of SIO pier is used as the reference level to calculate set-up from the at 1m isobath observations and the model results.

5.2.1 Case 1: Wind sea (Oct 10)

Wave observations described in Section 2.3 demonstrated that the canyon does not influence the propagation of wind waves as much as of swell waves, which may explain why, large set-up gradients did not develop along the coast for the October 10 case.

Figure 5.7 shows the mean and standard deviation of observed wave set-up on October 10 binned by water depth. A maximum cross-shore set-up increases from 9cm at Ray 1149 to 11cm at Ray 1450. The maximum mean wave set-up north of the focus zone decreases from 9cm at Ray 1911 to 6cm at Ray 2700.

The set-up decreases with increasing water depth. However, the alongshore difference between neighbouring mean set-up observations remains approximately constant, suggesting that the alongshore gradient of the water surface is about the same during the day.

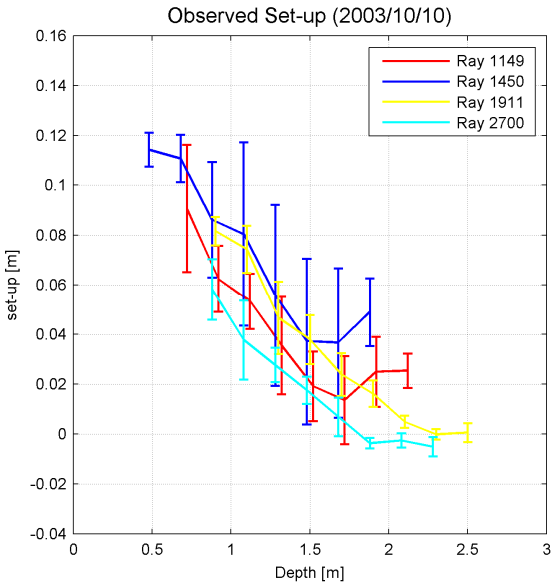

Figure 5.7 Mean and standard deviation of observed set-up as function of water depth (2003/10/10)

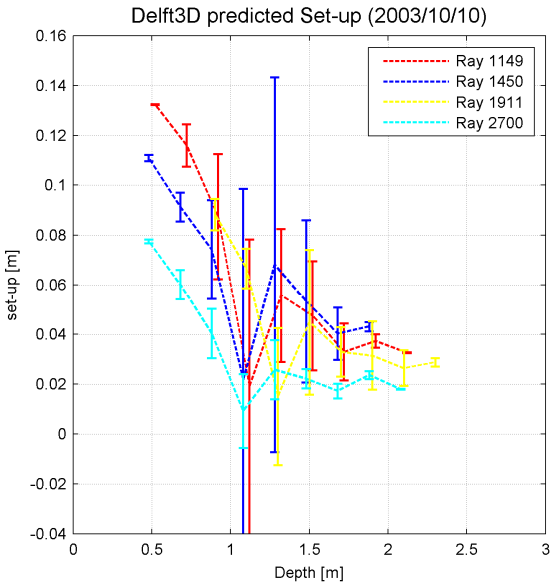

Figure 5.8 Mean and standard deviation of predicted set-up as function of water depth (2003/10/10)

Figure 5.8 represents the set-up prediction of the model. The model overpredicts the set-up in shallow water at Ray 1149 by about 2cm higher. Another odd phenomenon is sudden decrease of set-up in water depths around 1m. The model predictions of wave set-up when the water depth is about 1m coincide with the moment that the water level is rising and falling relatively fast owing to the tide. At these moments also small instabilities occur along the coastal boundary in the model predictions of the flow velocity. The high velocities could be related to the large standard deviations of wave set-up.

5.2.2 Case 2: Swell (Oct 28)

Observed means and standard deviations of the set-up binned by water depth on October 28, 2003 are shown in Figure 5.9. This day had approximately constant offshore wave heights (over time) and large wave height differences along the shore, due to the strong refraction effect of the canyon on the southwestern swell waves. The waves in the shadow zone are about 3 times smaller than in the focus zone, resulting in a large set-up gradient. The maximum cross-shore setup is 8cm at Ray 1450 and only 2cm at Ray 1149. North of the focus zone, the set-up gradients are smaller, increasing from 7cm at Ray 2700 to 9cm at Ray 1911.

Model predictions of set-up on October28, 2003 are displayed in Figure 5.10. The model also predicts the trend of increasing set-up towards the focus zone north of the canyon.

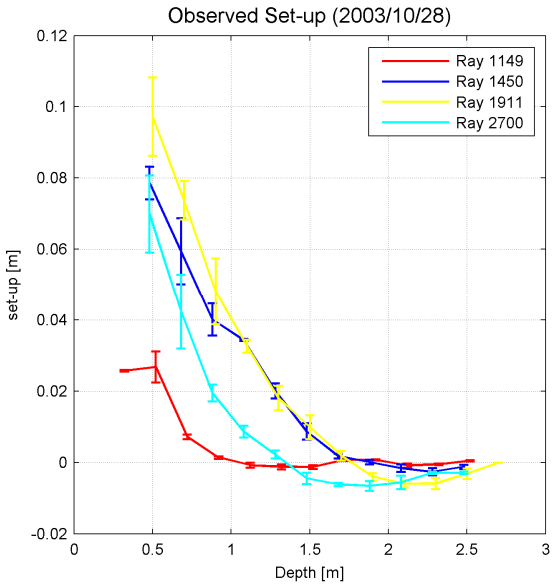

Figure 5.9 Mean and standard deviation of observed set-up as function of water depth (2003/10/28)

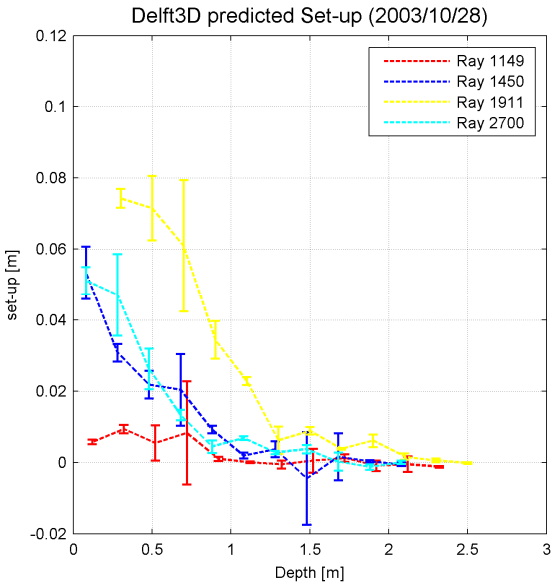

Figure 5.10 Mean and standard deviation of predicted set-up as function of water depth (2003/10/28)

5.2.3 Conclusions

Set-up has been considered for two wave conditions, short wind waves from the west and long swell waves from the south. In the first case, when wind waves with an offshore average significant wave height of 1.36m propagated to the shore, the setup was large at the shore throughout the domain and observed and predicted alongshore setup gradients were small.

Observations of set-up in the case of south swell showed a different pattern. Despite the smaller offshore mean significant wave height of 0.86m, the setup in the focus zone was similar to that on October 10. This large setup can be attributed to refraction of the swell waves caused by the submarine canyon. The observed set-up onshore of the canyon is significantly smaller, as the wave energy is smaller relative to that in the focus zone. As a result, there are large alongshore gradients in the water surface.

5.3 Nearshore currents

This section examines the comparison of observed and modelled flow velocities for the wind wave and swell wave cases, respectively on October 10 and October 28. Initially, time-series are shown of both alongshore and cross-shore flow predictions next to the observations. Subsequently, hourly averaged flow velocities are compared along the 2.5m water depth transect of one particular hour. Finally, the velocities along the alongshore transects at 1, 2.5 and 5m water depth are shown throughout the day.

5.3.1 Case 1: Wind sea (Oct 10)

On October 10, a convergent alongshore flow was observed along Black's beach. Also according to the model results the convergent flow was present between 0 and 5m water depth. In addition a rip current develops at about 1600m north of the SIO pier. The rip-current extends to over 10m water depth, shown in Figure 5.11.

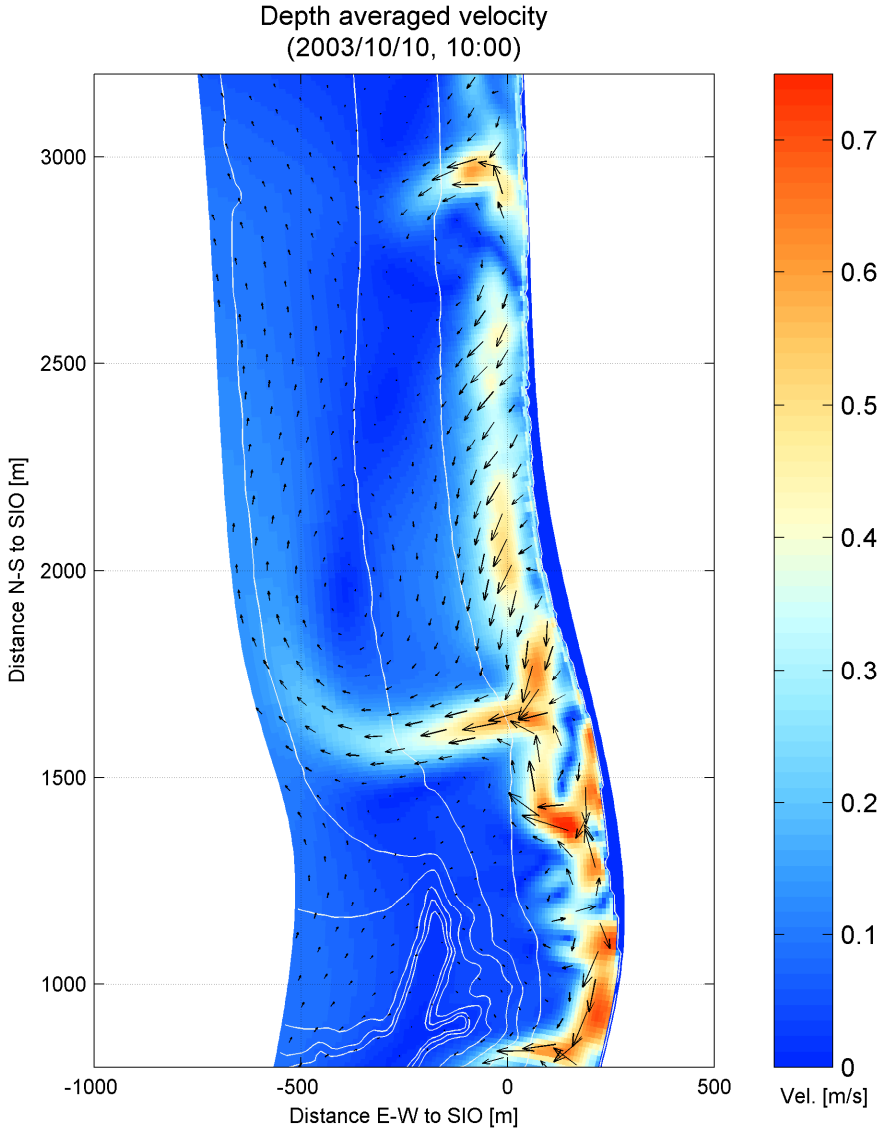

Figure 5.11 Model predictions of depth averaged velocity (2003/10/10, 10:00)

5.3.1.1 Flow time-series comparison

In this section, time-series of flow velocities in alongshore and cross-shore direction are shown. Model predictions are compared with observations at ray 1149, 1450, 1911 and 2450 in 2.5m water depth.

Alongshore flow

Time-series of the current meters described in section 2.3.3 showed a southward flow north of the focus zone and a northward flow south of the focus zone. Model predictions in Figure 5.12 also hindcast this convergent directed flow. In addition, alongshore flow velocities at Ray 1450 and 1911 (close to the focus zone) show larger magnitudes than at Ray 1149 and 2450 (further from the focus zone).

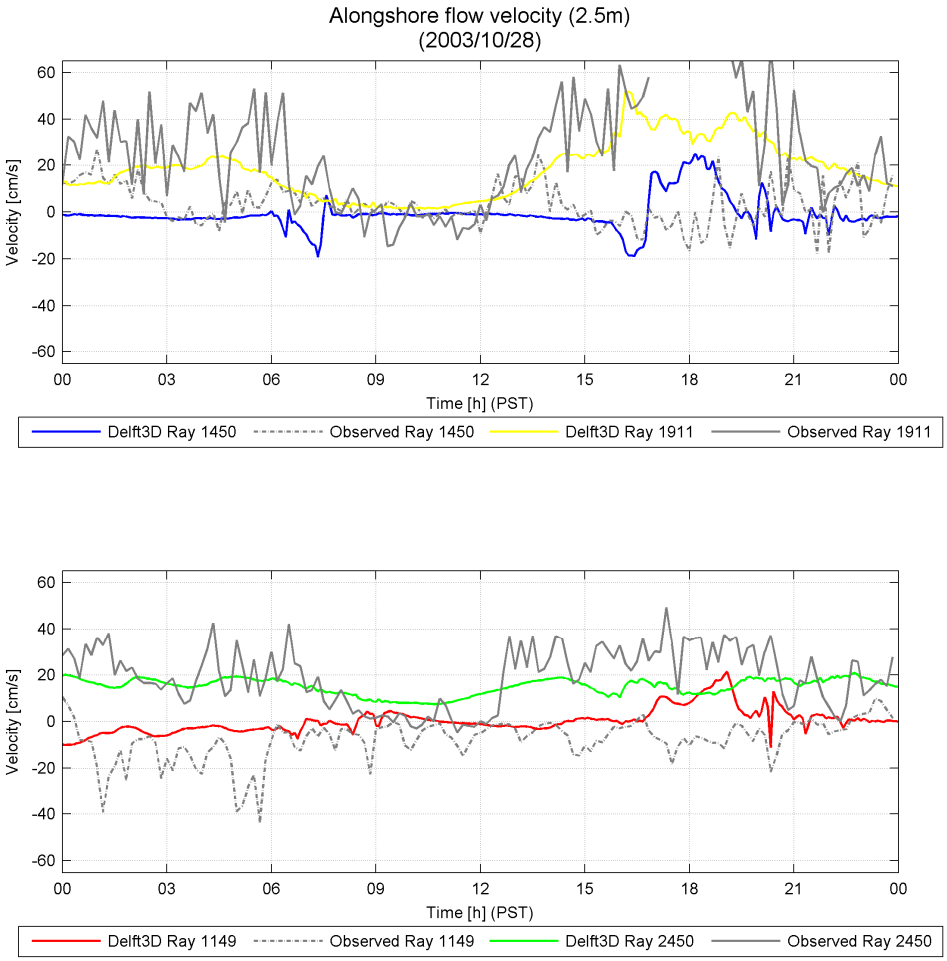

Figure 5.12 Time-series alongshore flow velocity comparison, 2.5m depth (2003/10/10)

Cross-shore flow

Cross-shore flow velocities (Figure 5.13) show smaller flow magnitudes than the alongshore flow velocities. Furthermore, the prevailing flow observations are offshore directed. The model predictions agree in most cases except for Ray 1149, where flow velocities are overpredicted and sometimes in the wrong direction.

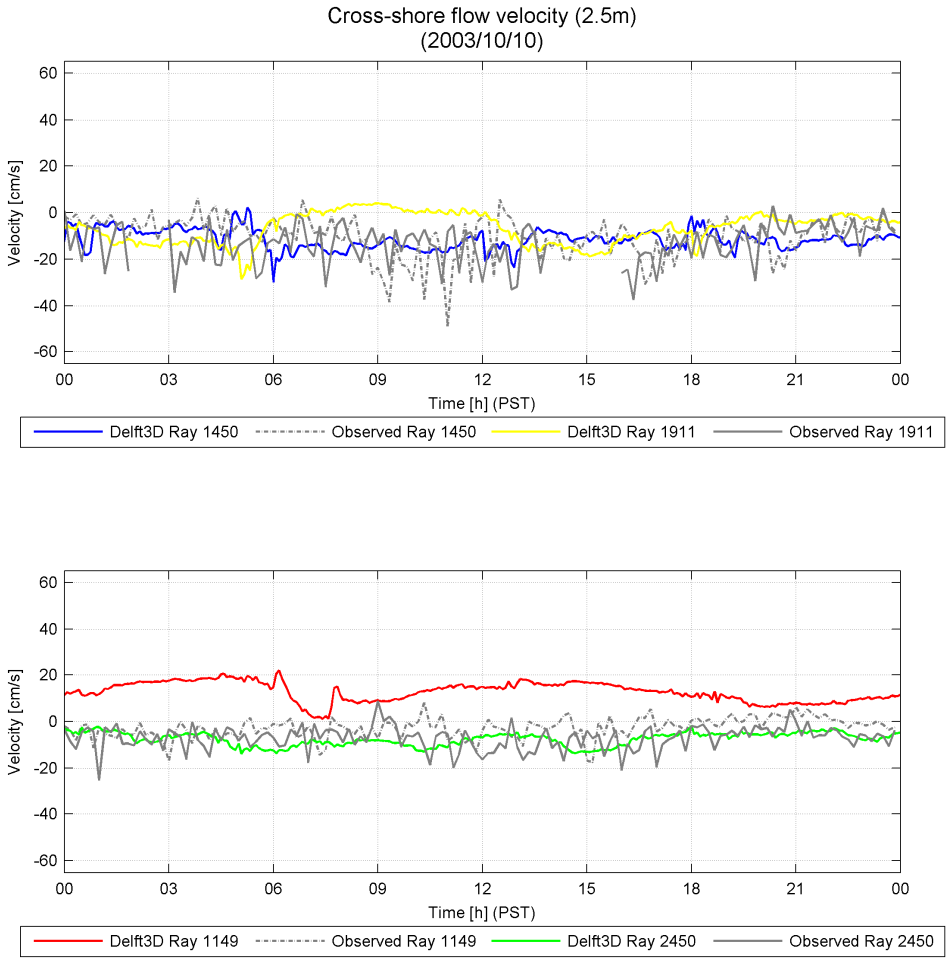

Figure 5.13 Time-series cross-shore flow velocity comparison, 2.5m depth (2003/10/10)

5.3.1.2 Flow velocity along transect

Time-series comparison of the flow velocities showed that the predictions not precisely correspond to the observations. The deviations do not necessarily mean that the model predicts the flow magnitudes wrong. Possibly, the model predicts the correct flow velocities, but at a wrong location. Therefore, a comparison is made of an hourly averaged flow velocity along an alongshore transect.

Alongshore flow

Figure 5.14 represents the alongshore flow velocity at 2.5m water depth. The comparison shows the averaged flow velocity between 10:00 and 11:00 am of the model next to 51.2-min averaged observations yellow pentagrams) and six 8.5-min averaged observations (blue dots).

Towards the focus zone (about 1600m), the magnitude of the flow velocities increase according to the observations and are convergent. Model predictions also show this convergent flow at 1600m. However, the model predictions south of the focus zone are not solely northward. Furthermore, are the velocities towards the focus zone slightly overpredicted.

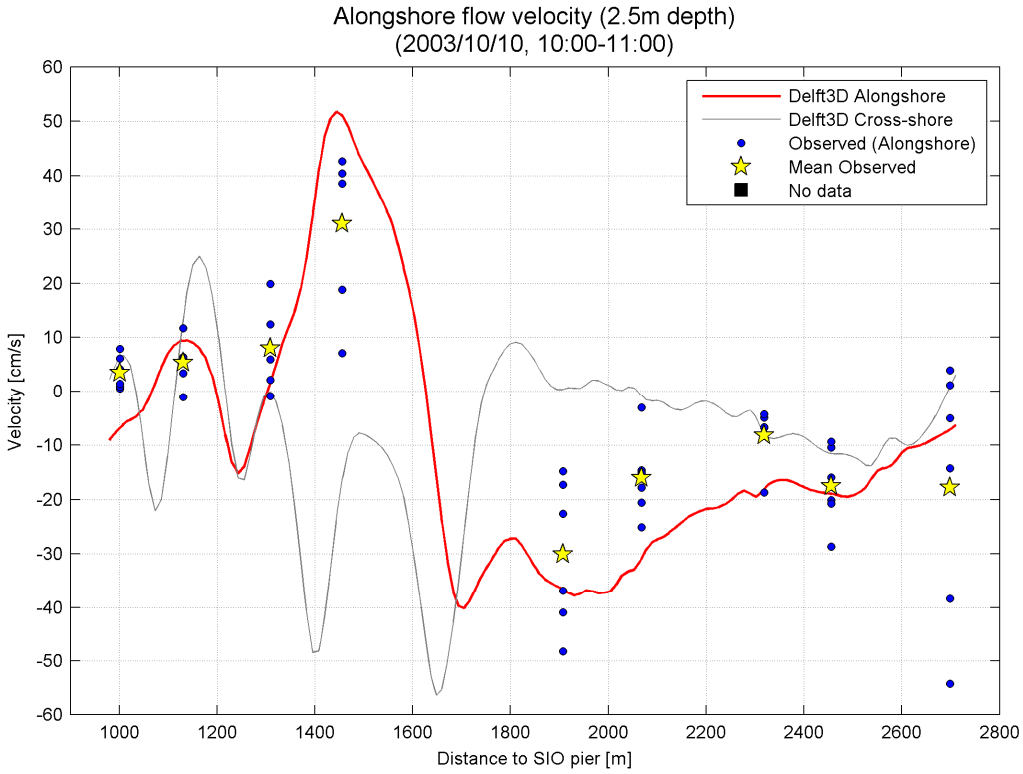

Figure 5.14 Hourly averaged alongshore flow velocity along 2.5m depth transect (2003/10/10, 10:00-11:00)

Cross-shore flow

The cross-shore flow velocities are prevailing offshore directed (Figure 5.15). The cross-shore flow velocity comparison along the 2.5m transect shows a reasonably well agreement. In addition, the model shows relatively higher cross-shore flows in between the observation locations.

The flow velocity between 1000 and 1700m shows spatial oscillation. The oscillation can possibly be related to the oscillating wave height as shown in Figure 5.1. For example the offshore directed flow predictions at 1100, 1250 and 1400m in Figure 5.15 coincide with locally low waves compared to the waves north and south of it.

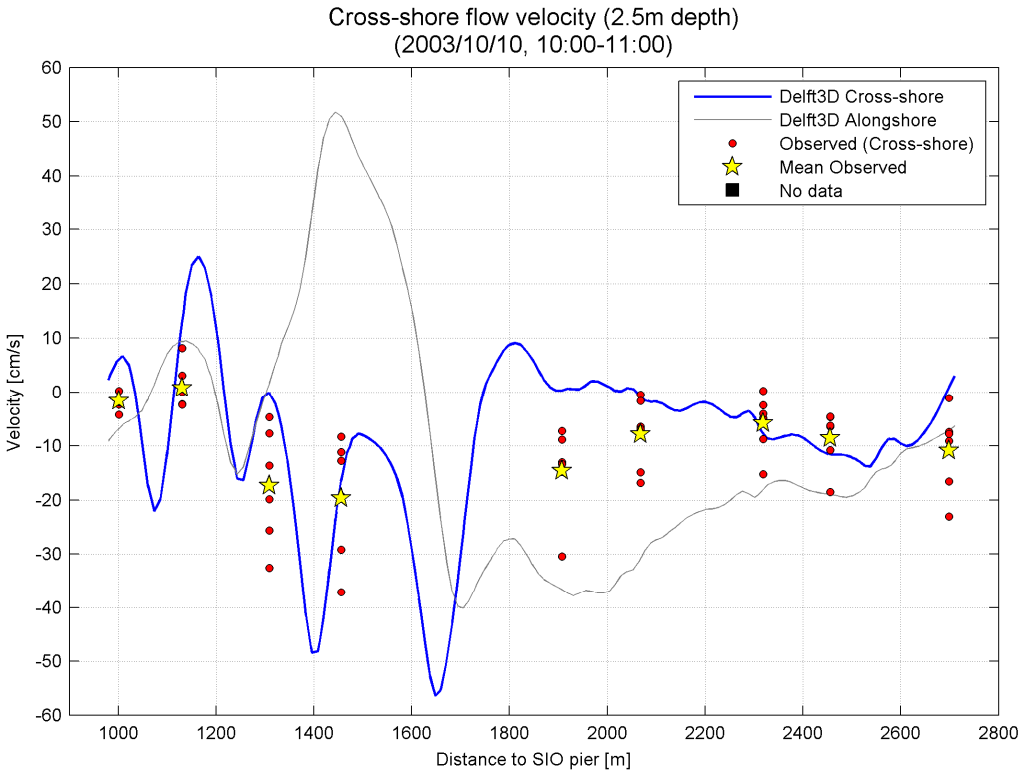

Figure 5.15 Hourly averaged cross-shore flow velocity along 2.5m depth transect (2003/10/10, 10:00-11:00)

5.3.1.3 Transect velocities throughout the day

The figures in this section represent the alongshore and cross-shore flow velocities along the alongshore transects (horizontal axes) in time (vertical axes). Where a transect crosses an observation point, a dot is plotted containing the hourly averaged observed flow velocity.

Northward and onshore-directed flow velocities are considered positive, which corresponds to a red colour. Southward and offshore-directed flows are considered negative and correspond to a blue colour. Black crosses are shown when observations were not available. The observed and modelled flow velocities are plotted in the same colour scale.

<u>1m depth contour</u>
The model results along the 1m depth transect in Figure 5.16 show flows in both the offshore and onshore direction. In particular, south of the focus zone, the alternating blue and red colours represent these opposite flow directions. Long and Özkan-Haller [2005] (section 2.4.2.1), found that for idealized conditions rip currents are predicted to be forced by strong alongshore wave height variations resulting from wave refraction over offshore bathymetric features (e.g. undulations at the rim of the canyon). North of the focus zone, this alternating pattern is less apparent which might be due to the larger distance from the surf zone to the canyon resulting in a smoother wavefield.
The observed (near bed) flows are offshore-directed. Differences in observed and predicted cross-shore flow directions at Ray 1000 and 1149 (onshore of the canyon) could be owing to the two causes detailed below:

1 The observations were collected 30 - 60cm above the bed, while the model predictions are depth averaged. According to Reniers [2004], cross-shore flow velocities have a

strong variation over the water column. Alongshore currents have been shown to be approximately depth uniform, meaning that a single observation point can represent a depth-averaged velocity

2 The predicted mean wave direction at these rays differs from the observations by about 5˚ (see par. 4.1.2.1), and thus the location of the predicted rip currents might be wrong.

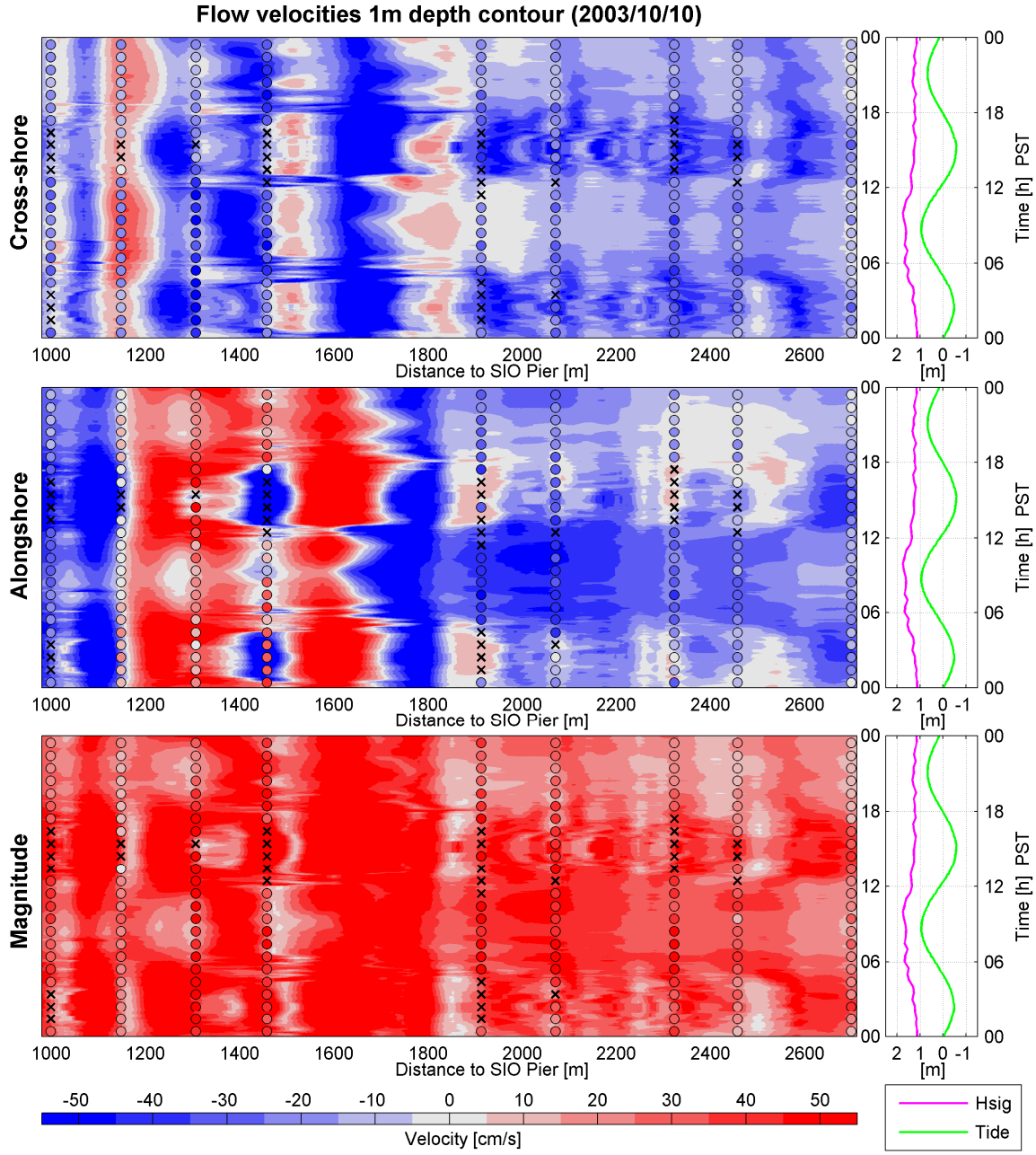

Figure 5.16 Flow velocities at 1m water depth on 2003/10/10

As shown in Figure 5.16, the alongshore flows are predominantly northward south of the focus zone and predominantly southward north of the focus zone. As the set-up during the day did not have a large spatial variation (section 5.2.1), these flows are mainly wave-driven. The mean observed and predicted wave directions south and north of the focus zone are from the south and from the north, respectively.

The model predictions show horizontally smoothed colour patterns just before and after low water periods, which is caused by an unrealistic flow forcing. Near low tide, the water level, which is updated every minute within Delft3D-Flow, is changing relatively fast. However, within Delft3D-Wave the water level is updated only every 20 minutes. Thus, flows calculated during those 20 minutes are driven by wave energy that is increasingly overestimated for a dropping water level and increasingly underestimated for a rising water level.

Wave observations at the offshore buoy show that relatively higher waves (up to 1.75m) propagated shoreward between 06.00 and 12.00 hours. Both the 1m depth (Figure 5.16) and the 2.5m depth transect (Figure 5.17) display that the southward flows north of the focus zone speed up during this period. However, the northward flow south of the focus zone is observed and predicted to decrease.

As only the southward flow increases, the rip current at about 1700m North of the SIO pier migrates slightly in southern direction.

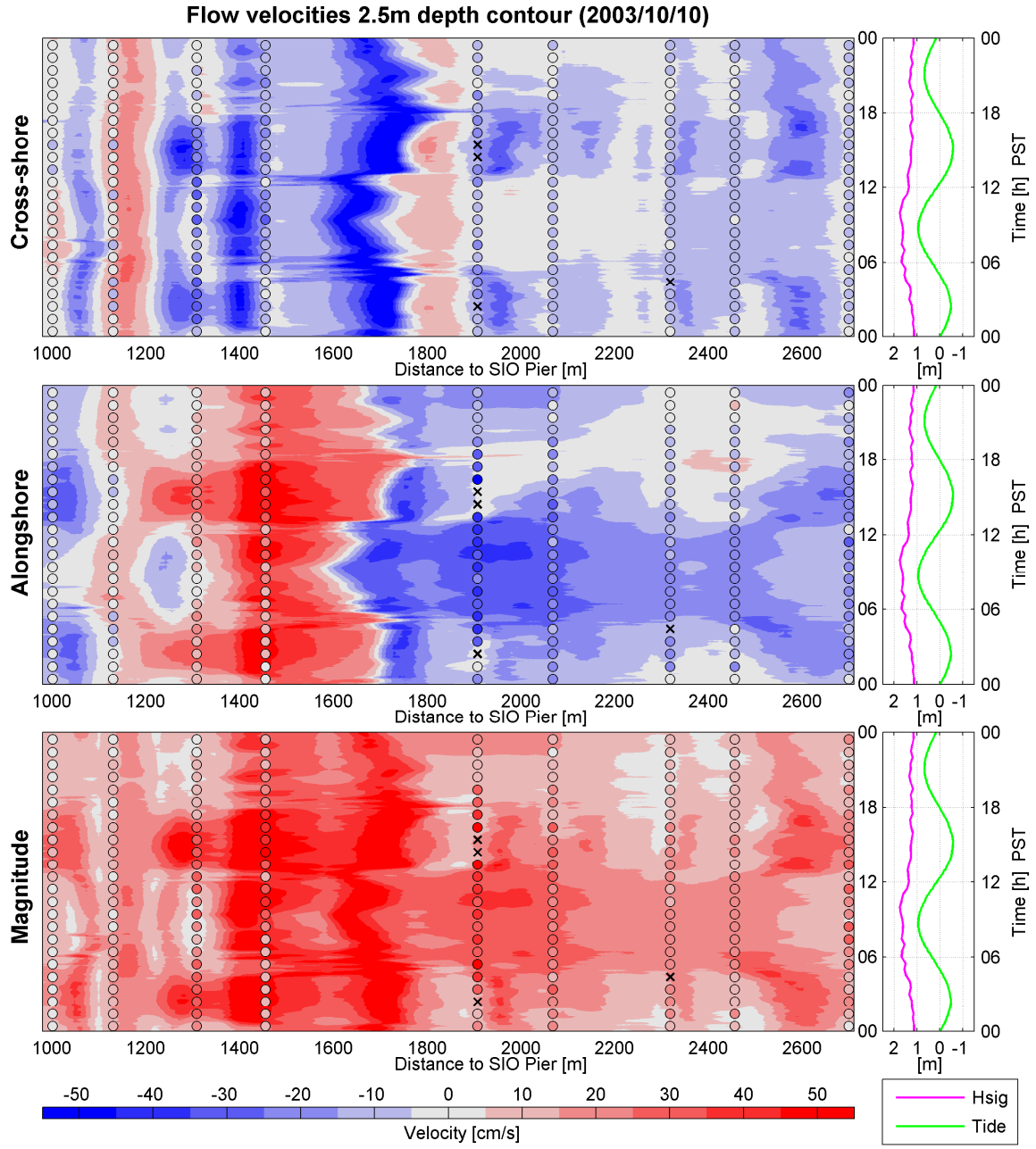

Figure 5.17 Flow velocities at 2.5m water depth on 2003/10/10

2.5m depth contour

Figure 5.17 shows the flow results along the 2.5m depth transect, which lies just inside of the surfzone. The flow patterns at this depth are similar to those on the 1m depth transect, but not as strong. As the waves start breaking, the radiation stress gradient forces the alongshore currents. However, due to a larger water depth the currents are not as strong.

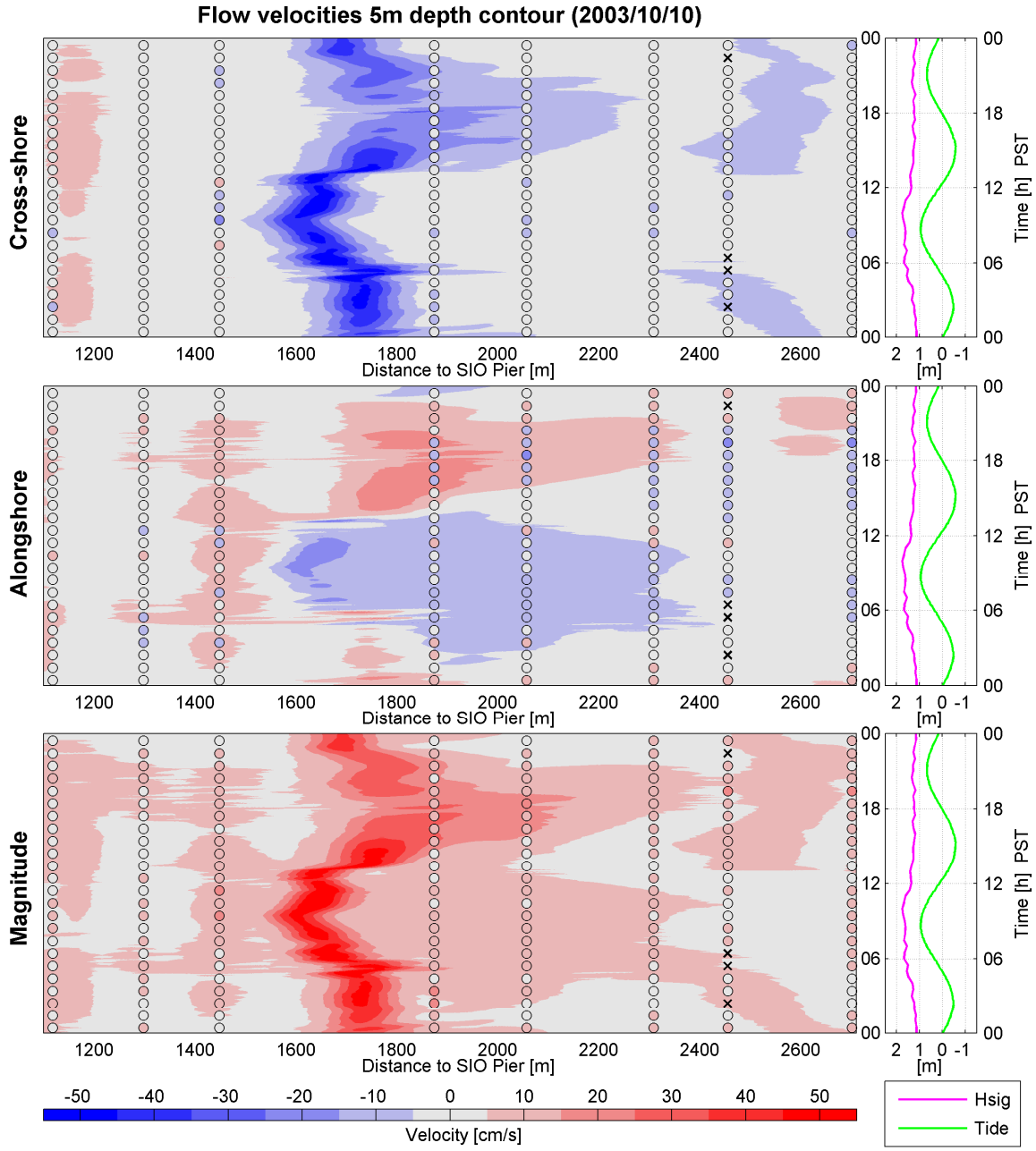

Figure 5.18 Flow velocities at 5m water depth on 2003/10/10

5m depth contour

Figure 5.18 represents the observed and predicted flow velocities at 5m depth transect. This transect lies outside of the surfzone, meaning that incident waves have not broken yet and the radiation stress gradient is negligible.

The modelled alongshore flow velocities between 1600 and 1800m north of the SIO pier are southward during the morning and northward during the afternoon, owing to the rip current that is not flowing perpendicular to the coast in this depth.

5.3.2 Case 2: Swell (Oct 28)

On October 28, a divergent alongshore flow was observed along Black's beach. The model predictions also show a divergent alongshore flow between 0 and 5m water depth (shown in Figure 5.19).

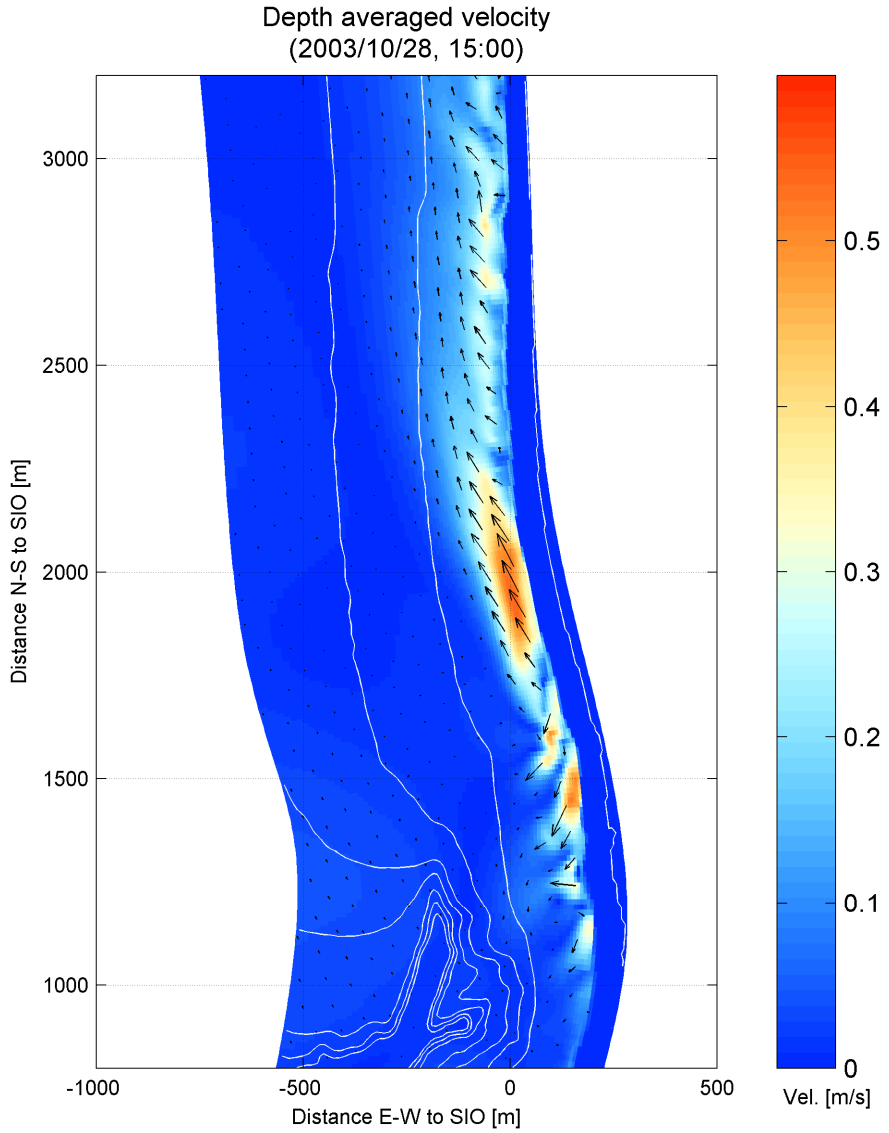

Figure 5.19 Model predictions of depth averaged velocity (2003/10/28, 15:00)

5.3.2.1 Flow time-series comparison

Time-series of the flow velocities in alongshore and cross-shore direction are shown of October 28. Model predictions are compared with observations of ray 1149, 1450, 1911 and 2450 in 2.5m water depth.

Alongshore flow

Time-series of the current meters described in section 2.3.3 showed a divergent flow, north of the focus zone a northward flow and vice versa. Model predictions in Figure 5.20 also hindcast this divergent directed flow during several periods of the day. However, the southward flows at both Ray 1149 and 1450 are slightly underpredicted, what makes the southward flow less significant.

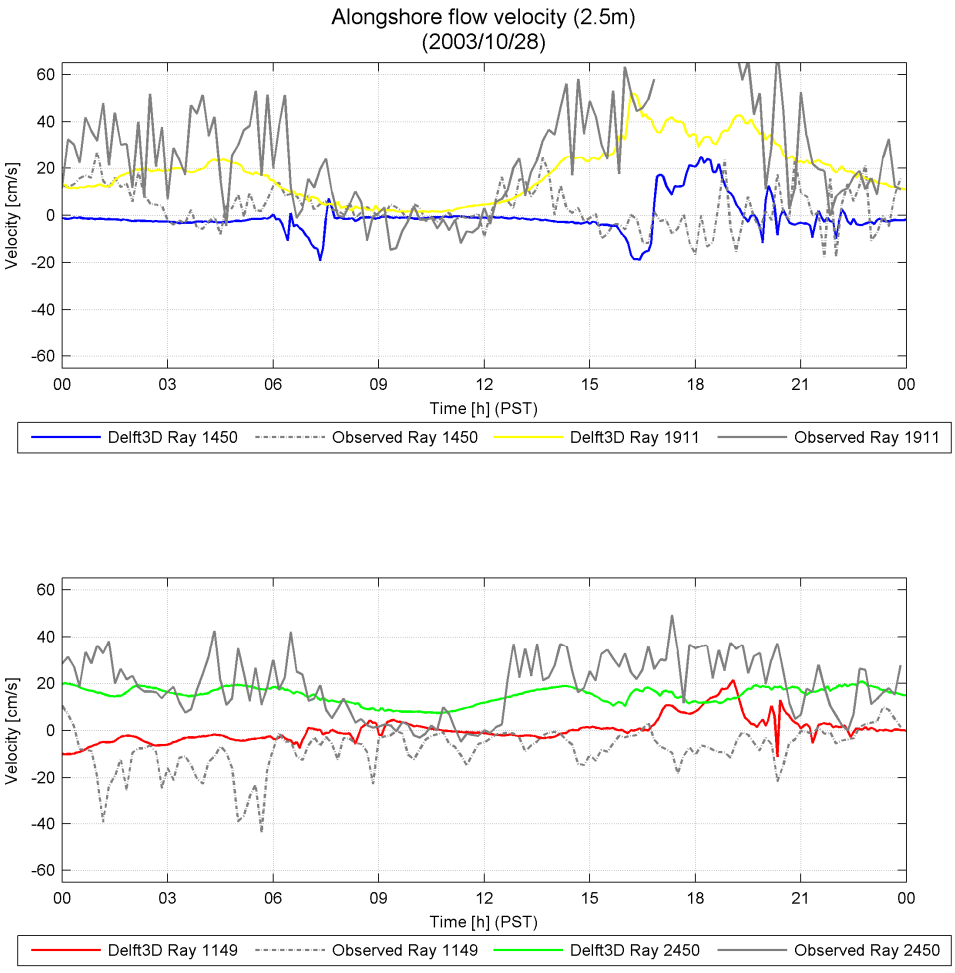

Figure 5.20 Time-series alongshore flow velocity comparison, 2.5m depth (2003/10/28)

Roughly between 00:00 and 06:00 and between 15:00 and 21:00, the time-series of the alongshore flow velocities show larger magnitudes. These moments correspond with the periods of low water levels owing to the tidal elevation.

Cross-shore flow

Cross-shore flow velocities (Figure 5.21) show smaller flow magnitudes than the alongshore flow velocities. Furthermore, also in this case the prevailing flow observations are offshore directed. The model predictions agree in most cases and show a significant larger offshore directed flow at Ray 1911 during the afternoon.

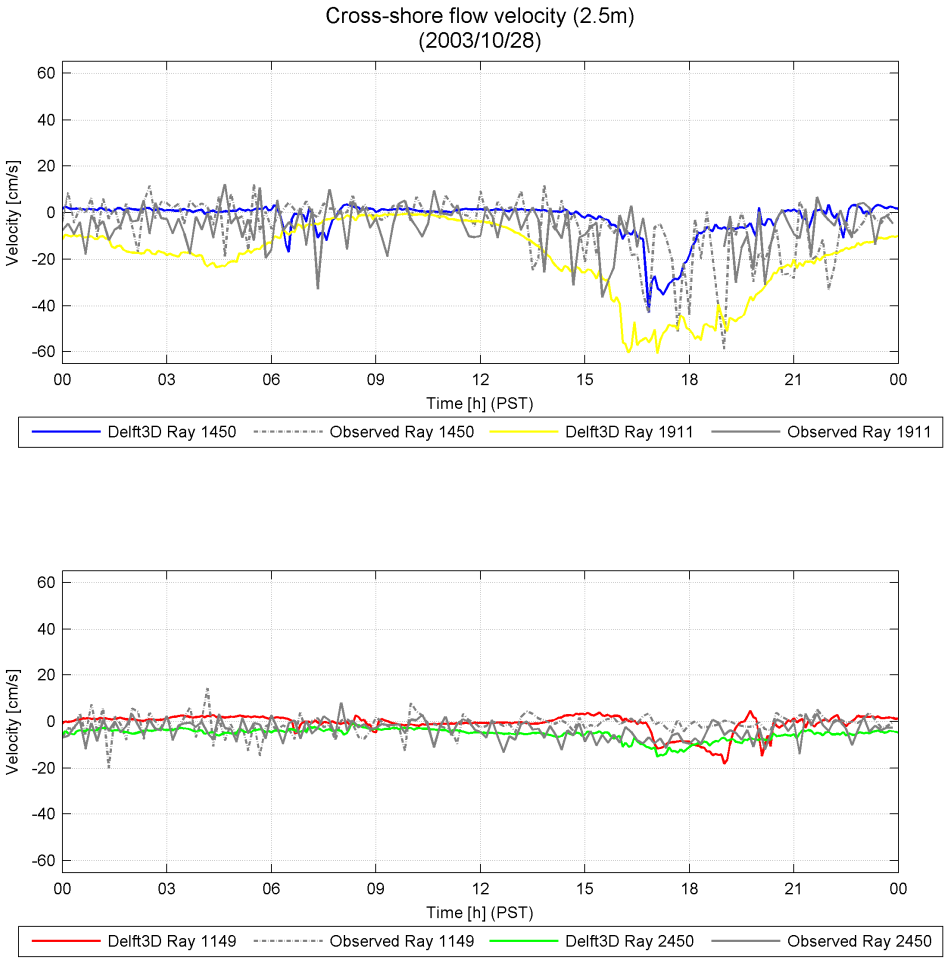

Figure 5.21 Time-series cross-shore flow velocity comparison, 2.5m depth (2003/10/28)

5.3.2.2 *Flow velocity along transect*

Time-series comparison of the flow velocities on October 28 showed that the predictions not precisely correspond to the observations. The deviations do not necessarily mean that the model predicts the flow magnitudes wrong. The model possibly predicts the correct flow velocities, but at a slightly wrong location. Therefore, a comparison is made of an hourly averaged flow velocity along an alongshore transect.

Alongshore flow

The hourly averaged alongshore flow velocity along the 2.5m depth transect is shown in Figure 5.22. The model predictions show a prevailing southward flow between 1000 and 1700m north of the SIO pier. Between 1700 and 2750m the model predictions are solely northward directed. Furthermore, the model underpredicts the alongshore flow velocities in both northward and southward direction.

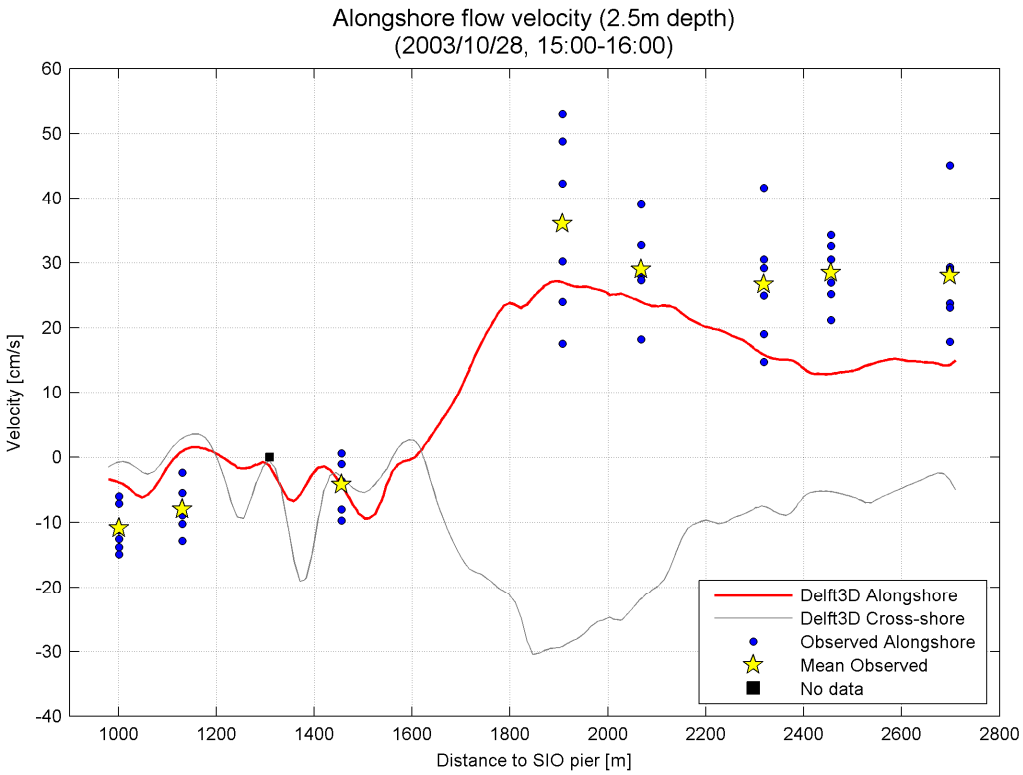

Figure 5.22 Hourly averaged alongshore flow velocity along 2.5m depth transect (2003/10/28, 15:00-16:00)

Cross-shore flow

The predicted cross-shore velocities along the alongshore transect show a prevailing offshore directed current. Except close to 1100 and 1600m, a onshore directed flow is observed. The onshore flow at 1600m is exactly where the alongshore flow changes sign.

A significant larger offshore current is observed between 1700 and 2100m, which corresponds with the alongshore currents. At this part also the alongshore flow has a larger magnitude.

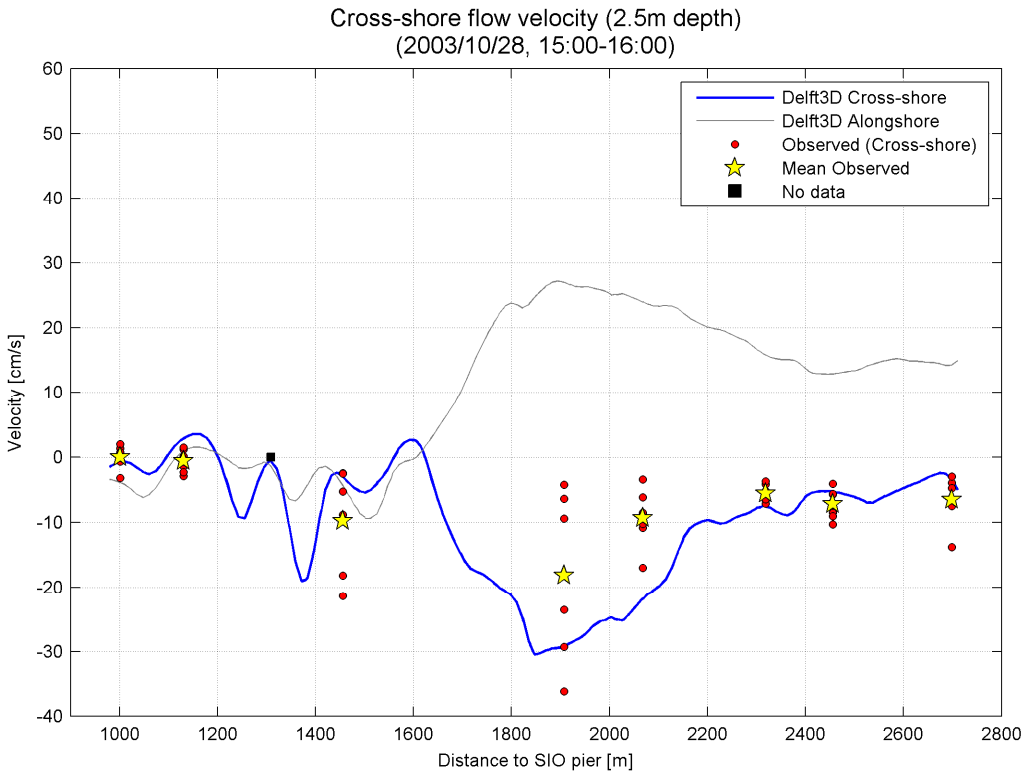

Figure 5.23 Hourly averaged cross-shore flow velocity along 2.5m depth transect (2003/10/28, 15:00-16:00)

Also in this case, the flow velocity between 1000 and 1600m shows spatial oscillation (Figure 5.23). Looking at Figure 5.4 the predicted significant wave height is relatively lower at about 1250 and 1350 north of SIO, which corresponds to the offshore directed flows in Figure 5.23.

5.3.2.3 Transect velocities throughout the day

The figures in this paragraph represent the alongshore and cross-shore flow velocities along these transects (horizontal axes) over time (vertical axes). Where a transect crosses an observation point, a dot is plotted containing the hourly averaged observed flow velocity. Northward and onshore-directed flow velocities are considered positive, which corresponds to a red colour in the figures. Southward and offshore-directed flows are considered negative and correspond to a blue colour. Black crosses are shown when observations were not available. The observed and modelled flow velocities are plotted in the same colour scale.

On October 28, the alongshore flows diverged at about 1600m north of the SIO pier. The flow direction south of the focus zone was southward, although wave forcing would have driven

northward flows, suggesting that water level gradients are driving the flows. North of the focus zone, the flows are northward as would be expected for the observed and predicted waves that approach the shore from the south.

1m depth contour

Figure 5.24 displays flow results along the 1m depth transect. Looking at the alongshore flow velocities, the model predicts an onshore-directed current at 1600m north of SIO pier. This model prediction cannot be tested with observations, since no current meters were deployed there. Nonetheless, this current is likely given the diverging alongshore flow at that point.

On October 28, the first low tide is at about 04.00 hours, and the second low tide is just before 18.00 hours. During the second low tide, the water level drops far enough that the instruments become dry (represented with black crosses in Figure 5.24). The white spots in the model predictions during the second low tide occur when the grid point is predicted to be dry.

The flow velocities at the 1m depth transect show a strong correlation with the tidal elevation. During low tide, the observation points are closer to the shoreline where the set-up is higher and set-up gradients are steeper. Since the wave conditions were constant throughout the day, it is likely that set-up was constant too. South of the focus zone the generated alongshore current was in opposite direction compared to the wave forcing, This is in accordance with Apotsos et al. [2008], who stated that set-up gradients become relatively more important in the middle- and inner surfzone.

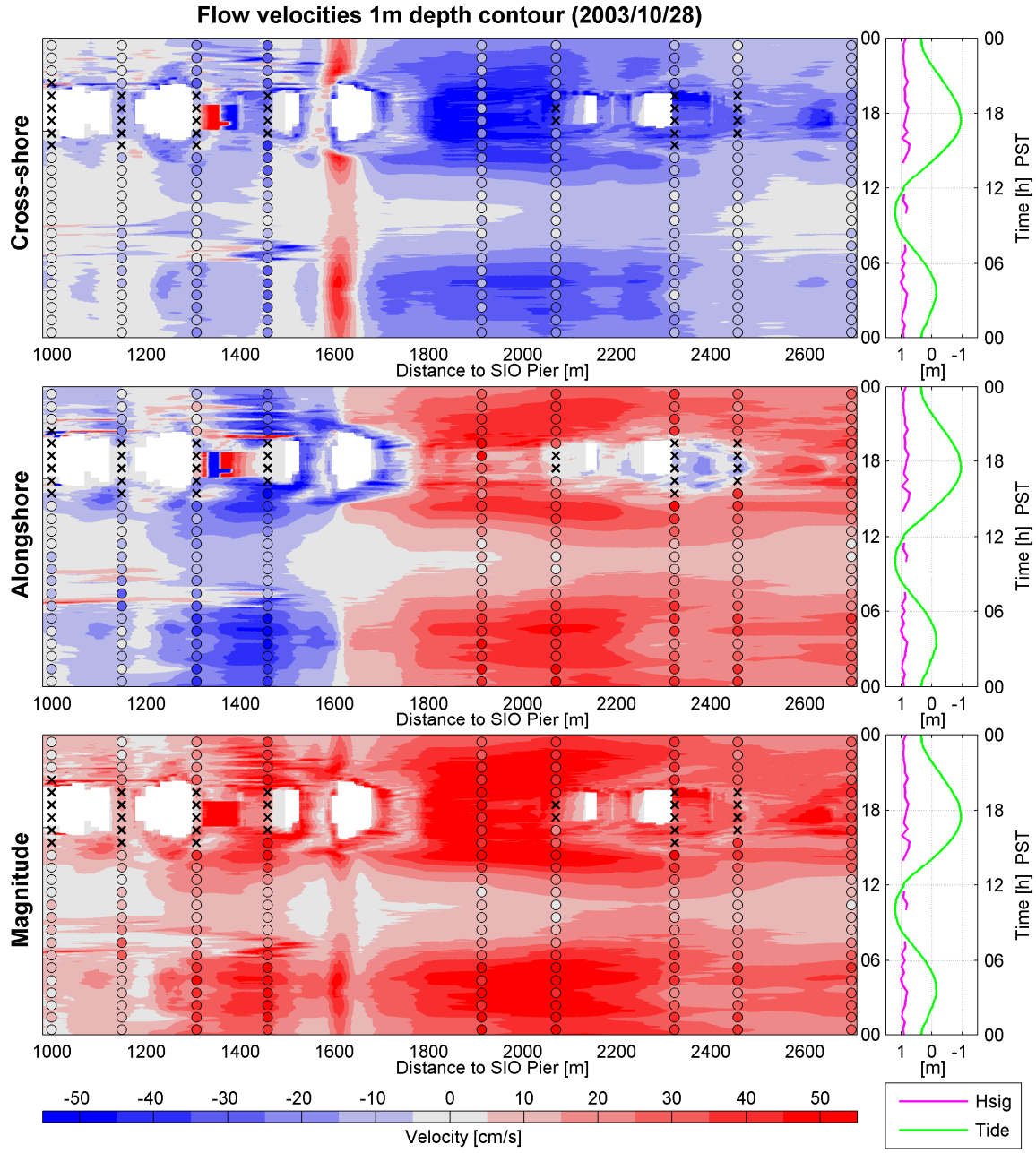

Figure 5.24 Flow velocities at 1m water depth on 2003/10/28

2.5m depth contour

Similar to the 1m depth flows, flows along the 2.5m depth contour show a strong correlation with tide. During low tide the instruments observations are closer to the shoreline, where the set-up gradient is larger than in the outer surfzone. Both model predictions and the observations show a higher velocity during low tide.

As shown on the 1m depth predictions, differences in the update rate for water depths in Delft3D-Wave and Delft3D-Flow lead to smoothed colour patterns just before and after low tide.

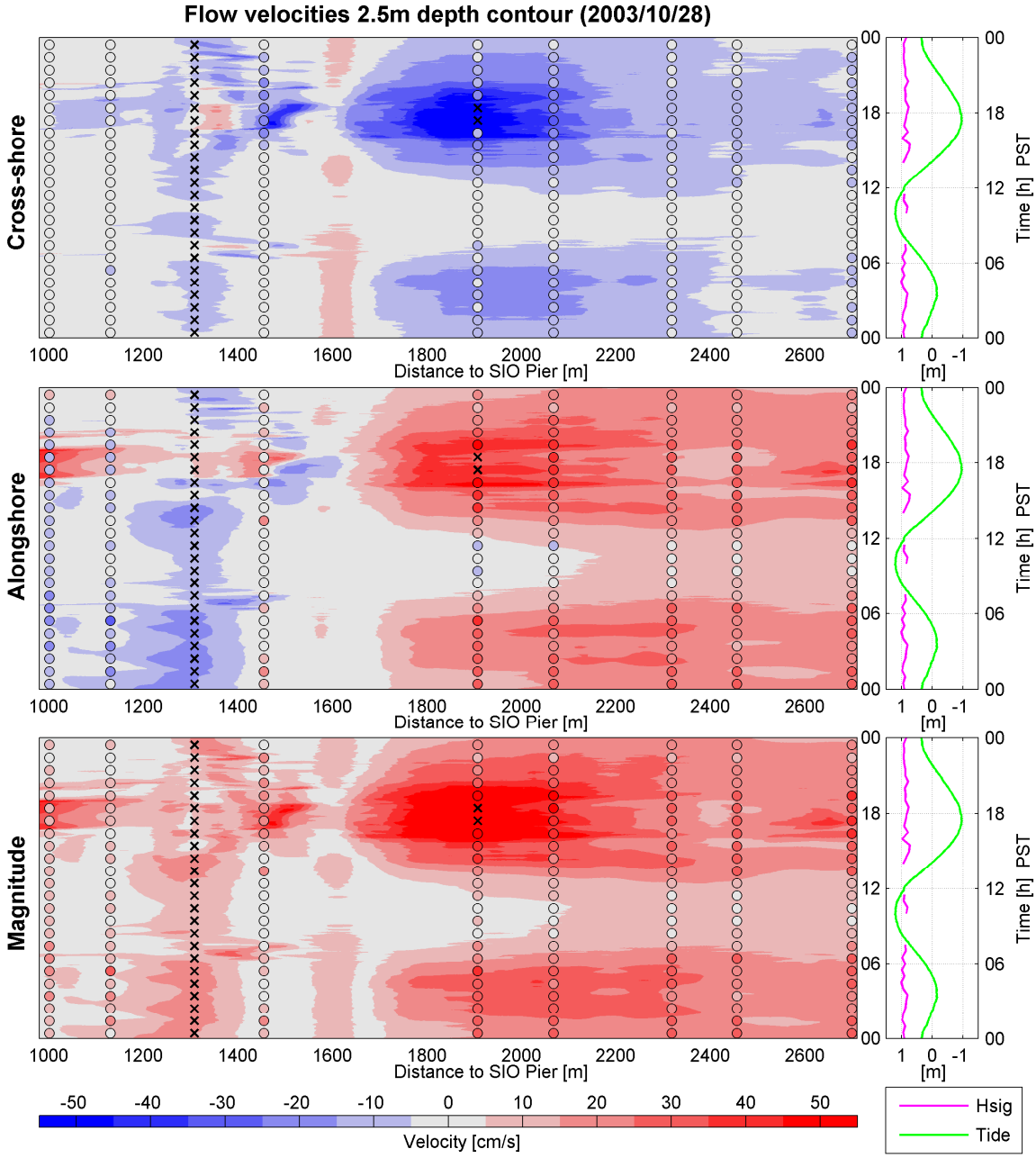

Figure 5.25 Flow velocities at 2.5m water depth on 2003/10/28

5m depth contour

Flow velocities at the 5m depth transect are shown in Figure 5.26. Both model predictions and observations show small cross-shore velocities. However, the model and data agreement is not as good for alongshore flows. In particular, the model predicts a northward flow north of the focus zone during low tide, similar to the flows predicted at 2.5m water depth. In contrast, the observed flows were southward directed. This model-data discrepancy is not well understood.

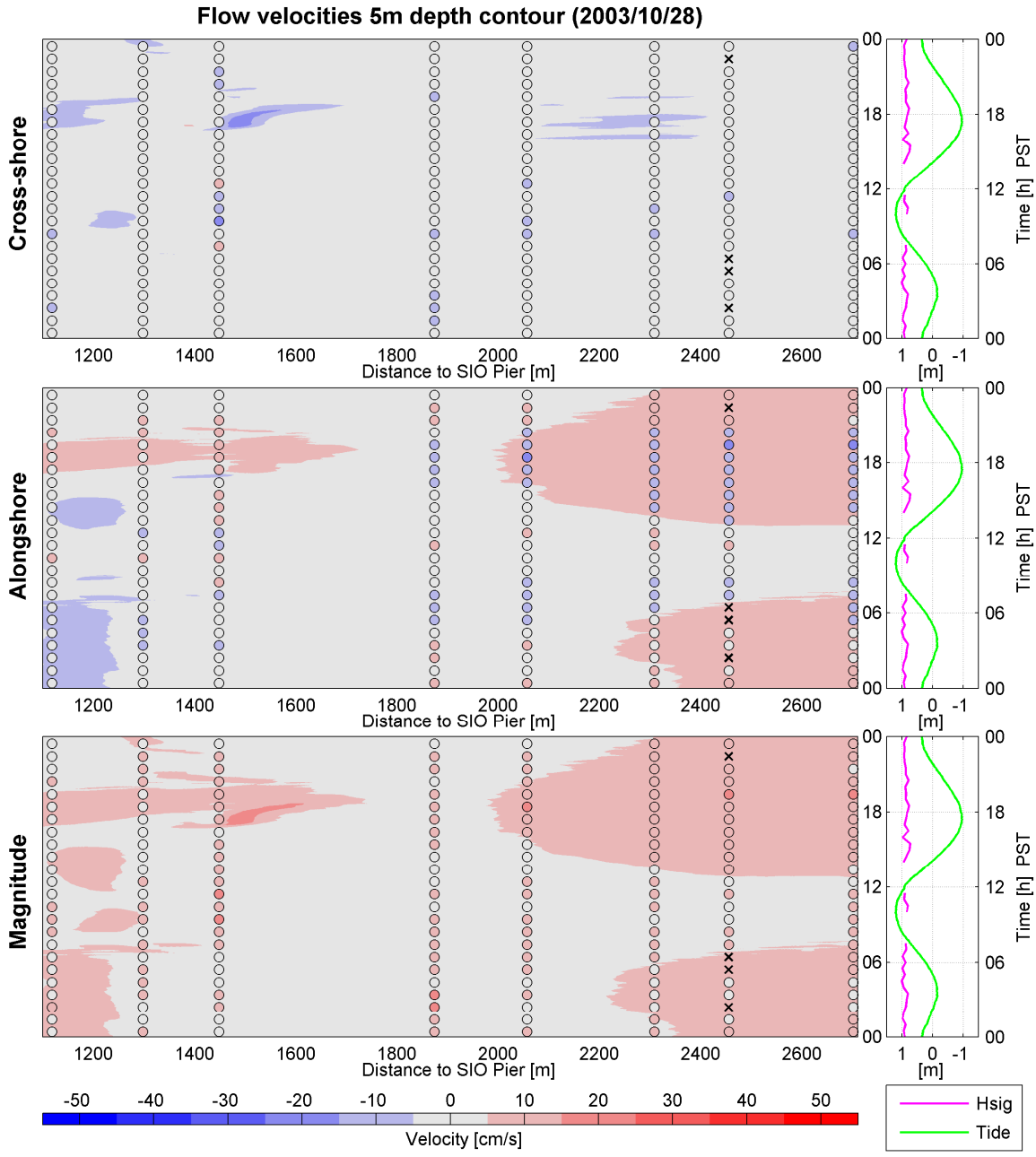

Figure 5.26 Flow velocities at 5m water depth on 2003/10/28

5.3.3 Conclusions

On October 10, currents along the coast are mainly wave-driven and converge close to the focus zone. The model predicts that multiple smaller rip currents develop, with one even extending outside of the surfzone. The observations do not provide evidence of the smaller rips. Model-data discrepancies could be owing to differences between depth-averaged and near-bed flows. For example, the rip could have existed in the top layer only. In addition, the rips may have occurred between the spatially sparse instruments.

On October 28, flow directions in the surfzone are opposite the direction of the wave forcing south of the focus zone. On this day strong set-up gradients develop, which are dominant to wave forcing. In the focus zone, an onshore directed flow develops feeding the diverging alongshore flow.

Model predictions represent the main features of the two cases reasonably well, including a convergent flow on October 10 and a divergent flow on October 28.

6 Conclusions and recommendations

In this last chapter, first the main conclusions will be summarized. Followed by an in-depth response to the research questions, which are used to address the objectives. Finally, recommendations are listed for further research.

6.1 Conclusions

6.1.1 Summary main conclusions

Below the main conclusions of this research are summarized:

Relevant physical processes

- The alongshore water level gradient is dominant to the alongshore currents in case swell waves are prevailing. In case of wind waves is the wave forcing dominant.
- In both conditions, the currents reach similar magnitudes.
- Swell (low frequency) waves are more influenced by the canyon than wind waves (high frequency). Therefore, a larger relative difference in energy is observed onshore of the canyon compared to north of the canyon.

Model performance

- Delft3D is able to reproduce the right flow direction even though the wave directions show inaccuracies onshore of the canyon of about 5˚.
- The trend of the alongshore set-up gradient is predicted by Delft3D.

6.1.2 Research questions

Relevant physical processes:

- How does the wave energy propagate across the submarine canyon?
- Does the canyon have more effect on longer waves?
- What is the incident wave angle relative to the shore?
- Does wind have an important role on the nearshore currents?

How does the wave energy propagate across the submarine canyon?
Incident waves are affected by the bathymetry, which causes refraction. The blue arrows in Figure 6.1 and Figure 6.2 show schematically the direction of wave propagation. In both cases wave energy rotates away from the canyon resulting in a focus zone north of the canyon and a shadow zone onshore of the canyon.

Does the canyon have more effect on longer waves?
A larger relative difference of energy over the canyon was observed when the swell waves were prevailing. Comparisons of the observed wave energy north of the canyon with observed wave energy onshore of the canyon show larger differences on October 28 than on October 10. In addition, wave spectra comparisons showed that predominantly energy distributed over the low frequencies was not able to cross the canyon. This indicates that swell waves are more influenced by the bathymetry.

What is the incident wave angle relative to the shore?
Between the focus zone ("H") and the shadow zone ("L") (see Figure 6.1 and Figure 6.2), the wave angle relative to the shore is south. This in both cases would cause a northward wave-driven flow.

Does wind have an important role on the nearshore currents?
Wind generates relative short waves. The short waves are not influenced as much by the canyon as the long swell waves. Therefore, the wavefield does not show large alongshore gradients in wave height and accompanying wave set-up and the wave-driven current will be dominant.

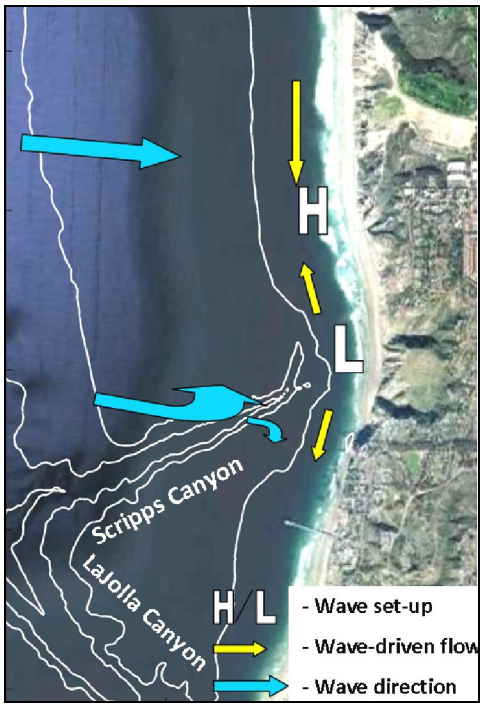

Figure 6.1 Wave-driven flow on October 10, 2003

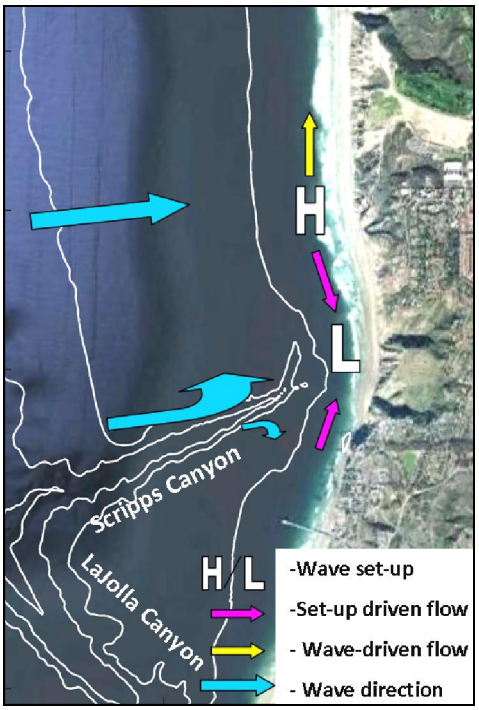

Figure 6.2 Set-up driven flow on October 28, 2003

Model performance:

- Are the wave heights predicted correctly within the surfzone?
- Do waves have the correct angle of incidence relative to the shore?
- Can the numerical model reproduce wave set-up, and its alongshore variations?

Are the wave heights predicted correctly within the surfzone?
Wave heights show reasonably well comparisons. However, small errors in the predictions occur. These errors may possibly be attributed to a not fully up to date bathymetry as no morphological updating is implemented.

Do waves have the correct angle of incidence relative to the shore?
North of the focus zone, the predictions of the incident wave angles relative to the shore show only small deviations. Onshore of the canyon, mean wave directions show deviations between 5 and 10˚. Within the Roller model mean wave directions are used from Delft3D-

Wave. This approach might be a too straight forward as the wave spectra close to the canyon are not narrow banded in direction.

Can the numerical model reproduce wave set-up, and its alongshore variations?
It reproduces the trend of set-up alongshore. However, there are large deviations compared to the observation. The deviations are possibly caused by boundary instabilities as the wave set-up predictions of interest lie close to the coastal boundary.

6.1.3 Main objectives

"What is the relative contribution to the alongshore current of (i) alongshore water level gradients due to the alongshore variation of wave set-up and (ii) obliquely incident waves?"

The offshore wave conditions on October 10 are defined as wind sea. Offshore, waves were observed with mean wave periods of 8 to 9 seconds. The offshore wave conditions on October 28 are defined as swell waves with mean wave periods of about 12 to a14 seconds.

The relative influence of the alongshore wave set-up gradient is strong on October 28. An alongshore water level gradient developed of 8cm over 400m. Conversely, on October 10 an alongshore water level gradient developed of 2cm over 400m.

Considering the mean incident wave direction in the surfzone, a northward flow direction was expected between the focus zone and the shadow zone on October 28. However, due to a large set-up gradient, the alongshore flow was in opposite direction. The reason for this significant set-up gradient is addressed to the larger influence of the submarine canyon on the relatively long swell waves.

The simultaneous occurrence of a large set-up gradient and a significant alongshore currents counteracting the wave forcing supports the relative large importance of a set-up gradient driven flow.

Can Delft3D reproduce the order of magnitude and direction of the nearshore currents?

The directions of the alongshore flows are reproduced well by Delft3D, as the observations showed a convergent current on October 10 and a divergent current on October 28 (see Figure 6.3 and Figure 6.4).

Model predictions for October 10 showed that a rip current developed. The rip could not be validated with observations of the current meters, as it developed in between the stations. However, the existence of this rip is likely as the convergent flow to the origin of the rip could be validated. Model predictions for October 28 clearly show a southward current from the focus zone together with a significant alongshore wave set-up gradient.

Errors in model data comparison of the flow velocity can be attributed to errors in wave predictions and to the comparison of a depth averaged prediction to an observation at a single point of the water column.

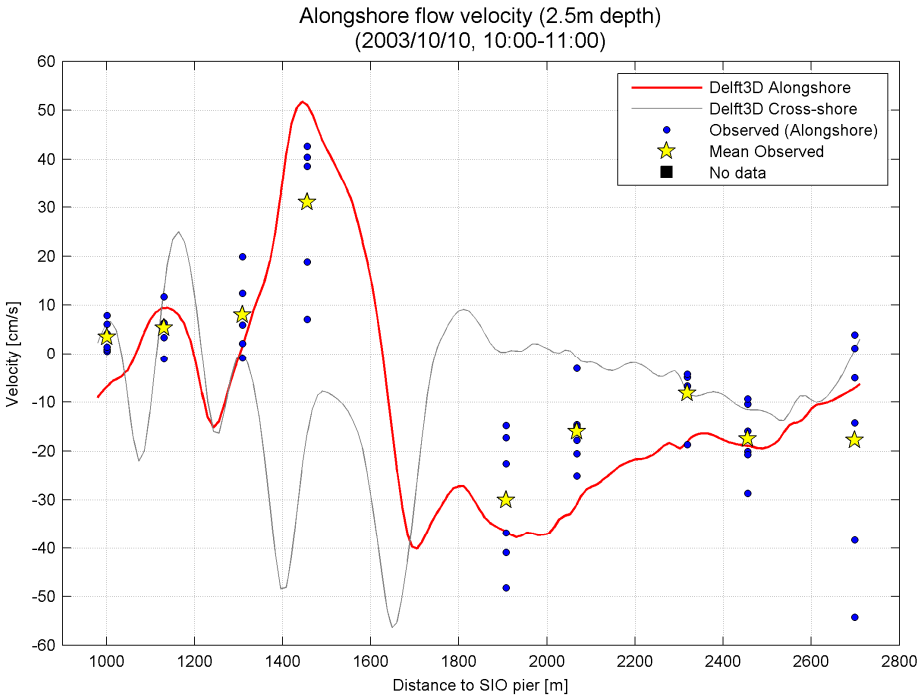

Figure 6.3 Hourly averaged alongshore flow velocity along 2.5m depth transect (2003/10/10, 10:00-11:00)

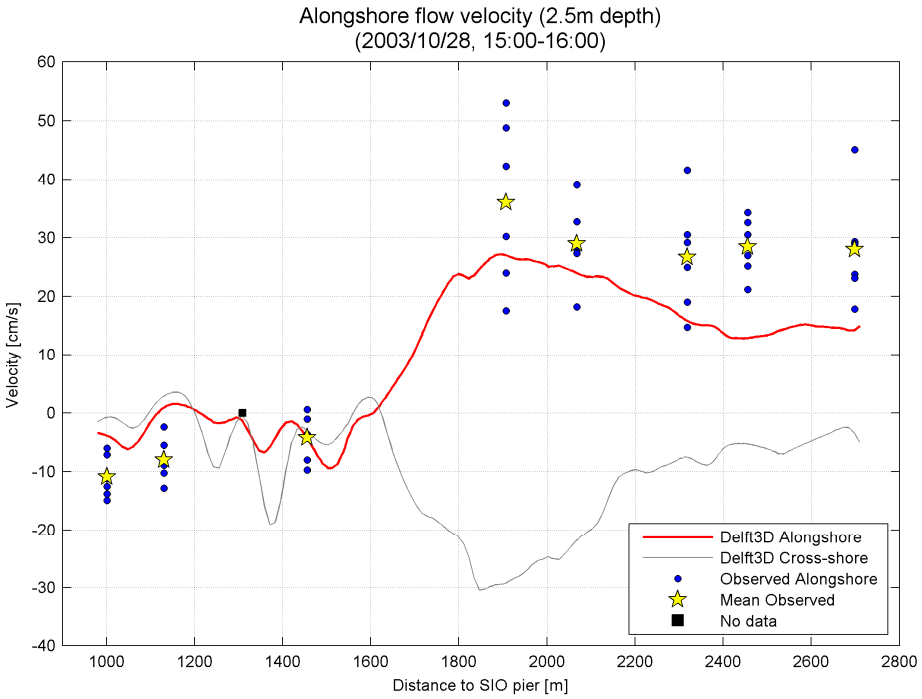

Figure 6.4 Hourly averaged alongshore flow velocity along 2.5m depth transect (2003/10/28, 15:00-16:00)

6.2 Recommendations for further research

Below a number of topics for further research.

Accuracy of the simulation

- The boundary conditions of Delft3D-Wave were formed from data of the Torrey Pine wave buoy. More wave buoys were deployed further south. Using data from these wave buoys could increase the accuracy of the offshore boundary conditions.

- Set up a model that covers the full period of the NCEX measurement campaign and implement morphological updating within the Flow domain. Updating the bathymetry would improve the spatial accuracy within the surfzone. As result of the updated bathymetry, waves and currents will be more accurate.

- Set up a 3D model to be able to account for layered flow velocities. Flow velocities can vary and even be opposite over the water column. E.g. a offshore directed undertow and a onshore directed top layer in the cross-shore. This creates the opportunity to make a better comparison with the observations, which are executed 30 to 60cm above the bed.

Extension of study

- The individual forcing terms for the currents in the surfzone can be determined from Delft3D. It would give more insight to the relative influence of the individual physical processes to the currents.

- Investigate a case in which the offshore wave direction is similar to the investigated cases in this study, but has other wave conditions. This study concentrates on a case with wind waves and a case with swell waves, but to make a better comparison of the influence of the different cases, the offshore wave direction should be the same.

- Verify the use of the Roller model. As the wave spectra close to the canyon are not narrow-banded it might not be good to use the Roller model.

- Bathymetric surveys showed that a significant sand wedge developed in the surfzone between October 6 and October 13 (Section 2.3.4). Modelling the morphological behaviour throughout the measurement campaign could give more insight to the influence of the wave and flow conditions on the bathymetry.

7 References

7.1 Books and papers

d'Angremond, K. and E.T.J.M. Pluim-Van der Velden [2001], "Introduction to Coastal Engineering", VSSD, Delft, Page 7.

Apotsos, A., B. Raubenheimer, S. Elgar, and R.T Guza [2008], "Wave-driven setup and alongshore flows observed onshore of a submarine canyon", J. Geophys. Res., 113, C07025, doi:10.1029/2007JC004514.

Benedet, L., C.W. Finkl, and W.M. Hartog [2007], "Processes controlling development of erosional hot spots on a beach nourishment project", Journal of Coastal Research, 23(1), 33-48. West Palm Beach (Florida), ISSN 0749-0208.

Benedet ,L, List, J.H. [2008], "Evaluation of the physical process controlling beach changes adjacent to nearshore dredge pits", Coastal Engineering, Vol. 55, Issue 12, December 2008, Pages 1224-1236, doi:10.1016/j.coastaleng.2008.06.008.

Booij N. *et al.* [1999], "A Third-generation Wave Model for Coastal Regions, Part 1,Model Description and Validation". Journal of Geophysical Research, Volume 104, No. C4, 7649-7666.

Datawell BV [2009], "Oceanographic instruments", Datawell Waverider Reference Manual, WR-SG, DWR-MkIII, DWR-G, Heerhugowaard, The Netherlands.

Deltares [2010], "Delft3D-Flow, Simulation of Multidimensional Hydrodynamic Flows and Transport Phenomena, Including Sediments", Manual Version 3.14, Rev.11214, Delft, The Netherlands.

Deltares [2010], "Delft3D-Wave, Simulation of short-crested waves with SWAN", Manual Version 3.04, Rev. 11114, Delft, The Netherlands.

Graaff, van der, J. [2004] , "Coastal Morphology & Coastal Protection", lecture notes Delft University of Technology

Hartog, W.M., L. Benedet, D.J.R. Walstra, M. van Koningsveld, M.J.F. Stive, and C.W. Finkl [2008], "Mechanisms that influence the performance of beach nourishment: a case study in Delray Beach, Florida, U.S.A.", Journal of Coastal Research, 24(5), 1304-1319. West Palm Beach (Florida), ISSN 0749-0208.

Holthuijsen, L.H. [2007], "Waves in oceanic and coastal waters", Cambridge University Press.

Kuik, A.J., G. Ph. van Vledder, and L.H. Holthuijsen [1988], "A method for the routine analysis of pitch-and-roll buoy wave data", Journal of physical oceanography, 18, p. 1020-1034.

Lippmann, T.C., G.M. Smith, [2009], "Shallow surveying in hazardous waters", U.S. Hydrographic Conference (US HYDRO), Norfolk, VA, USA, May 11 - May 14, pp. 1 - 12. Conference Proceeding.

Long, J.W., and H.T. Özkan-Haller [2005], "Offshore controls on nearshore rip currents", J. Geophys. Res., 110, C12007, doi:10.1029/2005JC003018.

Magne, R., K.A. Blibassakis, T.H.C. Herbers, F. Ardhuin, W.C. O'Reilly, and V. Rey [2007], "Evolution of surface gravity waves over a submarine canyon", J. Geophys. Res., 112, C01002, doi:10.1029/2005JC003035.

Reniers, A.J.H.M., , E. B. Thornton, T. P. Stanton, and J. A. Roelvink [2004], "Vertical flow structure during Sandy Duck: observations and modeling", Coastal Engineering, Vol. 51, Issue 3, May 2004, Pages 237-260 doi:10.1016/j.coastaleng.2004.02.001.

Roelvink, J.A., Walstra D.J.R. [2004], "Keeping it Simple by using Complex Models", 6th International Conference on Hydroscience and Engineering, Advances inHydro-Science and -Engineering, Brisbane, Australia.

Stive, M.J.F., H.J. de Vriend, J. Dronkers, A. van Dongeren, and Z.B. Wang [2006], "Coastal Inlets and Tidal Basins", VSSD, Delft, Pages 11, 12.

Thomson, J., S. Elgar and T.H.C. Herbers, [2005], "Reflection and tunneling of ocean waves observed at a submarine canyon", Geophys. Res. Lett., 32, L10602, doi10.1029/2005GL022834.

Thomson, J., S. Elgar, T.H.C. Herbers, B. Raubenheimer, and R.T. Guza [2007], "Refraction and reflection of infragravity wavesnear submarine canyons", J. Geophys. Res., 112, C10009, doi:10.1029/2007JC004227.

Van Rijn, L.C., Walstra D.J.R. [2003], "Modelling of Sand Transport in Delft3D-Online", Report Z 3624, WL|Delft Hydraulics, The Netherlands.

7.2 Internet

CDIP, [2009/10/16], "CDIP historic data", http://cdip.ucsd.edu/?nav=historic&sub=data&units=metric&tz=UTC&pub=public&map_stati=1,2,3

Elgar, S., [2009/10/16], "Field data", http://science.whoi.edu/users/elgar/NCEX/fo-field_data.html.

NOAA, [2003/10/03], "Station information", http://tidesandcurrents.noaa.gov/station_info.shtml?stn=9410230%20La%20Jolla,%20CA

NPS, [2006/01/12], "Ocean waves laboratory", http://www.oc.nps.edu/wavelab/ncex.html

A Time-series of observed H_{sig}

Time-series of the significant wave height in 2.5m water depth were shown in section 2.3.2.3. Observations in 1 and 5m water depth are shown below to illustrate the behaviour of the waves shore ward.

Case: Wind sea (Oct 10)

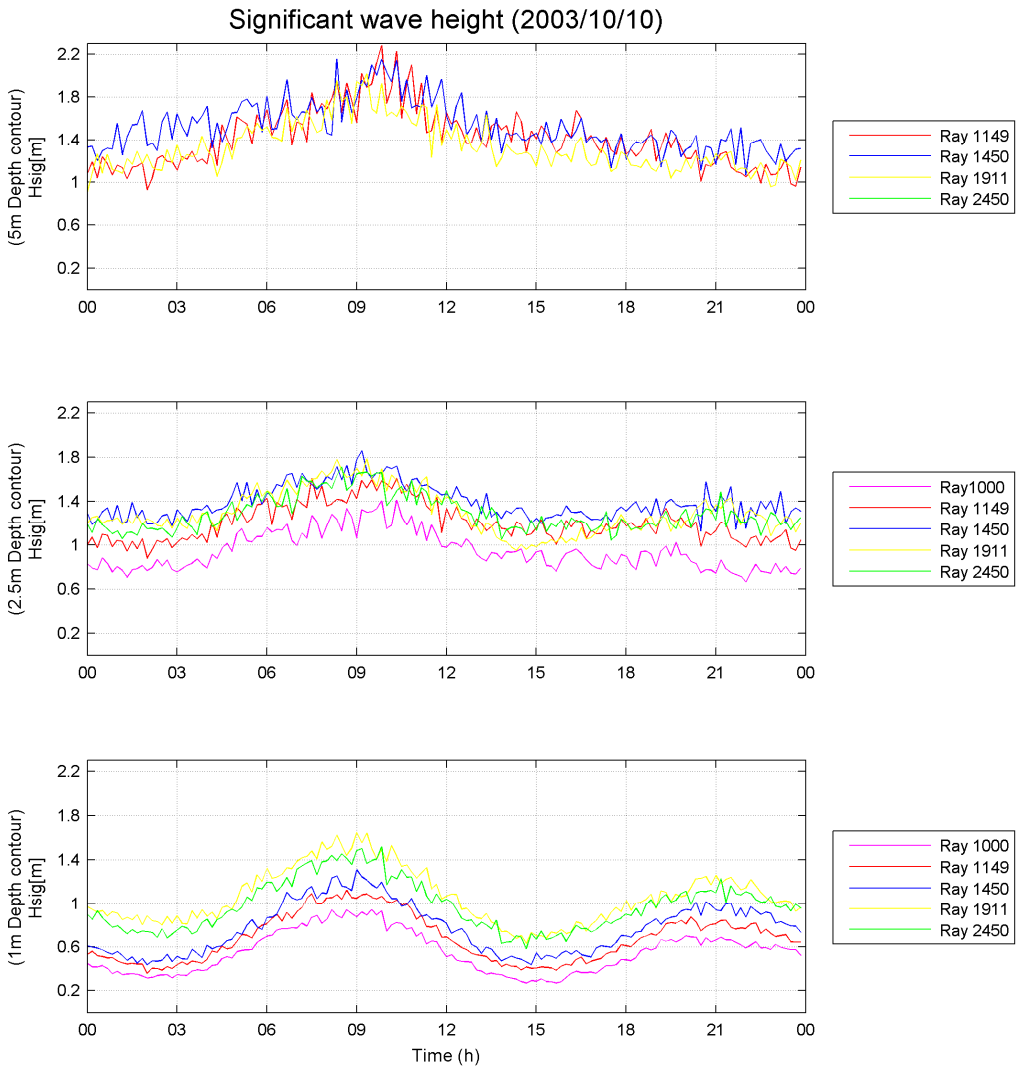

Case: Swell waves (Oct 28)

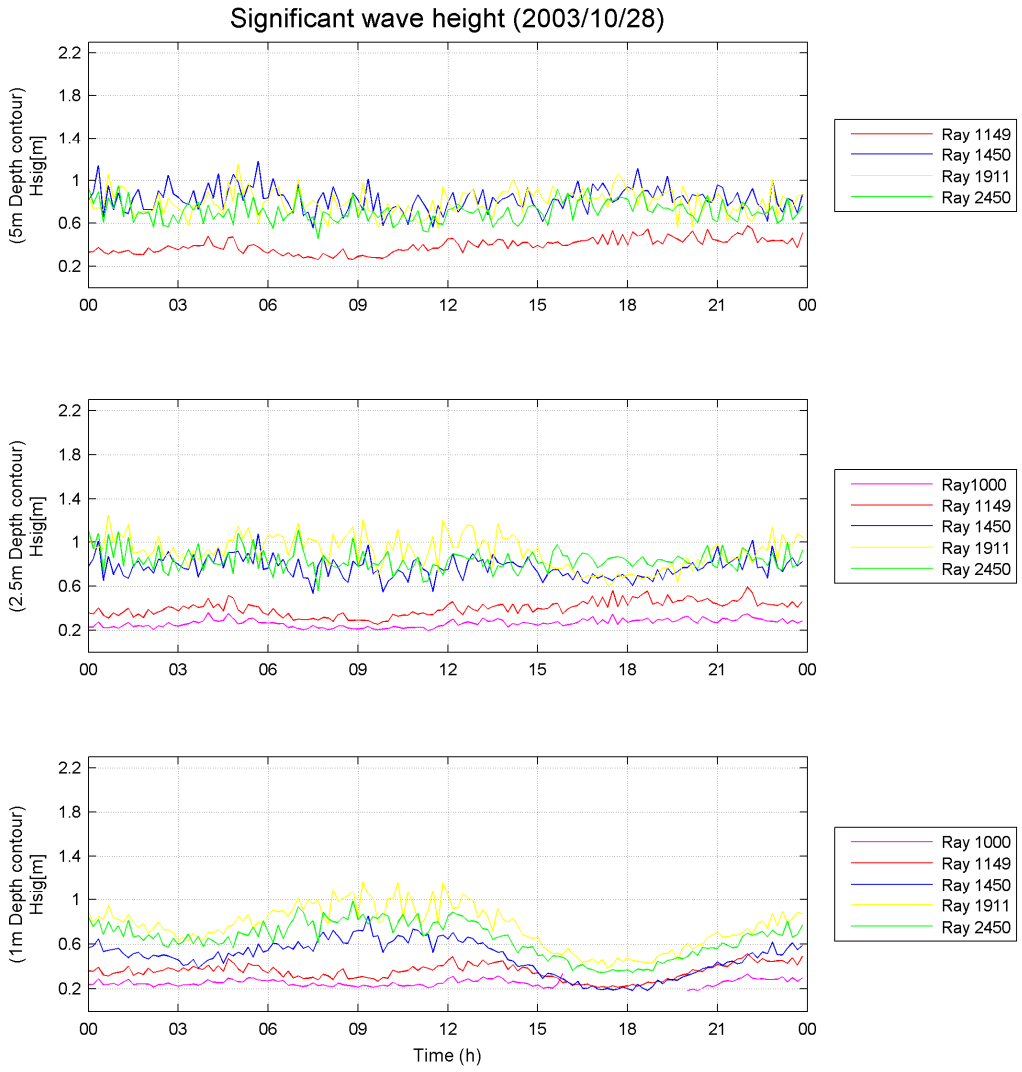

B Delft3D settings

An overview of the complete set of model settings is listed in the tables below. These settings are applied for all simulations unless mentioned otherwise.

B.1 Wave model

Hydrodynamics	Value	Details
Coupled	Use hydrodynamic results from flow	

Grids	Value	Details
Large grid	M*N = 99*65	Oreilly_large_SIO.grd
	Dir. Space = 360/90	Initially 360/36
	Wind use and extend	Initially no wind used
Intermediate grid	M*N = 100*113	Oreilly_mid_SIO.grd (nested)
	Dir. Space = 360/90	Initially 360/36
	Wind = use and extend	Initially no wind used
Small grid	M*N = 238*241	Orielly_small_SIO ext.grd (nested)
	Dir. Space = 360/90	Initially 360/36
	Water level = use and extend	
	Wind = use and extend	Initially no wind used

Boundaries	Value	Details
Orientation	North	Sp1-file
Orientation	West	Sp1-file
Orientation	South	Sp1-file

Physical parameter	Value	Details
Constants		
Gravity	9.81m/s^2	
Water density	1025kg/m^3	
North w.r.t. x-axis	90°	
Minimum depth	0.05m	
Convention	Nautical	
Wave set-up	None	
Forces	Radiation stress	
Processes		
Gen. Mode. Phys.	3rd generation	
Wave Set-up	False	
Breaking	True	
Break Alpha	1	
Break Gamma	0.5	
Triads	True	

Triads Alpha	0.1	
Triads Beta	2.2	
Bed Friction	JONSWAP	
Bed Friction Coef.	0.067 m^2/s^3	
Diffraction	False	
Various		
Wind growth	True	
White Capping	True	Komen et al.
Quadruplets	True	
Refraction	True	
Freq. Shift	True	

Numerical parameter	**Value**	**Details**
Geograph. space	First order (SWAN 40.01) Second order (SWAN 40.11)	
Directional space	0.5	
Frequency space	0.5	

B.2 Flow model

Domain	**Value**	**Details**
Grid	M*N = 346*86	Flow_strip_15.grd
Latitde	32.88°	
Number of layers	1	
Flow time step	3 sec	

Time frame	**Value**	**Details**
Reference date	09-10-2003	(dd-mm-yyyy)
Simulation start time	09-10-2003 18:00	(dd-mm-yyyy hh:mm)
Simulation stop time	11-10-2003 00:00	(dd-mm-yyyy hh:mm)
Flow time step	0.05 min (3 sec)	

Processes	**Value**	**Details**
Constituents	NONE	
Physical		
Wind	True	
Wave	True	
Online Delft3D-Wave	True	
Secondary flow	False	

Boundaries	Value	Details
North	M1 = 346, N1 = 2 M2 = 346, N2 = 85	Neumann, time-series
West	M1 = 2, N1 = 86 M2 = 345, N2 = 86	Water level, time-series
South	M1 = 1, N1 = 16 M2 = 1, N2 = 85	Neumann, time-series

Physical parameter	Value	Details
Constants		
Gravity	9.82 m^2/s	
Water density	1025 kg/m^3	
Air density	1 kg/m^3	
First breakpoint	0.00063	
Second breakpoint	0.00723	
Roughness		
Roughness formula	Chezy, Uniform U=65 V=65	Stress formulation Fredsoe
Wall roughness	Slip condition, free	
Viscosity		
Horizontal eddy viscosity	1 m^2/s	
Wind		
Turned on	Uniform	Hourly averaged
Interpolation	Linear	

Numerical parameter	Value	Details
Drying and flooding check	Grid cell centres and faces	
Depth specified at	Grid cell corners	
Depth at grid cell centres	Mean	
Depth at grid cell faces	Mean	
Threshold depth	0.3m	
Marginal depth	-999	
Smoothing time	60 min	
Advection scheme for momentum	cyclic	

Additional parameters	Value	Details
Coastal boundary	#yes#	
Roller model	#yes#	
Gamdis	0.5	
Betaro	0.05	